INFORMATION TO USERS

This material was produced from a microfilm copy of the original document. While the most advanced technological means to photograph and reproduce this document have been used, the quality is heavily dependent upon the quality of the original submitted.

The following explanation of techniques is provided to help you understand markings or patterns which may appear on this reproduction.

1. The sign or "target" for pages apparently lacking from the document photographed is "Missing Page(s)". If it was possible to obtain the missing page(s) or section, they are spliced into the film along with adjacent pages. This may have necessitated cutting thru an image and duplicating adjacent pages to insure you complete continuity.

2. When an image on the film is obliterated with a large round black mark, it is an indication that the photographer suspected that the copy may have moved during exposure and thus cause a blurred image. You will find a good image of the page in the adjacent frame.

3. When a map, drawing or chart, etc., was part of the material being photographed the photographer followed a definite method in "sectioning" the material. It is customary to begin photoing at the upper left hand corner of a large sheet and to continue photoing from left to right in equal sections with a small overlap. If necessary, sectioning is continued again — beginning below the first row and continuing on until complete.

4. The majority of users indicate that the textual content is of greatest value, however, a somewhat higher quality reproduction could be made from "photographs" if essential to the understanding of the dissertation. Silver prints of "photographs" may be ordered at additional charge by writing the Order Department, giving the catalog number, title, author and specific pages you wish reproduced.

5. PLEASE NOTE: Some pages may have indistinct print. Filmed as received.

University Microfilms International
300 North Zeeb Road
Ann Arbor, Michigan 48106 USA
St. John's Road, Tyler's Green
High Wycombe, Bucks, England HP10 8HR

Downloaded from SHAREOK. Persistent Handle URL: https://hdl.handle.net/11244/4302

77-21,403

ROUSEY, Carlton Earl, 1948-
EVIDENCE FOR SECONDARY GRAVITATIONALLY LENSED IMAGES IN RADIO QUASISTELLAR OBJECTS.

The University of Oklahoma, Ph.D., 1977
Physics, general

Xerox University Microfilms, Ann Arbor, Michigan 48106

THE UNIVERSITY OF OKLAHOMA

GRADUATE COLLEGE

EVIDENCE FOR SECONDARY GRAVITATIONALLY LENSED IMAGES IN RADIO QUASISTELLAR OBJECTS

A DISSERTATION

SUBMITTED TO THE GRADUATE FACULTY

in partial fulfillment of the requirements for the

degree of

DOCTOR OF PHILOSOPHY

By

CARLTON EARL ROUSEY

Norman, Oklahoma

1977

EVIDENCE FOR SECONDARY GRAVITATIONALLY LENSED

IMAGES IN RADIO QUASISTELLAR OBJECTS

A DISSERTATION

APPROVED FOR THE DEPARTMENT OF PHYSICS AND ASTRONOMY

By

Ronald Kantowski

Jack Cohn

William N. Huff

Ronald R. Bourassa

Mike Chiucchieri

David Branch

ACKNOWLEDGMENTS

I wish to extend my gratitude to Dr. Ronald Kantowski for his many helpful suggestions and ideas which helped to make this paper possible. I am also greatly indebted to Dr. Ronald R. Bourassa, Dr. David R. Branch, Dr. Guido L. Chincarini, and Dr. Jack Cohn for their many constructive comments and for reading and correcting the manuscript. I especially wish to acknowledge my wife, Jimmie Sue, for typing, retyping, and proofreading the manuscript with inexhaustible skill and patience. It is also my special pleasure to thank my parents, Mr. and Mrs. Lunt H. Gaines, for their inestimable moral and material support throughout the years of my education.

"A luminous star, of the same density as the Earth, and whose diameter should be two hundred and fifty times larger than that of the Sun, would not, in consequence of its attraction, allow any of its rays to arrive at us. It is therefore possible that the largest luminous bodies in the Universe may, through this cause, be invisible."

P. S. Laplace, 1798

TABLE OF CONTENTS

Page

LIST OF TABLES..... vii

LIST OF ILLUSTRATIONS..... viii

CHAPTER

I. INTRODUCTION..... 1

II. THE THEORETICAL FRAMEWORK OF GRAVITATIONAL IMAGING..... 4

The Gravitational Deflection of Light
Gravitational Imaging
The Point-Mass Lens

III. THE OBSERVATIONAL DATA AND THE RADIO IMAGING CRITERIA.... 20

Selection of the Appropriate Types of Sources
Description of the Present Types of
Radio-Quasar Data
The Radio Imaging Criteria and the Initial
Selection of Image Candidates
--Similar Radio Spectra of Components
--Conservation of Surface Brightness
--Notes to Particular Sources Listed in Table III
--Maximum Angular Separations of Images

IV. FURTHER SELECTION CRITERIA AND IMAGE MODELS..... 75

Observability of the Secondary Optical Images
Image Modeling Procedure
--The Deflector Mass-Distance Curves
--Estimation of the Deflector Distance
Image Models for the Extended Sources
--1704+60 (3C 351)
--1229-021 (4C-02.55)
--1111+40 (3C 254)
--0003-00 (3C 2)
--1206+43 (3C 268.4)

TABLE OF CONTENTS (continued)

CHAPTER Page

Image Models for the Compact Sources
--0538+49 (3C 147)
--1328+307 (3C 286)
--0420-01 (OF-035)
--2230+114 (CTA 102)
--1328+254 (3C 287)
--0333+32 (4C 32.14)
--1416+067 (3C 298)

V. CONCLUSION..... 112

Summary of the Results
Suggestions for Further Investigations

APPENDIX A: COSMOLOGICAL DISTANCE PARAMETERS..... 116

Luminosity Distances
Apparent Angular Diameter Distances
Imaging Distance Parameters

APPENDIX B: MAXIMIZATION OF $D(q_o:Z_d,Z_s)$..... 124

APPENDIX C: VALUES AND DIMENSIONS OF CONSTANTS..... 127

Fundamental Physical Constants
Derived Constants

LITERATURE CITED..... 128

References to Tables II and III
References to Notes to Table III
Bibliography

LIST OF TABLES

TABLE		Page
I.	Statistical Breakdown of the Studied Radio-Quasar Sample	31
II.	Different Component Spectra Radio Quasars	34
III.	Similar Component Spectra Radio Quasars	40
IV-1.	Image Model for the Extended Quasar 1704+60 (3C 351)	85
IV-2.	Image Model for the Extended Quasar 0003-00 (3C 2)	86
IV-3.	Image Model for the Extended Quasar 1206+43 (3C 268.4)	87
V-1.	Image Model for the Compact Quasar 0538+49 (3C 147)	98
V-2.	Image Model for the Compact Quasar 1328+307 (3C 286)	99
V-3.	Image Model for the Compact Quasar 0420-01 (OF-035)	100
V-4.	Image Model for the Compact Quasar 2230+114 (CTA 102)	101
V-5.	Image Model for the Compact Quasar 1328+254 (3C 287)	102
V-6.	Image Model for the Compact Quasar 0333+32 (4C 32.14)	103
V-7.	Image Model for the Compact Quasar 1416+067 (3C 298)	104

LIST OF ILLUSTRATIONS

FIGURE		Page
2-1.	The Gravitational Deflection of Light, Showing the Relative Distances of the Source, Lens, and Observer.....	8
2-2.	Gravitational Images of a Circularly Shaped Source Projected Onto the Plane of a Point-Mass Deflector.....	13
2-3.	Image Shapes of a Circular Source Due to a Point-Mass Deflector Which is "Exactly" Centered Over the Source and "Nearly" Centered Over the Source.....	15
2-4.	Image Shapes of a Circular Source Due to a Point-Mass Deflector Positioned at a Distance (h) from the Source.....	16
2-5.	Image Shapes of a Circular Source Due to a Point-Mass Deflector Which is "Off-Centered" from the Source.....	17
3-1.	Sketch of Typical Types of Radio Quasar Spectra.....	24
3-2.	A Typical Radio-Contour Map of the Radio Quasar, 3C 205.....	26
3-3.	Plot of Component Angular Separations Versus the Redshifts of the Sources for the "Extended" Radio Quasars.....	72
3-4.	Plot of the Component Angular Separations Versus the Redshifts for the "Compact" Radio Quasars.....	73
4-1.	Positional Sketch of the Radio and Optical Systems in the Quasar 1704+60 (3C 351).....	89
4-2.	Logarithmic Plot of the "Deflector-Mass" and "Defelctor-Luminosity" Curves for the Image Candidate 1704+60 (3C 351).....	90

LIST OF ILLUSTRATIONS (continued)

FIGURE		Page
4-3.	Logarithmic Plot of the "Deflector-Mass" and "Deflector-Luminosity" Curves for the Image Candidate 0003-00 (3C 2).....	93
4-4.	Positional Sketch of the Proposed Imaging System in the Quasar 1206+43 (3C 268.4).....	95
4-5.	Logarithmic Plot of the "Deflector-Mass" and "Deflector-Luminosity" Curves for the Image Candidate 1206+43 (3C 268.4).....	96
4-6.	Logarithmic Plot of the "Deflector-Mass" and "Deflector-Luminosity" Curves for the Image Candidate 0538+49 (3C 147).....	106
4-7.	Logarithmic Plot of the "Deflector-Mass" and "Deflector-Luminosity" Curves for the Image Candidate 1328+307 (3C 286).....	108
4-8.	Logarithmic Plot of the "Deflector-Mass" and "Deflector-Luminosity" Curves for the Image Candidate 0420-01 (OF-035).....	110
A-1.	Plot of A(Z) Versus Z for Various Values of q_o	118
A-2.	Plot of D_d Versus Z_d for Various Values of q_o	119
A-3.	Plot of D_{ds} Versus Z_d (with $Z_s = 2$) for Various Values of q_o	120
A-4.	Plot of D Versus Z_d (with $Z_s = 2$) for Various Values of q_o	121
A-5.	Plot of ΦD Versus Z_d (with $Z_s = 2$) for $q_o = 0$ and $q_o = 1$.....	122
A-6.	Plot of ΦD Versus Z_d (with $Z_s = 4$) for $q_o = 0$ and $q_o = 1$.....	123
B-1.	Plot of the Quantity, $(Z_d)_{max}$, Versus the Source Redshift, Z_s, for $q_o = 0$ and $q_o = 1$.....	126

CHAPTER I

INTRODUCTION

The rather novel nature of the radio emitting quasistellar objects (QSS's), along with their presumably large cosmological redshifts, gives rise to the hope that we may begin to explore the farthest depths of our universe. In these regions of darkened knowledge shines the inescapable truth of gravity, that entity which has determined the past and which will govern the future. One of the most esthetic aspects of gravity is the half-century-old idea that light from a distant source can be bent, or even focused, around a region of concentrated mass. However, the search for such "gravitational lenses" has, for the most part, been met with only limited success.

In the more likely cases where the secondary image (i.e., the weaker image) of a light source is too weak to be directly observable optically, it is still possible that the "lensed object" may be appreciably intensified by a gravitational lens (i.e., primary imaging). In particular, Barnothy and Barnothy[1] have proposed that the majority of the optical quasars (QSO's) are such gravitationally intensified Seyfert galaxies. Opponents to this proposition (for example,

---

[1]J. M. Barnothy and M. F. Barnothy, Soviet Astronomy (Astrophysics), Vol. 11, No. 5, (1968), p. 895.

Pacholczyk and Weymann[2]) argue that the ratio of Seyfert galaxies to quasars is much too low (i.e., ~1/100) to justify such an assertion. These arguments, however, are based on an incomplete knowledge of the spatial distributions of both classes of objects. So, even though the present observational data suggests that most quasars (i.e., ≳90%) cannot be explained as such simple "lensed" Seyfert galaxies, one cannot at this point exclude the possibility that at least a measurable fraction of the observed quasars are exhibiting primary imaging.

In the case of secondary optical images, Sanitt[3] has suggested that there may exist gravitational imaging in the quasar, 3C 268.4, but he finds that the secondary optical image must be very faint (~21^m). To this end, one must be adequately equipped to observe such faint secondary images. Thus, through the use of comparatively more sensitive radio telescopes, one might quite possibly be able to observe secondary gravitational images at radio wavelengths. (This particular source has, in fact, been found by the methods employed in this paper to be a prime candidate for the observability of secondary radio images.)

The author has previously[4] attempted to give evidence for gravitational imaging in QSS's with only modest success. Since then,

---

[2]A. G. Pacholczyk and R. Weymann, Astronomical Journal, Vol. 73, (1968), p. 836.

[3]N. Sanitt, Monthly Notices of the Royal Astronomical Society, Vol. 174, (1976), p. 91.

[4]C. E. Rousey, "Possible Evidence of the Gravitational Lens Effect from Observations of the Radio Properties of Quasistellar Objects," (unpublished M. S. thesis, University of Oklahoma, 1974).

considerably more and improved QSS data has been obtained, and, along with an improved method of approach, as a result is able to provide good evidence for the presence of secondary gravitationally lensed images in radio emitting quasistellar objects.

CHAPTER II

THE THEORETICAL FRAMEWORK OF GRAVITATIONAL IMAGING

The Gravitational Deflection of Light

The gravitational bending of light is a direct consequence of most gravitational theories, although the exact quantitative description of the effect varies somewhat among them. Perhaps the simplest and most realistic such theory is that of the linearized Einstein theory for static and weak gravitational fields.[5] Under this formulation, for small bending angles (i.e., the angle between the photon's deflected and undeflected paths), we can express the bending angle in the vector form,

$$\vec{\beta} = \frac{-2}{c} \cdot \int_{-\infty}^{+\infty} \vec{\nabla\phi}\, dt \qquad \text{(II-1)}$$

where c is the speed of light, $\vec{\nabla\phi}$ is the vector gradient of the Newtonian gravitational potential, ϕ, which is assumed to satisfy the boundary conditions that $\vec{\nabla\phi}$ and $\phi \to 0$ at ∞, and the integration is taken with respect to the flight time of the photon along the photon's orbit in the absence of the gravitational field. The bending angle has been expressed in vector from here to allow for the general case of non-spherical symmetry in the gravitational field of the deflector.

---

[5] P. G. Bergmann, Introduction to the Theory of Relativity, (New York: Prentice-Hall, Inc., 1950), p. 184.

To the limit of the above approximation, three very useful properties of the gravitational deflection of light can be seen:

1. The bending angle is independent of the photon's energy or frequency. This is particularly useful for comparing the deflection of light at optical wavelengths to radiation at radio wavelengths.

2. The bending angle has no component along the photon's trajectory. This property allows one to write relatively simple expressions for gravitational imaging systems.

3. The bending angle is linear in the gravitational potential, ϕ. This property enables one to calculate the effects of extended gravitational deflectors by summing up the contributions due to point-masses.

Gravitational Imaging

The concept of gravitational bending of light almost naturally leads one to the idea that a massive object in front of a source of light will act as a "gravitational lens" which produces intensified image(s) of the light source. Gravitational imaging has, of course, been known and applied for a long time. Einstein[6] as early as 1936 used his predicted "point-mass" deflector to calculate the intensification of background stars due to suitably alined foreground stars (primary imaging). Zwicky[7] later showed that under proper conditions of source-lens alinements, crescent shaped images of the source might

---

[6]A. Einstein, Science, Vol. 84, (1936), p. 506.

[7]F. Zwicky, Physical Review, Vol. 51, (1937), p. 679.

be observed. Since then, numerous papers have been published which make theoretical predictions concerning gravitational imaging using various types of source-lens systems, ranging from very naive to highly sophisticated. Refsdal[8] and Liebes[9] were perhaps the first to successfully formulate the imaging effects due to concentrated and opaque gravitational lenses. Barnothy and Barnothy[10] have considered opaque and distributed mass deflectors, while Bourassa, et.al.[11] have employed the more general opaque lens having elliptical symmetry. Such "extended" mass deflectors have been incorporated in gravitational lensing theories in order to mimic more physically realistic lenses such as galaxies. To this end, some of the more recent theories allow for "transparency" of the galaxy-lens. For example, Clark[12] has considered transparent galaxies with spherical symmetry; Sanitt[13] uses cylindrical symmetry in transparent mass systems; Bourassa and Kantowski[14] have developed a method applicable to transparent galaxies

---

[8]S. Refsdal, Monthly Notices of the Royal Astronomical Society, Vol. 128, (1964), p. 295.

[9]S. Liebes, Physical Review, Vol. 133, (1964), p. 835.

[10]J. M. Barnothy and M. F. Barnothy, Science, Vol. 162, (1968), p. 348.

[11]R. R. Bourassa, R. Kantowski, and T. D. Norton, Astrophysical Journal, Vol. 185, (1973), p. 747.

[12]E. E. Clark, Monthly Notices of the Royal Astronomical Society, Vol. 158, (1972), p. 233.

[13]N. Sanitt, Nature, Vol. 234, (1971), p. 199.

[14]R. R. Bourassa and R. Kantowski, Astrophysical Journal, Vol. 195, (1975), p. 13.

with spheroidal symmetry. Because the latter work is very generally developed and is easily reducible to concentrated-mass lenses, this writer will follow their formulation in this paper (henceforth referred to as the B and K Formulation).

In view of the consideration of property (2) of Equation II-1, B and K have written the bending angle in the complex form, $\alpha = \alpha_x + i\alpha_y$, where x and y are orthogonal Cartesian coordinates fixed to the center of mass of the deflector (see Figure 2-1). B and K have also introduced a convenient complex function (the scattering function), $I(x_o,y_o)$, given by:

$$I(x_o,y_o) = \frac{c}{2G} \cdot \left\{ \int_{-\infty}^{+\infty} \frac{\partial \phi(x_o,y_o,ct)}{\partial x_o} \cdot dt - i \cdot \int_{-\infty}^{+\infty} \frac{\partial \phi(x_o,y_o,ct)}{\partial y_o} \cdot dt \right\};$$

where as before ϕ is the Newtonian gravitational potential function, G is the Newtonian gravitational constant, and x_o and y_o are the impact parameters for the deflected photon. With the above definition of the complex scattering function, the complex bending angle can then be expressed as, $\alpha = \frac{-4G}{c^2} \cdot I^*$, where the asterisk denotes complex conjugation. This complex formulation greatly facilitates the algebraic manipulation of imaging expressions since, for example, by considering property (3) of Equation II-1, one can compute the total deflection of light due to generally distributed-mass deflectors by simply summing up all the contributions of the scattering function due to the point-masses which comprise the mass deflector system. Another advantage of this complex description is that the light source can be conveniently projected onto the plane of the deflector, so that in effect one needs only to work in two dimensions.

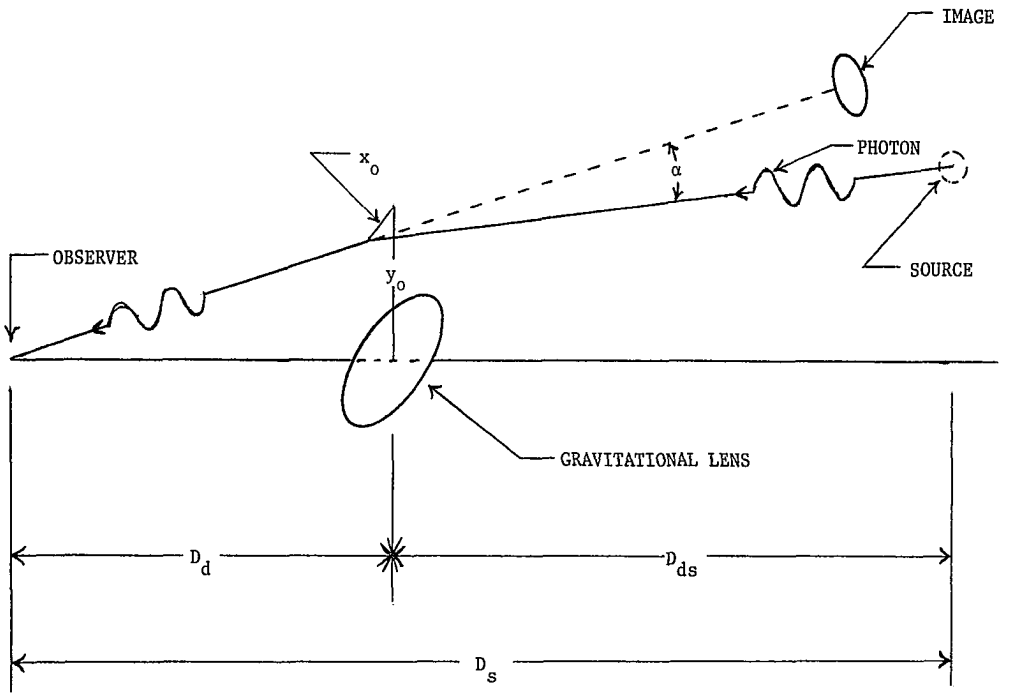

FIGURE 2-1: The gravitational deflection of light, showing the relative distances of the source, lens, and observer

If the bending angle is small, then a simple geometrical consideration provides a simple relation between the relative positions of the source and images. Letting z and z_o denote the complex positions projected onto the deflector plane of the source and image(s), respectively, (see Figure 2-1) one can write, $z = z_o - \frac{4GD}{c^2} \cdot I^*$. (II-2) Here, the quantity D (the position-distance parameter) is defined by $D = \frac{D_d \cdot D_{ds}}{D_s}$, where the deflector-source distance, D_{ds}, the observer-deflector distance, D_d, and the observer-source distance, D_s, are distances measured by "apparent angular size" if calculations are performed in a Robertson-Walker spacetime. To allow for cosmological expansion where large distances are involved, D_d must be evaluated at the time light passes the deflector, while D_s and D_{ds} are measured at the time of light emission from the source. More explicit expressions for these distance parameters are presented in Appendix A for the case of a general Friedmann-type universe.

Now, using the source-image position expression (Equation II-2), one can also calculate the shapes of the images by varying the source position z around the boundary of the source. The first order variation can be written in the matrix form,

$$\begin{vmatrix} \delta x_o \\ \delta y_o \end{vmatrix} = |T| \cdot \begin{vmatrix} \delta x \\ \delta y \end{vmatrix} ,$$

where the complex matrix T is given by,

$$|T| = \frac{1}{\Gamma^2 - |F|^2} \cdot \begin{bmatrix} \Gamma + R_e(F), & -I_m(F) \\ -I_m(F) & , \Gamma - R_e(F) \end{bmatrix},$$

and where the complex functions F and Γ are defined by,

$$\Gamma = 1 - \frac{4GD}{c^2} \cdot \frac{1}{2} \cdot \left[\frac{\partial I}{\partial x_o} + i \cdot \frac{\partial I}{\partial y_o} \right] \quad \text{and}$$

$$F = \frac{4GD}{c^2} \cdot \frac{1}{2} \cdot \left[\frac{\partial I}{\partial x_o} - i \cdot \frac{\partial I}{\partial y_o} \right] .$$

These equations approximate elliptically-shaped images, as long as the source is not two profusely extended. The projected axial ratio (i.e., the ratio of the minor axis to the major axis) of each image is then

$$P = \left| \frac{\Gamma - |F|}{\Gamma + |F|} \right| ,$$

where a value is calculated for each root of z_o (i.e., for each image).

Another useful quantity in the description of gravitational imaging is the "intensification" of the images (i.e., the ratio of the intensity of an image to the intensity of the source). The B & K Formulation (in the view of a suitable definition of distances in General Relativity[15]) leads to the result that the intensity of the images is proportional to their apparent areas. Thus, by using the above image-shape relations, we can express the image intensification by, $AMP = \frac{1}{\Gamma^2 - |F|^2}$, where again this expression assumes a value for each image position Z_o.

It follows from Equation II-2 that since the scattering function is in general a function of z_o, the number of roots for z_o (i.e., the number of images) depends on the exact nature of the mass distribution of the deflector. However, to a reasonably good approximation the

---

[15] I. M. H. Etherington, Philosophical Magazine, Vol. 15, (1933), p. 761.

relative positions and relative intensifications of the images are obtainable with a simple "point-mass" type of deflector system, whereas only the more detailed properties of the images, such as relative shapes and orientations, would be gained by using more sophisticated mass distributions, such as the ones discussed above.

The Point-Mass Lens

In the case of a "point-mass" gravitational lens, one obtains very simple lensing relations. For example, the complex scattering function for such a system can be expressed as $I = M/z_o$, where M is the gravitational mass of the deflector. Then, the relation between the source position (z) and image position(s) (z_o) (projected onto the plane of the deflector) becomes,

$$z = z_o - \frac{4GDM}{c^2} \cdot \frac{1}{(z_o)^*} \cdot \qquad \text{(II-3)}$$

Owing to the complete spherical symmetry in this case, only one of the two orthogonal components of z and z_o need to be considered insofar as source-image separations are concerned. Taking the imaginary components (i.e., letting $z_o \to i \cdot y_o$ and $z \to i \cdot y$), Equation II-3 can be written as $y = y_o - \chi^2/y_o$, where $\chi^2 = 4GDM/c^2$ and has the dimensions of length squared. For a given source displacement (y), there exists two real solutions for y_o, each root corresponding to an image. In fact, the image positions can be written as,

$$y_o^{\pm} = \tfrac{1}{2} \cdot \left[y \pm \sqrt{y^2 + 4\chi^2} \right],$$

where the superscripts (+ and -) refer to the "primary" and "secondary" images, respectively. As a convenient point of reference, we shall take $y \geq 0$, so that $y^+ \geq 0$ and $y^- \leq 0$.

Now, from an observational point of view, relative angular distances are usually more accessible than actual linear distances. Letting $\phi_d{}^+$ and $\phi_d{}^-$ denote the apparent angular separations between the deflector and the primary and secondary images, respectively, then we can write $\phi_d{}^\pm \simeq \pm\, y_o{}^\pm/D_d$ (see Figure 2-2), so that the angular separation of the images is $\phi_d = \phi_d{}^+ + \phi_d{}^- \simeq (y_o{}^+ - y_o{}^-)/D_d$. In terms of the source position (y), this relation becomes

$$\phi_d{}^2 \simeq \frac{y^2 + 4\cdot\chi^2}{D_d{}^2} \,. \qquad \text{(II-4)}$$

Likewise, the observation of imaging intensifications is made more convenient by comparing the relative intensifications of the images. Denoting (R) as the ratio of the light intensity (or flux ratio) of the primary and secondary images, we have $R = -AMP^+/AMP^-$, where the minus sign is used to make R positive, since the two images are inverted in a geometrical sense. Using the above expressions for the general amplification factors given by B and K, this quantity can be written as

$$R = \frac{|F^-|^2 - \Gamma^2}{\Gamma^2 - |F^+|^2} \,.$$

For point-mass deflectors, the scattering function, $I = M/z_o$, is analytic in the complex variable z_o, so that, $\frac{\partial I}{\partial x_o} = -i \cdot \frac{\partial I}{\partial y_o}$. Thus the functions F and Γ simplify to $\Gamma^\pm = 1$ and $F^\pm = \chi^2/(y_o{}^\pm)^2$, so that we have, $R \simeq \frac{(\chi/y_o{}^-)^4 - 1}{1 - (\chi/y_o{}^+)^4}$. Upon consideration of the above

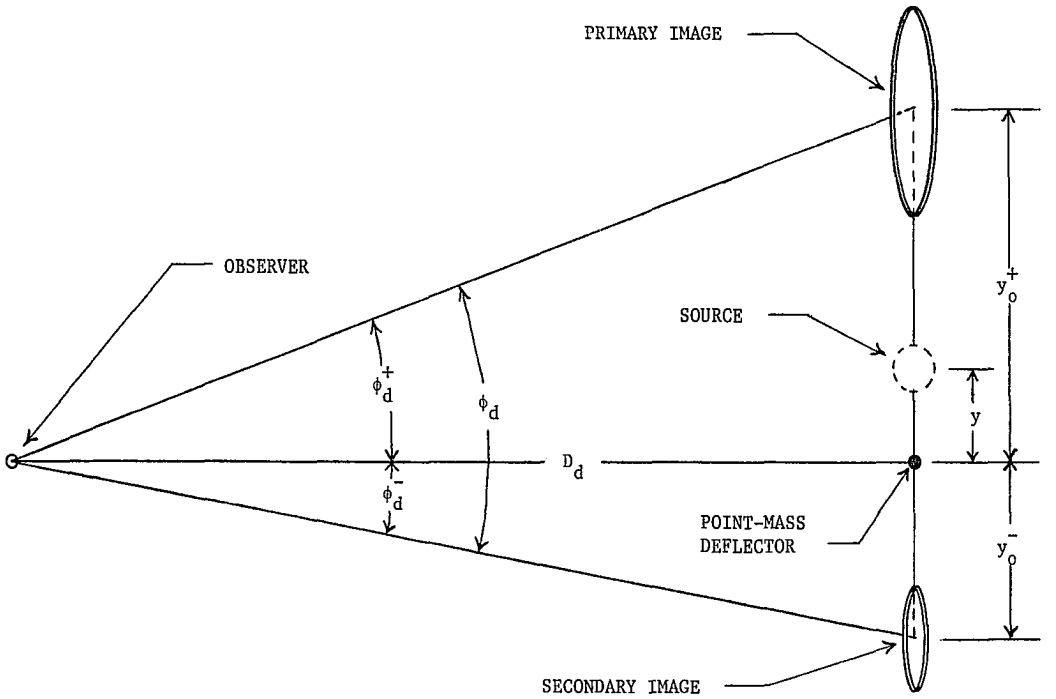

FIGURE 2-2: Gravitational images of a circularly shaped source projected onto the plane of a point-mass deflector

expression for $y_o^{\pm}$, the useful identity, $y_o^+ \cdot y_o^- = -\chi^2$, can be used to eliminate one of the image position roots (for example, y_o^-), and thus obtain $\sqrt{R} = (y_o^+)^2/\chi^2$, or again in terms of y as

$$\sqrt{R} = \frac{1}{2\cdot\chi^2} \cdot \left[y^2 + 2\chi^2 + y \cdot \sqrt{y^2 + 4\cdot\chi^2} \right] . \qquad \text{(II-5)}$$

Now, eliminating the source position, y, (which is not a directly observable quantity) from Equation II-4 and II-5, the following relation between the two observable quantities, ϕ_d and R can be obtained:

$$\phi_d^2 = \frac{(1 + \sqrt{R})^2}{\sqrt{R}} \cdot \frac{\chi^2}{D_d^2} \qquad \text{(II-6)}$$

Also, in the case that both the primary and secondary images may be observed separately, their apparent angular separations from the deflector can be simply expressed as

$$\phi_d^+ = \left(\frac{R}{1+\sqrt{R}}\right) \cdot \phi_d \quad \text{and} \quad \phi_d^- = \left(\frac{1}{1+\sqrt{R}}\right) \cdot \phi_d \ .$$

Here, it may be noted that as $R \to 1$ (equal intensity images), $\phi_d^+ \simeq \phi_d^- \to \phi_d/2$ (equally separated images), while as $R \to \infty$ (essentially primary imaging), it can be seen that $\phi_d^+ \to \phi_d$ and $\phi_d^- \to 0$ (the primary and secondary images become congruent to the source and deflector, respectively). In Figure 2-2, a flux ratio of 4 has been used, hence $\phi_d^+ = 2/3 \cdot \phi_d$ and $\phi_d^- = 1/3 \cdot \phi_d$.

Regarding the shapes of the images due to a simple point-mass deflector, we consider a circular source of radius (r) centered at a projected distance (h) from the deflector. The exact shapes can then be calculated as described above using Equation II-3. As an illustration, Figures 2-3 through 2-5 show a sequence of images of a circular

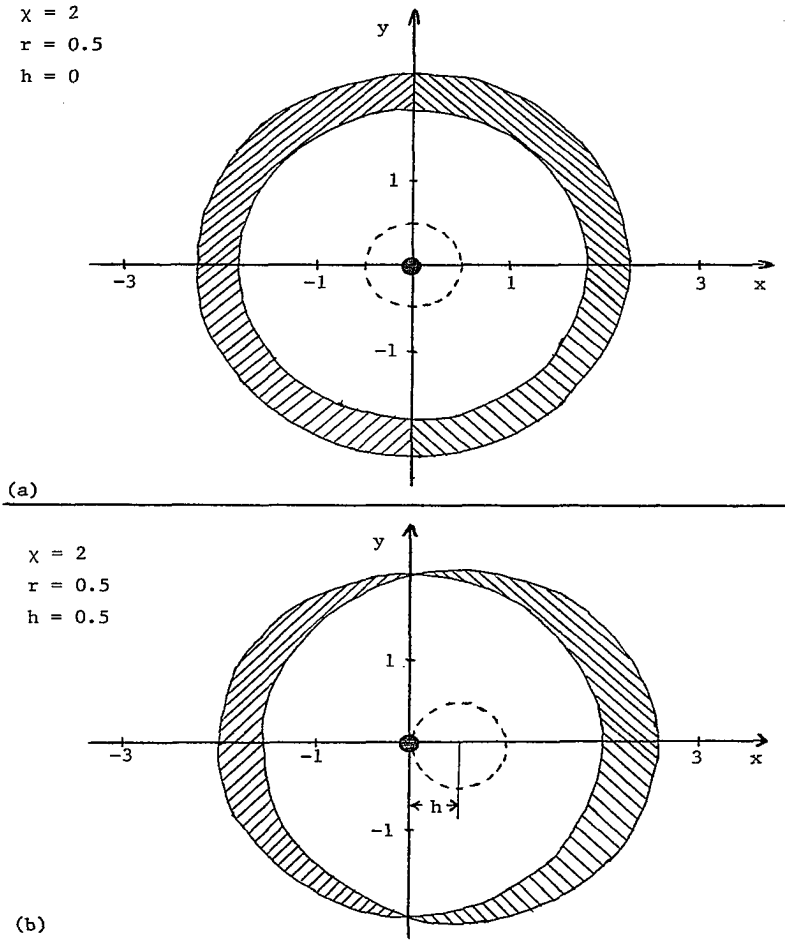

FIGURE 2-3: Image shapes of a circular source of radius r (dashed circle), due to a point-mass deflector (solid circle) which is, (a) "exactly" centered over the source, (b) "nearly" centered over the source

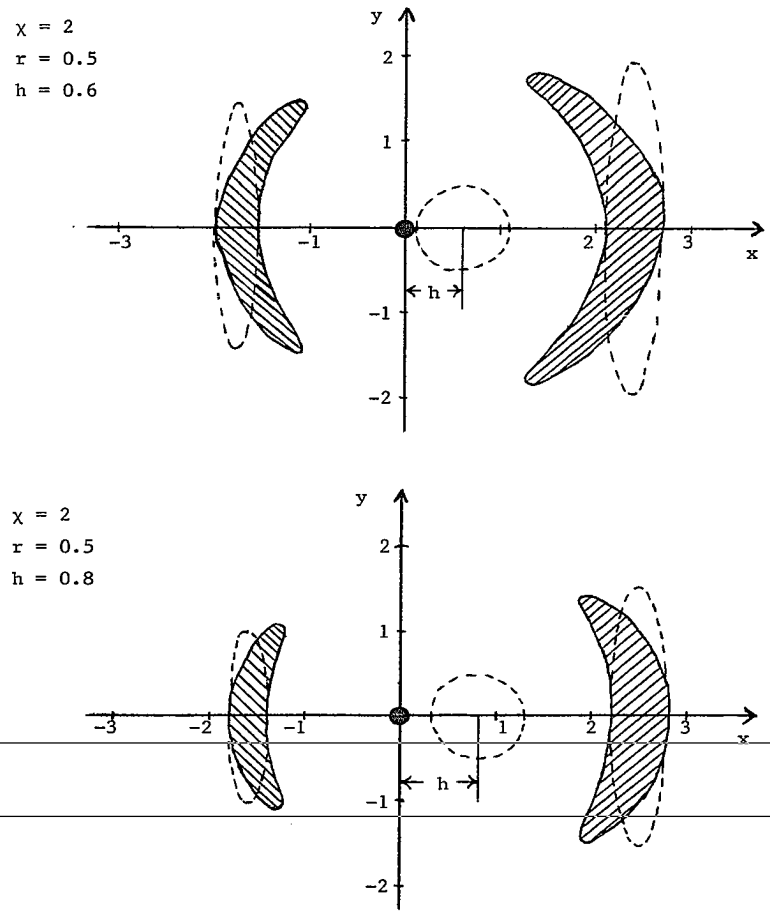

FIGURE 2-4: Image shapes of a circular source of radius r (dashed circle), due to a point-mass deflector positioned at a distance (h) from the source. The "image-ellipse approximations" are shown by the dashed curves.

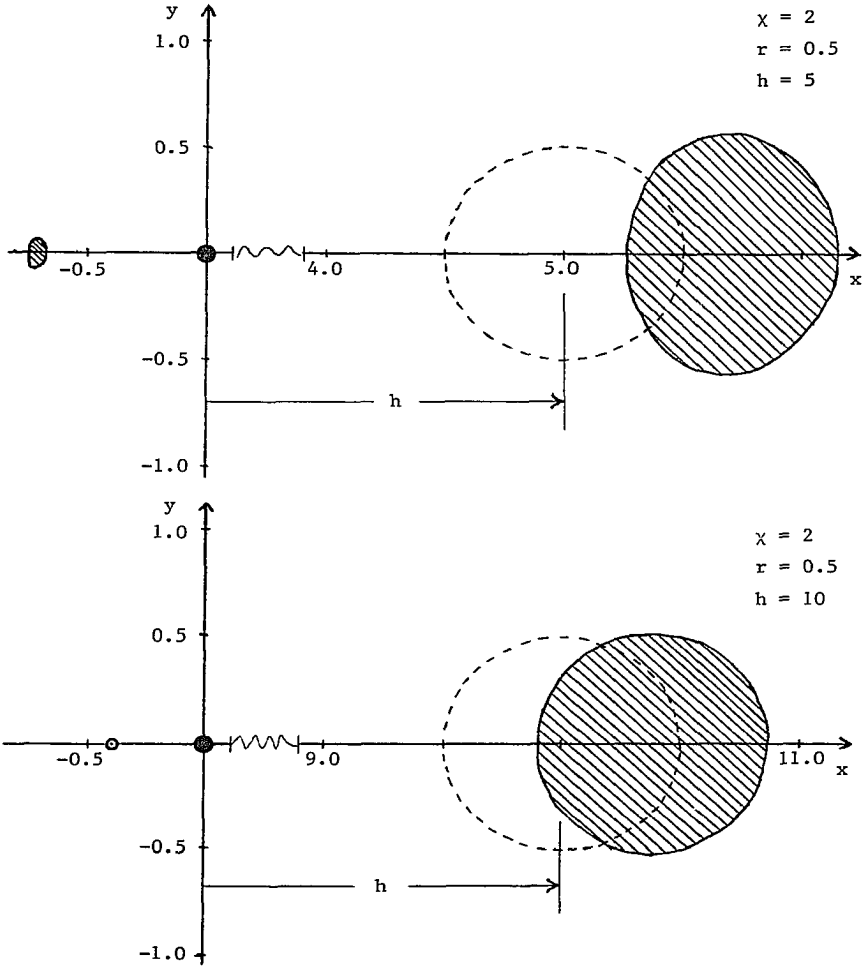

FIGURE 2-5: Image shapes of a circular source of radius r (dashed circle), due to a point-mass deflector which is "off-centered" from the source. The "image-ellipse approximations" are arbitrarily close to the actual shapes.

source, as the source position (h) is varied, keeping the parameter (χ) and the projected source radius (r) fixed. ($\chi = 2$ and $r = 0.5$), here for illustration purposes only). When the source is "exactly" centered, the images form a circular ring of width,

$$w = \tfrac{1}{2}\cdot\left[r + \sqrt{r^2 + 4\cdot\chi^2}\right] - \chi \ .$$

As the source is gradually moved from behind the deflector, the ring decomposes into two crescent shaped images, with the primary image approaching the size and position of the source, while the secondary image rapidly shrinks to a point centered on the deflector. Although the equations for these crescent shaped curves are very unwieldy, the geometrical center of each crescent ($h_o^{\pm}$) is still given by the simple equation,

$$h_o^{\pm} = \tfrac{1}{2}\cdot\left[h \pm \sqrt{h^2 + 4\cdot\chi^2}\right].$$

However, as the crescents shrink, they rapidly approach perfect ellipses. The first-order shape variations given by B and K as described above are then, $\delta x_o^{\pm} = \delta x/(1-F^{\pm})$ and $\delta y_o^{\pm} = \delta y/(1+F^{\pm})$, where here $F^{\pm} = (h_o^{\pm})^2/\chi^2$. Thus, by scaling with the size of the source, r, the semi-major and semi-minor axes of the image-ellipses can be written as $a^{\pm} = (\pm r)/(1-F^{\pm})$ and $b^{\pm} = (\pm r)/(1+F^{\pm})$, respectively. These image-ellipse approximations are compared to the actual image shapes in Figures 2-3 through 2-5.

Before turning to the more observational aspects, it should be noted that there is another interesting consequence of the gravitational imaging theory. Owing to the difference in the photons' path lengths

of the primary and secondary images, the observer will see a "time delay" of the arrival times of the radiation from the images. Thus, if any variation of the radiation field of the source exists, one may be expected to observe a similarly delayed variation in its images. Such time delays have been computed previously[16] by considering the geometrical differences in the optical path lengths. However, Cooke and Kantowski[17] have recently shown that a significant contribution to the time delays arises from the presence of a "gravitational potential well" due to the mass deflector. These latter writers have developed a general theory of gravitational image time delays, which is congruent to the B and K Formulation as described above. They write the total time delay, $(\Delta t)_{tot}$, as the sum of two terms; the usual geometrical term, Δt_g, and the gravitational potential term, Δt_p. That is, $(\Delta t)_{tot} = \Delta t_g + \Delta t_p$. In the limit of the point-mass deflector, using the quantities ϕ_d and R, these two terms can be expressed as,

$$\Delta t_g = \frac{(1 + z_d)}{2 \cdot c \cdot \mathfrak{D}} \cdot \left(\frac{\sqrt{R} - 1}{\sqrt{R} + 1}\right) \cdot \phi_d{}^2 , \qquad \text{(II-7)}$$

and

$$\Delta t_p = \frac{4 \cdot G}{c^3} \cdot M \cdot \ln(\sqrt{R}), \qquad \text{(II-8)}$$

where (z_d) is the cosmological redshift of the deflector, $\mathfrak{D} = D_{ds}/(D_s \cdot D_d)$, and all the other symbols are as previously defined.

---

[16] J. R. Gott and J. E. Gunn, Astrophysical Journal (Letters), Vol. 190, (1974), p. L105.

[17] J. H. Cooke and R. Kantowski, Astrophysical Journal (Letters), Vol. 195, (1975), p. L11.

CHAPTER III

THE OBSERVATIONAL DATA AND THE RADIO IMAGING CRITERIA

Selection of the Appropriate Types of Sources

From the theoretical work set forth in the previous chapter, one can see that even for suitably alined sources and very massive lenses, the observed angular separations of gravitational images should be at most a few seconds of arc, and most probably on the order of fractions of arc-seconds. For example, a compact source with a cosmological redshift of $z_s \sim 2$ situated almost directly behind a massive ($M \sim 10^{13}\ m_\odot$) concentrated galaxy deflector at a redshift, $z_d \simeq \frac{1}{2}$, would produce images with an angular separation, $\phi_d \sim 6"$, while if the galaxy's mass were reduced to $\sim 10^{10}\ m_\odot$, then the image separation would decrease to about $\frac{1}{2}"$ (assuming a flux ratio, $R \sim 4$, and a simple cosmology with $H_o = 50$ (Km/Sec)/Mpc and $q_o = 0$). For worse source deflector distances and alinements, the flux ratio of the images would tend to be much larger (i.e., weaker secondary images).

In view of the above considerations, if one wishes to observe the gravitational lens effect using the present technological techniques, sources must be restricted to those whose radiation fields can be measured with high sensitivity and whose internal structures can be determined down to a scale on the order of 0.001" to 0.1". Additionally, one seeks sources which are reasonably compact, so as not to substantially

deviate from the simple imaging theory presented here. Finally, sources must be sought whose distances are known, or are at least derivable, and which are sufficiently far away to allow for a reasonable probability of chance alinements of intervening galaxy-lenses. Such sources meeting the above properties nicely include the radio emitting quasistellar objects and N-galaxies, whose radio spectra and structures, as well as optical redshifts, have been determined. The former class of radio sources, QSS's, are particularly good candidates to search for gravitational imaging, because of their large redshifts (i.e., $z_s \sim 0.5$ to 3.0) and a wealthy collection of radio astronomical data obtained over the past decade.

Description of the Present Types of Radio-Quasar Data

In order to utilize to the fullest extent the present published data on radio emitting quasars in the search for gravitational imaging, one must consider carefully the various types of techniques used in deriving the internal structures of radio sources and must reconcile any ambiguous interpretations therein. Most of these observational techniques are a modification or blend of the following:

1. Single-antenna radio telescopes
2. Radio interferometers
3. Lunar occultation observations
4. Interplanetary scintillation observations

The single-antenna radio telescopes are the most fundamental of the observing instruments, and as such provide the least ambiguous

information about radio sources. They are, however, limited in their power of resolution (typically on the order of 10"). Since the majority of QSS's lie beneath this resolution limit, single-antenna radio telescopes alone are not usually adequate to determine their detailed internal structure. These fundamental instruments are, of course, very useful in determining the sky positions of QSS's and, hence, in their identifications with the associated optical objects. In addition, they are very well suited for conducting large-scale sky surveys and for obtaining the "overall" sizes of QSS's. With the aid of many recent technological improvements, single-antenna radio telescopes are becoming increasingly important in the determination of accurate radio intensities of QSS's at several observational frequencies. This latter property has allowed for an increase in the knowledge of the "overall" source spectra of QSS's at radio wavelengths and has added yet another link in the chain of strange properties associated with quasistellar objects (one such peculiar property being that most QSS's appear to have a dominant "non-thermal" component in their radio spectra).

The most directly measurable quantity from single-antenna radio telescopes is the spectral flux density, S_ν, (i.e., the received radiation power per unit area per unit frequency range), which is usually given the specific MKS unit, Jansky (Jy), which is defined as, Jy ~ 10^{-26} watts/m^2/Hz. Typical spectral flux densities for QSS's range from 0.1 Jy to 10 Jy at a frequency (ν) around 1,000 MHz. The "overall" radio spectra of many QSS's can be approximated quite well

over a broad frequency range (100 MHz to 8,000 MHz) by a simple power law of the form, $S_\nu = K \cdot \nu^\alpha$, where K and α are constants (referred to as the "spectral constant" and the "spectral index," respectively) and where for typical QSS's α = -0.1 to -2.0, which is in contrast to "black body" radiators whose spectral index is positive over the same frequency range. However, as if to add to their long list of peculiarities, some QSS's exhibit radio spectra which substantially deviate from such a simple power law, having "low-frequency cutoffs" (around 100 MHz) and "high-frequency upturns" (around 7,000 to 8,000 MHz). As a matter of illustration, a few QSS's exhibiting some of the more distinctive types of radio spectra are indicated in Figure 3-1.

In contrast to single-antenna radio telescopes, "radio interferometers" are capable of much higher resolutions, and as such are more suitable for studying the detailed structures of radio sources. In point of fact, some rather recent intercontinental baseline interferometer systems, such as that between the Owens Valley Radio Observatory of California and the Parkes Radio Observatory in Australia[18] have achieved useful resolutions down to 0.0005". The price one has to pay for this great increase of resolution is a considerable amount of ambiguity in the interpretation of the data, as well as a great reduction in the ability to observe many sources at differing frequencies. The ambiguities in the derived source structures arise in part because of the difficulty in preserving the "relative phases" of the interference

---

[18]K. I. Kellermann, et.al., Astrophysical Journal, Vol. 169, (1971), p. 1.

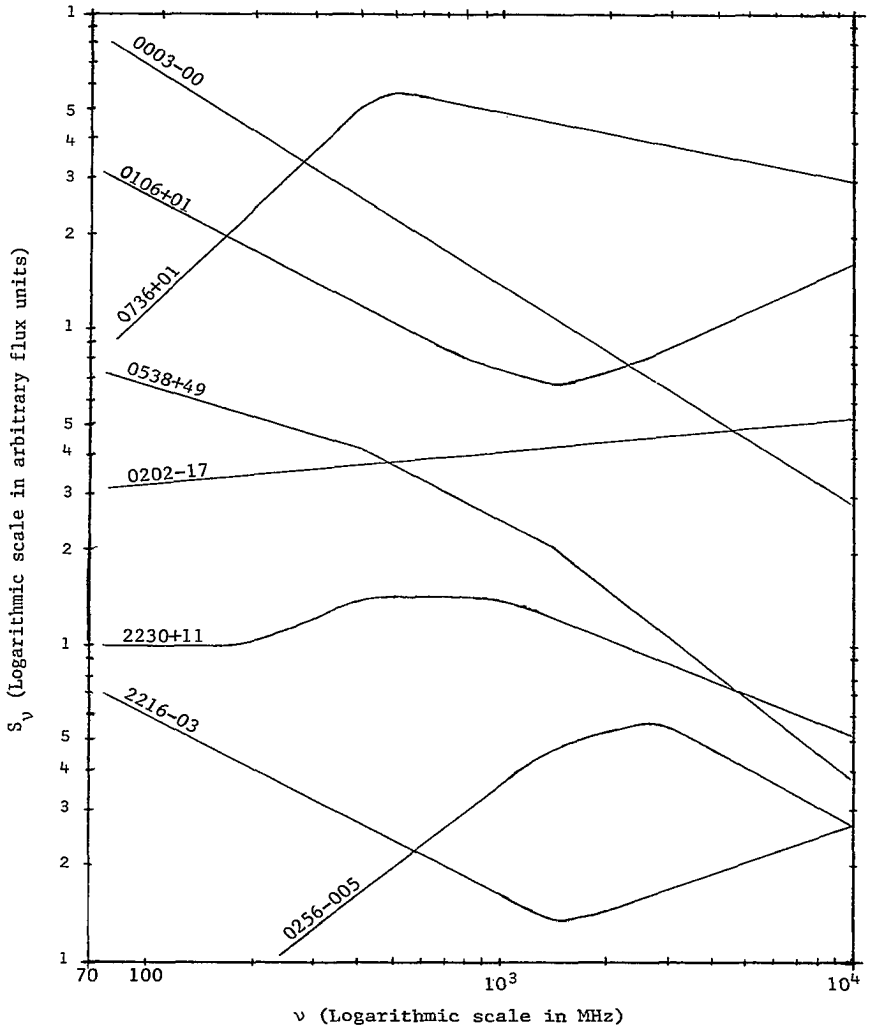

FIGURE 3-1: Sketch of typical types of radio quasar spectra (The spectrum of each source is labeled by its PKS name.)

patterns, as well as considerable changes in the resolution due to different observing frequencies. The former difficulty can, of course, be reduced by using improvements in interferometric techniques, but with the present state of the art, the usual method employed to recover this loss of information is by using "model-fitting" techniques. In these model-fitting methods, the source structure is derived by fitting various simple structural models to the observed interference fringes (i.e., the surviving amplitudes of the interference patterns). Naturally, the accuracy of the fitted models is inversely proportional to the number of parameters used. However, with good interferometric data, one can reasonably deduce such structural parameters as: the number of components, their relative angular separations, and their relative intensities (i.e., flux ratios). Other more subtle quantities, such as component sizes, component shapes, and their relative orientations, can only be obtained with meager confidence. Figure 3-2 is an illustration of a typical radio-contour map of the radio quasar, 3C 205, derived from interferometric model-fitting of data collected by Pooley and Henbest[19] using the Cambridge 5-Km Interferometer, operating at 5,000 MHz. This particular model assumes three components (A, B, and C) with Gaussian intensity distributions. The Gaussian halfwidths (i.e., the characteristic width in which the total component intensity distribution drops by a factor of e^{-1}) are indicated for each component. Also, the orientation of each component is specified by the "position angle," PA, which is taken as the angle between its major axis and

[19]G. G. Pooley and S. N. Henbest, Monthly Notices of the Royal Astronomical Society, Vol. 169, (1974), p. 477.

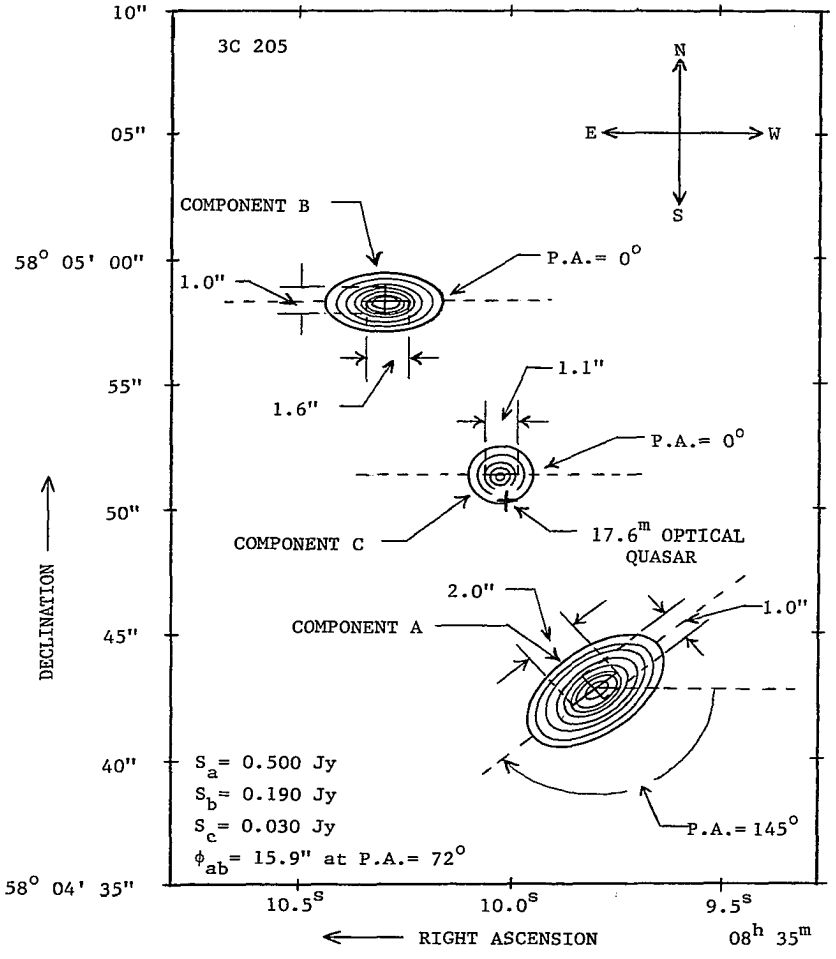

FIGURE 3-2: A typical radio-contour map of the radio quasar, 3C 205, showing the three-component model fit as described in the text (The derived component intensities and separations are shown in the lower left corner.)

the east-west direction, as measured clockwise from west to south, in the astronomical sense.

The two other principal radio astronomical techniques mentioned above, "lunar occultations" (LO) and "interplanetary scintillations of radio sources" (IPS) are rather recent in their practical use, but they have already added a nice complement to the more conventional radio telescope systems. Both of these techniques are fundamentally the same in principle, in that the former employs the diffraction of radio waves by the lunar disk, while the latter utilizes the solar plasma as the scintillating medium. In practice, however, there are some substantial differences between the two.

Lunar occultations can provide internal structures of only a limited number of radio sources, namely those which lie near the lunar ecliptic. In addition, the operating frequencies of the observing radio telescopes are restricted to a few hundred megahertz in order to avoid spurious signals arising from topographical irregularities of the lunar limb. In this last regard, the angular resolutions of the occulted source is generally limited to a few seconds of arc, especially when using single-antenna receivers[20], while somewhat better resolutions (~0.3") can be achieved with interferometers[21]. The methods used to determine the detailed source structure from lunar occultations are essentially the same as for regular interferometers,

---

[20]V. K. Kapahi, et.al., Astronomical Journal, Vol. 78, No. 8, (1973), p. 673.

[21]A. G. Lyne, Monthly Notices of the Royal Astronomical Society, Vol. 158, (1972), p. 431.

and thus the reliability of the derived structural parameters is equivalent to that of "moderately long" baseline interferometers.

Interplanetary scintillation observations, on the other hand, can cover a much larger region of the sky, owing to the larger angular extent of the interplanetary medium, but this technique is also limited to low frequencies (80 MHz to 450 MHz) due to the physical nature of the interplanetary medium[22]. This method can normally determine source structure on the scale of ½" or so[23], but because of the unknown variational nature of the solar plasma[24], only crude estimates of relative component intensities can be made. Although only crude source structures can be made at the present epoch using IPS observations, when coupled with the higher frequency observations of radio interferometers, one can obtain reasonably good knowledge of the detailed structures of radio sources, especially the radio emitting quasistellar objects.

The Radio Imaging Criteria and the Initial Selection of Image Candidates

In the search for gravitationally imaged quasars, the writer has researched the existing published data concerning the radio structure

---

[22]A. Hewish and S. J. Burnell, Monthly Notices of the Royal Astronomical Society, Vol. 150, (1970), p. 141.

[23]D. E. Harris, Astronomical Journal, Vol. 78, No. 5, (1973), p. 369.

[24]S. J. Burnell, Astronomy and Astrophysics, Vol. 16, (1972), p. 379.

of QSS's, as well as any relevant optical information, and has compiled, sorted, and evaluated, without undue bias, data of varying degrees of quality. This compiled sample consists of some 255 quasars with known redshifts. Many more quasars, or at least quasar candidates, have been cataloged. Barbieri and others[25], for example, have recently listed over 500 quasars with known redshifts. Some of these objects may actually be N-galaxies, Markarian galaxies, Seyfert galaxies, or the like, since such a clear distinction is often debatable in many cases. These sources, regardless of any subtle classifications, or even of the lack of knowledge of their physical nature, are still appropriate potential imaging candidates because of their optical compactness as well as their great distances.

Not all of the cataloged quasars are strong radio emitters (e.g., the Tonantzintla objects). These "radio quiet" or "radio weak" quasars are often found by spectroscopic analysis of certain blue stellar objects (BSO's) which appear on optical sky survey plates, but which have not been detected by any previous radio surveys covering the same general region of the sky. The researched sample contains 47 such radio quiet quasars, which represents about 18% of the total sample. These objects are not directly useful with respect to the method of approach used in this paper, but future, more intensive radio surveys may reveal some applicable information regarding gravitational imaging.

---

[25]C. Barbieri, M. Capaccioli, and M. Zanban, Memorie Della Società Astronomica Italiana, Vol. 46, No. 4, (1975), p. 461.

The statistical breakdown of the researched quasar sample is given in Table I. The radio emitting quasars classified as "single structured" are those sources in which no significant internal structuring has been observed. These systems are generally very compact (<1") in their region of radio emission, although some of these sources have not been observed in detail with high-resolution interferometers. The "multiple structured" quasars have, however, by virtue of their observed structural nature, generally been studied with quite high radio resolutions ($\lesssim$0.0001") but have not necessarily (and quite often not) been observed at more than one radio frequency. This latter situation is reflected in Table I, where 56% of the multiple structured quasars have undetermined radio spectra for their constituents.

With the observation that at least two out of every three radio quasars have two or more distinct components, one may be hastily tempted to conclude that these are gravitational images of one radio region in a manner somewhat indicative of the proposal by Barnothy and Barnothy[26] that the majority of quasars are optical effects produced by gravitational lenses. Such a high probability of observing gravitational images is not consistent with most lensing probability studies (for example, Press and Gunn[27]) and certainly is not borne out by the present observational facts, as this paper will in fact show. Granting that most of the multiple structured quasars are not gravitational images, but at the

---

[26]J. M. Barnothy and M. F. Barnothy, Astronomical Journal, Vol. 70, (1965), p. 666.

[27]W. H. Press and J. E. Gunn, Astrophysical Journal, Vol. 185, (1973), p. 397.

TABLE I

STATISTICAL BREAKDOWN OF THE STUDIED RADIO QUASAR SAMPLE

† Two or more conclusive frequency observations.

†† Component flux ratios are constant, within errors, over all observed frequencies.

TOTAL QUASAR SAMPLE 255	RADIO QUIET QUASARS 47 (18%)			
	RADIO EMITTING QUASARS 208 (82%)	SINGLE STRUCTURE 70 (34%)		
		MULTIPLE STRUCTURE 138 (66%)	UNKNOWN COMPONENT SPECTRA 78 (56%)	
			KNOWN COMPONENT SPECTRA† 60 (44%)	DIFFERENT COMPONENT SPECTRA 20 (33%)
				SIMILAR COMPONENT†† SPECTRA 40 (67%)

same time not conceding that none are, we must filter out the most likely candidates by using some appropriate selection criteria. The initial criteria, based on the "point-mass deflector" theory and its application to the observed radio quasar data, are discussed below.

Similar Radio Spectra of Components

The first main selection criterion imposed on the multiple structured radio quasars is a consequence of the frequency independence of the gravitational deflection of radiation. Thus, whatever energy spectrum the radio source may have intrinsically, if the observed components are gravitational images, then they must have similar radio spectra. This test is most easily realized by finding those sources which have components with flux ratios which are constant with respect to all observing frequencies. In order to achieve the flux ratio test reliably, one must consider the following observational restrictions:

1. With the present quality of data, we shall confine our attention to only those multiple structured sources which are clearly double structured or have a well-observed simple triple structure. Some sources are observed to consist of at least four or more distinct radio components. In order to measure the energy spectrum of each such component, several good high-resolution observations must have been made. With the present radio data, this is not usually the case.

2. For the simple double or triple component sources, one must require that at least two, and preferably more, good sets of observations at distinctly different frequencies are available.

3. The errors of estimating the flux ratio of the components must be carefully considered. Most radio frequency observations are limited in their sensitivity to about 5% to 10%, which results in flux ratio errors of 10% to 20%.

In the studied sample of radio quasars, 20 sources out of the 60 with known component spectra were found to have components with differing energy spectra (i.e., their flux ratios appeared to depend on the observing frequency). These "different component spectra" components are presented in Table II. The relevant data are entered in columns under the following format:

1. The source names (SOURCE): The first source name given is the "positional name," which is mainly the same as that listed in the "Parkes Catalogues of Radio Sources." The first four digits give the source's position of right ascension in hours and the nearest value of minutes. The following two or three digits, preceded by a (+) or (-) sign, specify the source's position of declination in degrees and the nearest one-tenth of a degree. (Some sources' names are listed with only two digits in declination because of their standardly used names in most radio catalogs.) Underneath the positional names, the other most commonly used names are listed. For example, (3C and 4C) denotes sources listed in the "Third Cambridge Radio Catalogue" and the "Fourth Revised Cambridge Radio Catalogue," respectively, (OA to OZ) denotes sources listed in the "Ohio Survey Radio Catalogue," and (NRAO) denotes source listings in the "National Radio Astronomical Observatory Catalogue of Radio Sources."

2. The optical "visual" magnitude (V) of the optical quasar object.

3. The redshift (Z) of the optical quasar.

4. A "structure code" (STR.) for the radio structure of the observed radio quasar having the following meanings:

TABLE II

DIFFERENT COMPONENT SPECTRA RADIO QUASARS

SOURCE	V	Z	STR.	COMP. FLUX RATIO	REF.	COMP. SIZE	COMP. SEP.
0106+01 4C 01.02 0C 012	18.39	2.107	D	R(2300) = 3.5 ± 0.7 R(5010) = 5.6 ± 1.2 R(7840) ≈ 9	{23} {24} {8}	θ_a = 0.0004" θ_b = 0.0008"	$\phi_{ab} \simeq 0.1"$
0152+43 NRAO 84 3C 54	15.7	1.460	D	R(151) = 3.5 ± 0.7 R(408) = 1.9 ± 0.5 R(1407) = 1.8 ± 0.4	{10} {10} {26}	θ_a = 4.6" x 2.3" θ_b = < 2" x < 2"	ϕ_{ab} = 51.4" ± 5.0"
0336-01 0E-063 CTA 26	18.41	0.852	D	R(2300) = 1.8 ± 0.3 R(5010) = 4.5 ± 0.8 R(7840) = 1.4 ± 0.3	{23} {24} {8}	$\theta_a \simeq 0.001"$ $\theta_b \simeq 0.005"$	ϕ_{ab} < 1"
0518+165 4C 16.12 3C 138	18.84	0.759	D	R(448) = 1.5 ± 0.2 R(1670) = 2.3 ± 0.4 R(2694) = 1.4 ± 0.2	{7} {24} {13}	θ_a = 0.04" θ_b = 0.30"	ϕ_{ab} = 0.38" ± 0.05"
0725+147 4C 14.24	18.92	1.382	D	R(2695) = 1.0 ± 0.1 R(5000) = 1.9 ± 0.3	{19} {30}	θ_a < 4" x < 1" θ_b = 4.1" x 2.8"	ϕ_{ab} = 5.9" ± 0.6"

TABLE II (continued)

SOURCE	V	Z	STR.	COMP. FLUX RATIO	REF.	COMP. SIZE	COMP. SEP.
0923+39 4C 39.25 OK 340 DA 267	17.86	0.698	D	R(1670) ≃ 2 R(2300) = 2.2 ± 0.3 R(5010) = 4.5 ± 0.5 R(7840) ≃ 4	{24} {23} {24} { 8 }	θ_a = 0.0007" θ_b = 0.0200"	ϕ_{ab} < 0.2"
1047+096 4C 09.37	17.85	0.786	D	R(2695) = 4.5 ± 0.5 R(8085) = 3.0 ± 0.4	{32} {32}	θ_a = 3.0" x 3.0" θ_b = 4.5" x 4.0"	ϕ_{ab} ≃ 66"
1127-145 OM-146	16.90	1.187	D	R(448) = 5.7 ± 0.6 R(1670) = 1.6 ± 0.2 R(2300) ≃ 0.2 R(5010) ≃ 0.6 R(7840) 0.8	{ 7 } {22} {23} {22} { 8 }	θ_a = 0.005" θ_b = 0.001"	ϕ_{ab} ≃ 0.03"
1222+216 4C 21.35	17.50	0.433	D	R(430) = 4.2 ± 0.5 R(2695) = 3.5 ± 0.4	{17} {27}	θ_a ≃ 2" θ_b ≃ 0.5"	ϕ_{ab} ≃ 10"
1318+113 4C 11.45	19.13	2.171	D	R(2695) = 3.4 ± 0.4 R(8085) = 4.5 ± 0.5	{32} {32}	θ_a = 1.0" x 1.0" θ_b = 2.0" x 1.0"	ϕ_{ab} = 5.3" ± 0.6"

TABLE II (continued)

SOURCE	V	Z	STR.	COMP. FLUX RATIO	REF.	COMP. SIZE	COMP. SEP.
1354+195 4C 19.44	16.02	0.720	D_1	R(2700) = 1.0 ± 0.1 R(5000) ≃ 0.4	{15} {15}	$\theta_a \simeq 10''$ $\theta_b \simeq 5''$	$\phi_{ab} \simeq 13''$
2134+004 OX 057 PHL 61	17.0	1.936	D	R(2300) = 2.1 ± 0.3 R(5010) = 3.5 ± 0.7 R(7840) = 7.5 ± 0.8	{23} {24} {8}	$\theta_a = 0.0015''$ $\theta_b = 0.0015''$	$\phi_{ab} = 0.017'' \pm 0.003''$
2145+067 4C 06.69 OX 076 DA 562	16.47	0.367	D	R(1670) = 1.3 ± 0.3 R(2300) = 1.8 ± 0.4 R(5010) = 2.1 ± 0.6 R(7840) = 4.0 ± 1.0	{24} {23} {24} {8}	$\theta_a = 0.0008''$ $\theta_b = 0.0004''$	$\phi_{ab} \simeq 0.015''$
2223-052 4C-05.92 3C 446 OY-039 NRAO 687	18.39	1.404	D	R(327) > 1 R(1666) = 1.1 ± 0.2 R(2300) = 4.1 ± 0.8 R(5010) = 2.5 ± 0.5 R(7840) = 1.3 ± 0.2	{2} {6} {23} {24} {8}	$\theta_a = 0.0004''$ $\theta_b \simeq 0.02''$	$\phi_{ab} \simeq 0.25''$

D: Indicates a simple double radio structure. Any subscripts denote which radio component has been observed to coincide with the optical object. For example, (D_1) means that the brightest radio component is coincident with the QSO, (D_2) indicates that the second most bright component coincides with the QSO, while if no subscripts are used, then either the QSO is between the radio components or the present data is insufficient to determine either case.

T: Indicates that at least three distinct radio components have been observed. Any subscripts here denote a similar meaning as that used for the D codes.

5. The component flux ratio (R): These values give the measured or derived ratio of the components' radio fluxes at the observing frequency (ν) denoted by $R(\nu)$, where ν is expressed in MHz. These flux ratios generally refer to the bright component compared to the weakest component, as observed at most frequencies, so that usually $R(\nu) \geq 1$, however, some sources have components with inverted spectra which may cause the flux ratio defined in this manner to become less than unity. Also included in this column are the estimated errors of the flux ratio.

6. Source of data (REF.): At each observing frequency, a numeric code is listed which refers to the source of information. This list of references can be found in a special section of the Literature Cited.

7. The angular sizes of the components (θ): The sizes of the components are usually the derived "Gaussian-halfwidths" (measured in seconds of arc) of the radio emitting region of each component, and the values which are given are obtained from the best resolutional observation. If the resolution and/or the accuracy of a particular observation was sufficient, then the values given are the semi-major and semi-minor dimensions of an assumed elliptical-Gaussian intensity distribution. If not, then most of the single dimensional values are assumed to be indicative of a circular-Gaussian intensity distribution. Errors in the sizes are not included but are typically on the order of 10% to 20%, or worse.

8. The angular separation of the components (ϕ): These values are generally the measured or derived angular separation (in arc-seconds) between the centers of maximum radio intensity of each component. These values are generally accurate to less than 5%, although in some cases, the only reliable measure is determined from the "Largest Angular Separation (LAS)" observed, in which case the separation values should be considered to be an upper limit.

Six radio quasars were not included in Table II because they all have been observed to have at least four components which have complex structures which vary with the observing frequencies. These sources are: 0232-04 (4C-04.06), 0734+80 (3C 184.1), 0856+17 (4C 17.46), 1226+02 (3C 273), 1253-05 (3C 279), and 2251+15 (3C 454.3).

The remaining 40 out of the 60 radio quasars with known component spectra have been classified as "similar component spectra" sources. These sources are presented in Table III, where the data format is essentially the same as Table II, with the following modifications and additions:

1. The sources are listed in order of increasing redshifts for convenience.

2. In the "structure code" column, a dagger (†) indicates that a note is made for the source. These notes, placed immediately after Table III, are used to provide clarification of the listed data, other pertinent information, and remarks concerning unusual features about the particular source, such as galaxies or other objects which have been observed to be in the "projected neighborhood" of the optical quasar.

3. In the flux ratio column, special care has been taken to present the observed flux ratios of all the observed components. The components are labeled by (a, b, and c), where component a is generally the strongest radio emitting component, component b is the next brightest, and component c (if observed) is taken to be the

weakest emitter. Thus, $R_{bc}(\nu)$, for example, means the flux ratio of component b to component c at the observing frequency (ν, in MHz). If no "component subscripts" are used, the flux ratio is assumed to be that of the only two components observed.

4. Since these sources are assumed to have constant flux ratios with respect to the observing frequencies, an average value of the flux ratio ($\bar{R}_{bc}$, for example) is computed, weighted according to the quoted errors, for the pair of components which appear to have constant flux ratios.

5. An additional quantity, the "surface brightness ratio, " Σ, (discussed as the next imaging criterion) appears as the last entry for each source.

From the results so far obtained, one sees that 40 sources out of the 130 which have known structures and component spectra apparently have similar spectra components and, thus, meet the first selection criterion for imaging. This result implies that about 31% of these sources have similar component spectra. We next consider a second radio selection criterion for gravitational imaging.

Conservation of Surface Brightness

It was pointed out in the previous chapter that surface brightness (i.e., radiation intensity per unit area) is preserved under the process of gravitational imaging. Thus, as a consequence, if a source is gravitationally imaged, the brightest image should have the largest apparent angular size. In particular, for point-mass deflectors, where the images are elliptically shaped, the apparent geometrical area of the image can be written as, AREA = $(\pi \cdot \theta_1 \cdot \theta_2)\ D_s^2$, where θ_1

TABLE III

SIMILAR COMPONENT SPECTRA RADIO QUASARS

SOURCE	V	Z	STR.	COMP. FLUX RATIO	REF.	COMP. SIZE	COMP. SEP.
1049-09 NRAO 359 3C 246	16.79	0.344	D†	R(1427) = 1.1 ± 0.2 R(2695) = 1.1 ± 0.2 $\bar{R}_{ab}$ = 1.1 ± 0.1	{16} {27}	θ_a = <40" x <30" θ_b = <40" x <30" Σ_{ab} = 1.1 ± 0.4	ϕ_{ab} = 80" ± 5"
1510-089 MSH 15-006	16.52	0.361	D	R(327) > 1 R(2300) = 1.4 ± 0.2 R(2695) = 1.6 ± 0.2 R(5010) = 1.5 ± 0.3 R(7840) < 2 $\bar{R}_{ab}$ = 1.5 ± 0.1	{2} {23} {24} {24} {8}	$\theta_a \simeq 0.005"$ $\theta_b \simeq 0.0004"$ $\Sigma_{ab} \leq 0.1$	ϕ_{ab} = 0.15" ± 0.03"
0134+32 4C 32.08 0C 358 3C 48	16.20	0.367	D†	R(408) < 9 R(448) = 4.5 ± 0.3 R(2300) < 7 $\bar{R}_{ab}$ = 4.5 ± 0.5	{1} {7} {23}	$\theta_a \simeq 0.15"$ $\theta_b \simeq 0.035"$ Σ_{ab} = 0.5 ± 0.2	ϕ_{ab} = 0.35" ± 0.07"

TABLE III (continued)

SOURCE	V	Z	STR.	COMP. FLUX RATIO	REF.	COMP. SIZE	COMP. SEP.
1704+60 4C 60.24 3C 351	15.28	0.371	D†	R(408) = 2.5 ± 0.4 R(1423) = 3.0 ± 0.5 $\bar{R}_{ab}$ = 2.7 ± 0.3	{11} {11}	θ_a = 0.9" x 0.8" θ_b = 0.5" x 0.5" Σ_{ab} = 0.9 ± 0.3	ϕ_{ab} = 5.6" ± 0.8"
1229-021 4C-02.55 ON-049	16.75	0.388	D_1	R(318) < 3.5 R(327) > 2.3 R(2695) = 2.7 ± 0.4 $\bar{R}_{ab}$ = 2.7 ± 0.5	{17} { 2 } {27}	$\theta_a \simeq$ 1.0" $\theta_b \simeq$ 0.5" Σ_{ab} = 0.7 ± 0.3	ϕ_{ab} = 8.0" ± 0.5"
0903+169 4C 16.26 3C 215 OK 106 NRAO 315	18.27	0.411	T_3†	R_{ab}(2700) = 1.3 ± 0.3 R_{ab}(5000) = 1.1 ± 0.2 R_{ac}(5000) ≃ 8 $\bar{R}_{ab}$ = 1.2 ± 0.1	{ 3 } {30}	$\theta_a \simeq$ 8" $\theta_b \simeq$ 7" Σ_{ab} = 0.9 ± 0.3	ϕ_{ab} = 28" ± 2" $\phi_{ac} \simeq$ 20"
0133+20 4C 20.07 3C 47 OC 256 CTA 14	18.10	0.425	D†	R(1407) = 1.6 ± 0.3 R(2700) = 2.0 ± 0.3 R(5000) = 2.0 ± 0.4 $\bar{R}_{ab}$ = 1.9 ± 0.3	{26} { 3 } { 3 }	θ_a = 9" x 8" θ_b = 10" x 10" Σ_{ab} = 2.6 ± 0.9	ϕ_{ab} = 65" ± 5"

TABLE III (continued)

SOURCE	V	Z	STR.	COMP. FLUX RATIO	REF.	COMP. SIZE	COMP. SEP.
2019+09	20.0	0.469	T†	R(151) = 1.8 ± 0.3	{10}	$\theta_a \simeq 7''$	$\phi_{ab} = 21.3'' \pm 0.7''$
4C 09.67				R(408) = 1.5 ± 0.2	{10}	$\theta_b \simeq 5''$	$\phi_{ac} \simeq 10''$
3C 411				$R_{ab}(5000) = 1.6 \pm 0.5$	{30}	$\theta_c \simeq 4''$	
OW 032				$R_{ac}(5000) \simeq 10$			
NRAO 627							
DA 512				$\bar{R}_{ab} = 1.5 \pm 0.2$		$\Sigma_{ab} = 0.8 \pm 0.3$	
0538+49	17.80	0.545	T†	$R_{ab}(448) = 1.9 \pm 0.5$	{7}		
4C 49.14				$R_{bc}(448) = 1.0 \pm 0.3$		$\theta_a = 0.60''$	$\phi_{ab} \simeq 0.55''$
3C 147				$R_{ab}(1670) \simeq 1$	{24}	$\theta_b = 0.04''$	$\phi_{bc} = 0.14'' \pm 0.03''$
OG 465				$R_{bc}(1670) \simeq 1$		$\theta_c = 0.04''$	
NRAO 221				$R_{ab}(2694) \simeq 0.5$			
DA 186				$R_{bc}(2694) = 1.3 \pm 0.2$	{14}		
				$\bar{R}_{bc} = 1.2 \pm 0.1$		$\Sigma_{bc} = 1.3 \pm 0.4$	
1136-13	17.8	0.554	D_1†	R(408) = 1.5 ± 0.3	{9}	$\theta_a \simeq 3''$	$\phi_{ab} = 22''$ 1''
OM-161				R(2695) = 1.5 ± 0.3	{27}	$\theta_b \simeq 3''$	
MSH 11-108				$\bar{R}_{ab} = 1.5 \pm 0.2$		$\Sigma_{ab} = 1.5 \pm 0.6$	

TABLE III (continued)

SOURCE	V	Z	STR.	COMP. FLUX RATIO	REF.	COMP. SIZE	COMP. SEP.
1618+177 4C 17.68 3C 334	16.41	0.555	D†	R(1407) = 1.3 ± 0.2 R(2695) = 1.2 ± 0.2 $\bar{R}_{ab}$ = 1.3 ± 0.1	{26} {19}	θ_a = 15" x < 15" θ_b = 15" x < 10" Σ_{ab} = 0.9 ± 0.3	ϕ_{ab} = 41" ± 2"
0349-14 3C 95 NRAO 147	16.24	0.614	D†	R(408) = 2.7 ± 0.3 R(2695) = 3.1 ± 0.4 $\bar{R}_{ab}$ = 2.9 ± 0.2	{9} {27}	θ_a = 6.5" x 4.5" θ_b = 4.0" x 1.5" Σ_{ab} = 0.7 ± 0.4	ϕ_{ab} = 22" ± 2"
1104+16 4C 16.30 OM 109	15.70	0.634	D_2†	R(318) > 3 R(2695) = 5.0 ± 0.6 R(8085) = 5.0 ± 0.5 $\bar{R}_{ab}$ = 5.0 ± 0.3	{17} {32} {32}	θ_a = 1.0" x 1.0" θ_b = 0.5" x 0.5" Σ_{ab} = 1.2 ± 0.3	ϕ_{ab} = 6.8" ± 0.5"
0838+13 4C 13.38 3C 207 OJ 163 NRAO 300 DA 255	18.15	0.684	T_2†	R_{ab}(2695) = 1.0 ± 0.2 R_{ac}(2965) ≃ 2 R_{ab}(5000) = 1.1 ± 0.2 R_{ac}(5000) ≃ 3 $\bar{R}_{ab}$ = 1.1 ± 0.1	{19} {30}	θ_a ≤ 4" θ_b ≃ 3" θ_c ≤ 3" Σ_{ab} = 0.7 ± 0.4	ϕ_{ab} = 5.5" ± 0.6" ϕ_{ac} ≃ 10"

TABLE III (continued)

SOURCE	V	Z	STR.	COMP. FLUX RATIO	REF.	COMP. SIZE	COMP. SEP.
1828+48	16.81	0.691	D†	R(408) = 2.5 ± 0.4	{11}		
4C 48.46				R(1423) = 2.9 ± 0.5	{11}	$\theta_a \simeq 0.015''$	$\phi_{ab} = 0.75'' \pm 0.10''$
3C 380				R(1670) = 2.7 ± 0.3	{24}	$\theta_b \simeq 0.002''$	
OU 447				R(2694) > 1.5	{12}		
NRAO 565				R(5010) = 2.7 ± 0.4	{24}		
DA 452				$\bar{R}_{ab} = 2.7 \pm 0.2$		$\Sigma_{ab} < 0.1$	
1111+40	17.98	0.734	$D_1^\dagger$	R(81.5) < 2	{4}	$\theta_a = 1.6'' \times < 1.3''$	$\phi_{ab} = 13.4'' \pm 0.5''$
4C 40.28				R(2695) = 1.2 ± 0.3	{5}	$\theta_b = 1.4'' \times < 1.4''$	
3C 254				R(5000) = 1.1 ± 0.2	{30}		
NRAO 369				$\bar{R}_{ab} = 1.2 \pm 0.1$		$\Sigma_{ab} = 1.1 \pm 0.4$	
0710+11	16.60	0.768	D†	R(1407) = 1.5 ± 0.2	{28}	$\theta_a \simeq 6''$	$\phi_{ab} = 46'' \pm 2''$
4C 11.26				R(2695) = 1.6 ± 0.2	{19}	$\theta_b \simeq 6''$	
3C 175							
OI 117				$\bar{R}_{ab} = 1.5 \pm 0.2$		$\Sigma_{ab} = 1.5 \pm 0.6$	
NRAO 258							

TABLE III (continued)

SOURCE	V	Z	STR.	COMP. FLUX RATIO	REF.	COMP. SIZE	COMP. SEP.
1328+307	17.25	0.849	T†	$R_{ab}(408) \simeq 2$			
4C 30.26				$R_{ac}(408) > 5$	{1}		
3C 286				$R_{ab}(448) = 2.0 \pm 0.5$		$\theta_a = 0.053"\text{x}0.026"$	$\phi_{ab} = 0.37" \pm 0.05"$
OP 348				$R_{ac}(448) \simeq 6$	{7}	$\theta_b = 0.035"\text{x}0.026"$	$\phi_{ac} \simeq 0.2"$
NRAO 425				$R_{ab}(1667) = 2.6 \pm 0.5$		$\theta_c \lesssim 0.005"$	
DA 346				$R_{ac}(1667) \simeq 7$	{6}		
LHE 348				$R_{ab}(2300) \gtrsim 2$			
CTA 60				$R_{ac}(2300) \gtrsim 7$	{23}		
				$R_{ab}(2694) = 2.0 \pm 0.3$			
				$R_{ac}(2694) \simeq 8$	{13}		
				$\overline{R}_{ab} = 2.1 \pm 0.3$		$\Sigma_{ab} = 1.4 \pm 0.5$	
0440-004	18.5	0.850	D	$R(1670) = 1.2 \pm 0.7$	{24}		
NRAO 190				$R(2300) = 1.6 \pm 0.2$	{23}	$\theta_a \simeq 0.002"$	$\phi_{ab} = 0.10" \pm 0.02"$
DA 145				$R(5010) = 1.5 \pm 0.6$	{24}	$\theta_b \simeq 0.001"$	
				$R(7840) = 1.4 \pm 0.3$	{8}		
				$\overline{R}_{ab} = 1.5 \pm 0.2$		$\Sigma_{ab} \simeq 0.4$	

TABLE III (continued)

SOURCE	V	Z	STR.	COMP. FLUX RATIO	REF.	COMP. SIZE	COMP. SEP.
0809+48	17.79	0.871	T†	$R_{ab}(408) = 1.8 \pm 0.5$	{10}		
4C 48.22				$R_{ab}(1423) = 1.6 \pm 0.4$	{11}	$\theta_a = 1.3'' \times 1.2''$	$\phi_{ab} = 5.2'' \pm 0.6''$
3C 196				$R_{ab}(2695) = 1.4 \pm 0.3$	{19}	$\theta_b = 1.2'' \times < 1.2''$	
OJ 417				$R_{ab}(5000) = 1.6 \pm 0.3$		$\theta_c \simeq 1.5''$	$\phi_{ac} \simeq 8''$
NRAO 285				$R_{ac}(5000) \simeq 6$	{30}		
DA 246				$\bar{R}_{ab} = 1.6 \pm 0.2$		$\Sigma_{ab} \lesssim 1.3$	
1055+018	18.28	0.890	D†	$R(1422) < 2$	{12}		
4C 01.28				$R(1670) = 1.2 \pm 0.3$	{24}	$\theta_a = 0.0015''$	$\phi_{ab} = 0.25'' \pm 0.05''$
OL 093				$R(2300) = 1.2 \pm 0.2$	{23}	$\theta_b = 0.0005''$	
DA 293				$R(5010) = 1.0 \pm 0.4$	{24}		
MSH 10+010				$\bar{R}_{ab} = 1.2 \pm 0.1$		$\Sigma_{ab} \lesssim 0.2$	
1458+71	16.78	0.905	D†	$R(448) = 1.5 \pm 0.3$	{ 7 }		
4C 71.15				$R(1423) = 1.2 \pm 0.4$	{11}	$\theta_a = 0.23'' \times 0.06''$	$\phi_{ab} = 0.10'' \pm 0.02''$
3C 309.1				$R(1667) \gtrsim 1$		$\theta_b = 0.13'' \times 0.04''$	
NRAO 464				$R(2694) < 2$			
				$\bar{R}_{ab} = 1.4 \pm 0.2$		$\Sigma_{ab} \lesssim 0.5$	

TABLE III (continued)

SOURCE	V	Z	STR.	COMP. FLUX RATIO	REF.	COMP. SIZE	COMP. SEP.
0420-01 OF-035	18.0	0.915 (1.740)	D†	R(1670) = 1.1 ± 0.2 R(2300) = 1.3 ± 0.2 R(5010) = 1.3 ± 0.2 $\bar{R}_{ab}$ = 1.3 ± 0.2	{24} {23} {24}	$\theta_a \simeq 0.001"$ $\theta_b = 0.0007"$ $\Sigma_{ab} = 0.6 \pm 0.4$	$\phi_{ab} = 0.10" \pm 0.02"$
1622+238 4C 23.43 3C 336 OS 238 NRAO 501	17.47	0.927	T_3†	$R_{ab}(2695) = 2.0 \pm 0.2$ $R_{ab}(5000) = 2.1 \pm 0.2$ $R_{ac}(5000) \simeq 16$ $\bar{R}_{ab} = 2.1 \pm 0.1$	{19} {30}	$\theta_a = 2.3" \times 1.9"$ $\theta_b = 2.3" \times 1.8"$ $\theta_c = 3.7" \times 1.9"$ $\Sigma_{ab} = 2.0 \pm 0.6$	$\phi_{ab} = 21.7" \pm 1.0"$ $\phi_{ac} \simeq 15"$
1340+60 4C 60.18 3C 288.1 NRAO 428	18.12	0.961	D†	R(2695) = 2.0 ± 0.2 R(5000) = 2.1 ± 0.3 $\bar{R}_{ab}$ = 2.0 ± 0.2	{19} {30}	$\theta_a = 1.3" \times < 1.3"$ $\theta_b = 1.0" \times < 1.0"$ $\Sigma_{ab} = 1.2 \pm 0.4$	$\phi_{ab} = 13.5" \pm 0.7"$
1040+12 4C 12.37 3C 245 OL 166 NRAO 358 DA 289	17.29	1.028	T_1†	$R_{ab}(408) = 1.5 \pm 0.2$ $R_{bc}(408) = 2.2 \pm 0.3$ $R_{ab}(1420) = 3.0 \pm 0.4$ $R_{bc}(1420) = 2.4 \pm 0.3$ $\bar{R}_{bc} = 2.3 \pm 0.2$	{25} {25}	$\theta_a \simeq 0.5"$ $\theta_b \simeq 3.0"$ $\theta_c \simeq 2.0$ $\Sigma_{bc} = 1.0 \pm 0.4$	$\phi_{ac} \simeq 2"$ $\phi_{bc} = 7.0" \pm 1.0"$

TABLE III (continued)

SOURCE	V	Z	STR.	COMP. FLUX RATIO	REF.	COMP. SIZE	COMP. SEP.
0003-00	19.35	1.037	$D_1^\dagger$	R(178) = 1.0 ± 0.5	{ 2 }		
4C-00.01				R(318) > 1	{17}	$\theta_a \simeq 0.7''$	$\phi_{ab} = 3.5'' \pm 0.5''$
3C 2				R(327) = 1.5 ± 0.5	{31}		
OB-007				R(408) = 1.5 ± 0.3	{25}	$\theta_b \simeq 0.5''$	
NRAO 6				R(430) = 1.5 ± 0.5	{ 2 }		
DA 005				R(1400) < 2	{ 5 }		
MSH 00-001				R(2695) < 6	{27}		
				$\bar{R}_{ab} = 1.5 \pm 0.3$		$\Sigma_{ab} = 0.8 \pm 0.4$	
2230+114	17.32	1.038	$D^\dagger$	R(448) = 5.7 ± 0.6	{ 7 }		
4C 11.69				R(1666) < 6	{ 6 }	$\theta_a \simeq 0.007''$	$\phi_{ab} = 0.05'' \pm 0.01''$
OY 150				R(1670) > 4	{24}		
DA 582				R(2300) = 4.5 ± 0.6	{23}	$\theta_b \simeq 0.003''$	
CTA 102				R(2695) = 5.0 ± 0.6	{12}		
				$\bar{R}_{ab} = 5.1 \pm 0.5$		$\Sigma_{ab} = 0.9 \pm 0.4$	

TABLE III (continued)

SOURCE	V	Z	STR.	COMP. FLUX RATIO	REF.	COMP. SIZE	COMP. SEP.
1328+254	17.67	1.055	T†	$R_{ab}(448) = 1.3 \pm 0.3$			
4C 25.43				$R_{bc}(448) = 1.1 \pm 0.2$	{7}	$\theta_a \simeq 0.3"$	
3C 287				$R_{ab}(1422) < 4$			$\phi_{ab} \simeq 0.5"$
OP 247				$R_{bc}(1422) \simeq 1$	{13}	$\theta_b \simeq 0.04"$	$\phi_{bc} = 0.10" \pm 0.02"$
NRAO 424				$R_{ab}(1670) \simeq 2$		$\theta_c \lesssim 0.04"$	
DA 345				$R_{bc}(1670) = 1.1 \pm 0.2$	{24}		
				$R_{ab}(2300) \simeq 4$			
				$R_{bc}(2300) \simeq 1$	{23}		
				$\bar{R}_{bc} = 1.1 \pm 0.1$		$\Sigma_{bc} = 0.9 \pm 0.3$	
0833+65	18.21	1.112	D†	$R(1407) = 1.2 \pm 0.2$	{28}	$\theta_a = 2.0"$ x < 1"	$\phi_{ab} = 31.5" \pm 0.7"$
4C 65.09				$R(2695) = 1.0 \pm 0.2$	{19}	$\theta_b = 1.5"$ x < 1"	
3C 204				$R(5000) = 1.3 \pm 0.3$	{30}		
				$\bar{R}_{ab} = 1.2 \pm 0.1$		$\Sigma_{ab} \simeq 0.9$	
1046+05	18.94	1.115	D†	$R(430) < 2$	{17}	$\theta_a \simeq 1.0"$	
4C 05.46				$R(2695) = 1.4 \pm 0.3$	{32}	$\theta_b \lesssim 1.0"$	$\phi_{ab} = 9.7" \pm 0.8"$
OL 078				$R(8085) = 1.3 \pm 0.4$	{32}		
				$\bar{R}_{ab} = 1.4 \pm 0.2$		$\Sigma_{ab} \lesssim 1.0$	

TABLE III (continued)

SOURCE	V	Z	STR.	COMP. FLUX RATIO	REF.	COMP. SIZE	COMP. SEP.
0333+32	18.3	1.258	D†	R(610) = 1.6 ± 0.4	{20}		
4C 32.14				R(1670) ≳ 1.5	{24}	θ_a = 0.020"	
OE 355				R(2300) = 1.3 ± 0.4	{23}		ϕ_{ab} ≲ 0.3"
NRAO 140				R(5010) < 2	{24}	θ_b = 0.015"	
				R(7840) = 1.6 ± 0.2	{ 8 }		
				$\bar{R}_{ab}$ = 1.6 ± 0.2		Σ_{ab} = 0.9 ± 0.3	
1206+43	18.42	1.400	T_1†	R_{ab}(2695) = 4.2 ± 0.6	{19}	θ_a = 1.8" x 1.2"	ϕ_{ab} = 9.8" ± 1.0"
4C 43.23				R_{ab}(5000) = 5.0 ± 0.7	{30}	θ_b = ≲1.4" x <1.2"	ϕ_{ac} ≃ 6"
3C 268.4				R_{ac}(5000) ≃ 10		θ_c < 1.0"	
ON 411							
NRAO 393				$\bar{R}_{ab}$ = 4.6 ± 0.4		Σ_{ab} << 3	
1611+34	17.5	1.401	D	R(1666) = 1.1 ± 0.2	{24}		
OS 319				R(2300) = 1.2 ± 0.2	{23}	θ_a ≃ 0.001"	
DA 406				R(5000) < 2	{24}		ϕ_{ab} = 0.35" ± 0.05"
LHE 403				R(7840) < 1.5	{ 8 }	θ_b ≃ 0.005"	
				$\bar{R}_{ab}$ = 1.2 ± 0.1		Σ_{ab} ≳ 25	

TABLE III (continued)

SOURCE	V	Z	STR.	COMP. FLUX RATIO	REF.	COMP. SIZE	COMP. SEP.
1416+067 4C 06.49 3C 298 0Q 027	16.79	1.439	D	$R(408) = 1.7 \pm 0.2$ $R(1422) = 1.8 \pm 0.4$ $\bar{R}_{ab} = 1.8 \pm 0.2$	{1} {12}	$\theta_a = 0.47'' \times 0.47''$ $\theta_b = 0.40'' \times 0.40''$ $\Sigma_{ab} = 1.3 \pm 0.4$	$\phi_{ab} = 1.2'' \pm 0.2''$
0835+58 4C 58.16 3C 205 NRAO 298	17.62	1.534	$T_3^{\dagger}$	$R_{ab}(408) \gtrsim 2$ $R_{ab}(2695) = 2.0 \pm 0.3$ $R_{ab}(5000) = 2.6 \pm 0.5$ $R_{ac}(5000) \simeq 15$ $\bar{R}_{ab} = 2.3 \pm 0.3$	{2} {19} {30}	$\theta_a \simeq 2.0''$ $\theta_b \simeq 1.6''$ $\theta_c < 1.0''$ $\Sigma_{ab} = 1.5 \pm 0.6$	$\phi_{ab} = 15'' \pm 2''$ $\phi_{ac} \simeq 10''$
1258+40 4C 40.32 3C 280.1 NRAO 417	19.44	1.659	$D^{\dagger}$	$R(81.5) = 1.6 \pm 0.5$ $R(2695) = 1.2 \pm 0.2$ $\bar{R}_{ab} = 1.4 \pm 0.2$	{4} {19}	$\theta_a = 4.0'' \times 2.0''$ $\theta_b = 3.5'' \times 1.5''$ $\Sigma_{ab} = 0.8 \pm 0.3$	$\phi_{ab} = 19'' \pm 2''$
1023+06 4C 06.40 3C 243 0L 040	18.3	1.699	D	$R(2695) = 1.2 \pm 0.2$ $R(8085) = 1.5 \pm 0.4$ $\bar{R}_{ab} = 1.4 \pm 0.2$	{32} {32}	$\theta_a = 5.5'' \times 1.5''$ $\theta_b = 5.5'' \times 1.5''$ $\Sigma_{ab} = 1.4 \pm 0.4$	$\phi_{ab} = 11.4'' \pm 1.0''$

TABLE III (continued)

SOURCE	V	Z	STR.	COMP. FLUX RATIO	REF.	COMP. SIZE	COMP. SEP.
0926+117 4C 11.32 OK 142	19.06	1.754	D	R(318) = 2.3 ± 0.4 R(2695) = 2.0 ± 0.3 R(8085) < 2.5	{17} {32}	$\theta_a \simeq 2.0''$ $\theta_b \simeq 0.5''$	$\phi_{ab} = 6.3'' \pm 0.5''$
				$\bar{R}_{ab} = 2.2 \pm 0.2$		$\Sigma_{ab} \lesssim 0.3$	
0017+15 4C 15.02 3C 9 OB 129	18.21	2.012	D†	R(2695) = 3.0 ± 0.4 R(5000) = 3.4 ± 0.5	{29} {30}	$\theta_a = 10'' \times < 3.2''$ $\theta_b = 8'' \times 1.6''$	$\phi_{ab} = 10'' \pm 1''$
				$\bar{R}_{ab} = 3.2 \pm 0.2$		$\Sigma_{ab} = 1.7 \pm 0.5$	

Notes to Particular Sources Listed in Table III

1049-09: Bhandari, et.al., {2}* using IPS at 327 MHz has detected some small scale substructure with ~15% of the total flux contained in a region ~0.5". The position of the radio components A and B given by Fomalont {16} and the 16.8^m optical QSO position given by Hunstead[N-14]** are:

	R. A. (1950)	DEC (1950)
Component A:	$10^h\ 49^m\ 33.0^s \pm 0.5^s$	$-9^\circ\ 2'\ 27'' \pm 6''$
Component B:	$10^h\ 48^m\ 24.0^s \pm 0.5^s$	$-9^\circ\ 1'\ 57'' \pm 6''$
Optical QSO:	$10^h\ 48^m\ 59.42^s \pm 0.01^s$	$-9^\circ\ 2'\ 13.2'' \pm 0.5''$

0134+32: The low frequency observations by Anderson and Donaldson {1} and the high frequency observations by Kellermann, et.al. {23} were essentially unresolved, but both sets of observations are consistent with a double structure with component flux ratio ~4.5 as observed by Clarke, et.al. {7} at 448 MHz using a long baseline interferometer. Optically, Kristian[N-2] observes the 16.2^m QSO to have an apparent surrounding fuzzy image, which may be the QSO envelope itself or perhaps a galaxy centered in front of the optical QSO.

*Denotes reference as cited in Table III.

**In order to facilitate easier readability of the notes, references normally listed as footnotes are listed in a special section of the Literature Cited.

1704+60: The radio components (A and B) here are subcomponents of a larger source (~58") which has been observed by Hogbaum and Carlsson {18} at 1415 MHz to consist of at least three components, the weaker component (c) having a size ~5". Their radio positions and the position of the 15.3^m QSO are:

	R. A. (1950)	DEC (1950)
Component a:	$17^h\ 4^m\ 5.60^s \pm 0.05^s$	$60^\circ\ 48'\ 51.7'' \pm 0.5''$
Component b:	$17^h\ 4^m\ 1.99^s \pm 0.05^s$	$60^\circ\ 48'\ 10.7'' \pm 0.5''$
Component c:	$17^h\ 4^m\ 1.65^s \pm 0.05^s$	$60^\circ\ 48'\ 53.2'' \pm 0.5''$
Optical QSO:	$17^h\ 4^m\ 3.39^s \pm 0.02^s$	$60^\circ\ 48'\ 31.3'' \pm 0.3''$

The compact component (c) here is probably the overall region of the two components observed by Critchley, et.al. {11}. Optically, Wyndham[N-3] has observed a faint (~20^m) stellar object about 17" north of the 15.3^m QSO, and Bahcall, et.al.[N-4] notes that the optical QSO lies about 18' from NGC 6306 and two other faint galaxies.

0901+169: Pooley and Henbest {30} using the 5-km Cambridge interferometer at 5000 MHz find this source to consist of three components, the weaker component (c) being about 10 times weaker than component A and coinciding with the 18.3^m optical QSO. The positions of these radio components and the optical position given by Hunstead[N-5] are:

	R. A. (1950)	DEC (1950)
Component A:	$9^h\ 3^m\ 43.30^s \pm 0.20^s$	$16^\circ\ 58'\ 30.0'' \pm 3.0''$
Component B:	$9^h\ 3^m\ 44.73^s \pm 0.05^s$	$16^\circ\ 58'\ 12.8'' \pm 2.0''$
Component C:	$9^h\ 3^m\ 44.11^s \pm 0.02^s$	$16^\circ\ 58'\ 16.0'' \pm 1.0''$
Optical QSO:	$9^h\ 3^m\ 44.14^s \pm 0.02^s$	$16^\circ\ 58'\ 16.1'' \pm 0.5''$

Optically, Bahcall[N-6] has observed that the QSO lies in a field of several faint galaxies and is in the direction of the cluster ZW 0909.7 + 1814 ($Z \lesssim 0.01$).

0133+20: Pooley and Henbest {30} also find this source to have sub-structure components. They find a four-component structure, components (a, b, c, and d), which have the following relative positions with respect to the brightest component (A):

	Δ(R.A.)(1950)	Δ(DEC)(1950)
Component b:	4.4" ± 0.3" W	4.7" ± 0.5" N
Component c:	30.0" ± 0.2" E	51.3" ± 0.8" S
Component d:	16.2" ± 0.2" E	19.4" ± 0.5" S

Regarding the component groups, A → a + b and B → c + d, the flux ratio, $(a + b)/(c + d) \cong 1.8$, which is consistent with the lower resolution observation at 5000 MHz by Branson, et.al. {3}.

2019+09: Pooley and Henbest {30} observe a weaker third component (C) with $R_{ac}(5000) \sim 10$, which coincides with the 20^m optical object. They also suggest that owing to an apparent "radio bridge" between components A and C that this object may be an N-galaxy rather than a QSO.

0538+49: This source has been observed to consist of three principal components with component A about 15 times larger than components B and C. The intensity of component A appears to decrease with increasing

frequencies, while the smaller and equal components B and C seem to have a constant flux ratio from 448 MHz to 2695 MHz.

1136-13: Critchley, et.al. {9} observed that the brighter radio component A coincides with the 17.8^m QSO.

1618+177: The positions of the radio components given by MacDonald, et.al. {26} and the position of the 16.4^m QSO given by Hunstead[N-7] are:

	R. A. (1950)	DEC (1950)
Component A:	$16^h\ 18^m\ 5.6^s \pm 0.2^s$	$17^\circ\ 43'\ 48'' \pm 3''$
Component B:	$16^h\ 18^m\ 7.9^s \pm 0.2^s$	$17^\circ\ 43'\ 29'' \pm 3''$
Optical QSO:	$16^h\ 18^m\ 7.33^s \pm 0.03^s$	$17^\circ\ 43'\ 29.6'' \pm 0.4''$

Optically, the QSO is near the eastern side of the Hercules Cluster of galaxies; optical center at $16^h\ 3^m$ and 17° 53' (Carr, et.al.[N-8]).

0349-14: The components A and B here are probably subcomponents of a much larger source ~110" as observed by Donaldson, et.al. {12} at 1425 MHz. The position of these components (a and b) and the position of the 16.2^m optical QSO given by Hunstead[N-9] are:

	R. A. (1950)	DEC (1950
Component a:	$3^h\ 49^m\ 17.9^s \pm 0.5^s$	$-14^\circ\ 38'\ 51'' \pm 5''$
Component b:	$3^h\ 48^m\ 53.9^s \pm 0.5^s$	$-14^\circ\ 38'\ 7'' \pm 5''$
Optical QSO:	$3^h\ 49^m\ 9.45^s \pm 0.02^s$	$-14^\circ\ 38'\ 6.4'' \pm 0.3''$

Donaldson, et.al. {12} also estimate the size of their component b as $\lesssim$35', which suggests that this component is substructured into the listed components A and B.

1104+16: Wardle and Miley [32] find this radio source to consist of at least two components. They give the following position of component B with respect to component A as:

	Δ(R.A.)(1950)	Δ(DEC)(1950)
Component B:	5.3" ± 0.5" W	4.3" ± 0.4" N

They also suggest that this weaker component (B) coincides with the 15.7^m QSO.

0838+13: This source has been observed to have a triple component structure by Pooley and Henbest [30] at 5000 MHz. Their positions of these components and the position of the 18.2^m QSO are:

	R. A. (1950)	DEC (1950)
Component A:	$8^h\ 38^m\ 2.1^s \pm 0.1^s$	$13^o\ 23'\ 5" \pm 1"$
Component B:	$8^h\ 38^m\ 1.74^s \pm 0.02^s$	$13^o\ 23'\ 5.3" \pm 0.6"$
Component C:	$8^h\ 38^m\ 1.46^s \pm 0.02^s$	$13^o\ 23'\ 6.6" \pm 0.6"$
Optical QSO:	$8^h\ 38^m\ 1.75^s \pm 0.03^s$	$13^o\ 23'\ 5.6" \pm 0.5"$

It is most likely that component B coincides with the optical QSO, with the weaker component C displaced to the east of A and B. The lower resolution observations at 2695 MHz by Hogg [19] only discern the two brightest components A and B.

1828+48: Bahcall[N-10] notes that the 16.8^m QSO lies in the general direction of the cluster ZW 1916.8 + 4855 (Zc ~ 0.01).

1111+40: The radio positions of the components as given by Pooley and Henbest {30} and the optical position of the 18.0^m QSO as given by Wyndham[N-11] are:

	R. A. (1950)	DEC (1950)
Component A:	$11^h\ 11^m\ 53.41^s \pm 0.02^s$	$40^\circ\ 53'\ 40.6'' \pm 0.3''$
Component B:	$11^h\ 11^m\ 52.29^s \pm 0.02^s$	$40^\circ\ 53'\ 44.2'' \pm 0.03''$
Optical QSO:	$11^h\ 11^m\ 53.35^s \pm 0.05^s$	$40^\circ\ 53'\ 42.0'' \pm 2.0''$

Thus, the optical QSO is probably coincident with the strong component (A). Wyndham has also observed a red galaxy (~18^m) at about 20" NE of the optical QSO, which likely is a member of the cluster ZW 1111.3 + 4051 ($0.05 \leq Zc \leq 0.10$) which is near by as noted by Bahcall[N-12].

0710+11: The positions of the radio component as given by MacKay {28} and the optical position of the 16.6^m QSO as given by Hunstead[N-13] are:

	R. A. (1950)	DEC (1950)
Component A:	$7^h\ 10^m\ 16.41^s \pm 0.10^s$	$11^\circ\ 51'\ 33'' \pm 3''$
Component B:	$7^h\ 10^m\ 13.83^s \pm 0.10^s$	$11^\circ\ 51'\ 10'' \pm 3''$
Optical QSO:	$7^h\ 10^m\ 15.35^s \pm 0.01^s$	$11^\circ\ 51'\ 24.4'' \pm 0.5''$

Wyndham[N-14] has noted two near by stellar objects: the brighter one (~15.4^m) is ~10" NE of the optical QSO, the fainter object (~17.5^m) is only about 5" East of the optical QSO.

1328+307: Clarke {7} at 448 MHz observes a weak third component (C) with the intensity of the brighter component (A) being about 7 times brighter than component C, which is ~0.005" in size and is closer to

component B than it is to component A. Anderson and Donaldson [1] observing with a lower resolution at 408 MHz find the source unresolved with an overall size of ~0.37", which is likely the maximum separation of the components A and B observed by Clarke. Optically, this 17.3^m QSO is most interesting in that Brown and Roberts[N-15] have observed a 21 cm. absorption redshift line with a redshift of 0.692, which they attribute to the presence of an intervening galaxy.

0809+48: The higher resolution observations by Pooley and Henbest [30] show this source to consist of three components with the weaker component (C) ~ 6 times weaker than component A at 5000 MHz, while the other listed observations were not able to resolve this weaker component. The positions of the radio components and the 17.8^m optical QSO are:

	R. A. (1950)	DEC (1950)
Component A:	$8^h\ 9^m\ 59.28^s \pm 0.02^s$	$48^\circ\ 22'\ 4.9" \pm 0.2"$
Component B:	$8^h\ 9^m\ 59.50^s \pm 0.02^s$	$48^\circ\ 22'\ 9.7" \pm 0.2"$
Component C:	$8^h\ 9^m\ 59.8^s \pm 0.1^s$	$48^\circ\ 22'\ 8.0" \pm 1.0"$
Optical QSO:	$8^h\ 9^m\ 59.38^s \pm 0.05^s$	$48^\circ\ 22'\ 8.0" \pm 0.5"$

It appears likely that the optical QSO is between the radio components A and B, with the weaker component (B) being slightly closer than the strong component (A). The weakest component (C) appears to be distinctly separated from the above system, and hence may not be intrinsically a part of the QSO system. Optically, Kristian[N-16] suggests that the Palomar prints show some faint luminosity (21^m–22^m) about 1.5" to 2.0" SE of the optical QSO, which if real, may well be a foreground galaxy.

1055+018: Peterson[N-17] notes that this 18.3^m QSO is in the eastern edge of the Abell Cluster 1139 (Zc = 0.0376). In particular, he notes that a bright (~14.2^m) cluster member (Zg = 0.0382) is about 5.1' from the optical QSO.

1458+71: Wyndham[N-18] notes a near by red galaxy (~16.5^m) about 36" [illegible] of the 16.8^m QSO. Burbidge, et.al.[N-19] also have noticed that the galaxy (~13.5^m), NGC 5832, (Zg = 0.0020) lies about 6.2' from the optical QSO. Both of these galaxies may well be members of a cluster near the QSO.

0420-01: MacDonald and Miley {27} using a short baseline interferometer at 2695 MHz suggest that this radio source either has a large (~30") halo or is pronouncedly radio variable at this frequency. There is also some controversy as to the value of the redshift of this 18.0^m QSO; some researchers use a value of 1.740, while others adopt a lower value of 0.915. The latter value may be an absorption-redshift of the higher redshift system.

1622+238: Pooley and Henbest {30} observed a weak third component (c) which is about 20 times weaker than component A at 5000 MHz. The positions of the radio components and the position of the 17.5^m QSO are:

	R. A. (1950)	DEC (1950)
Component A:	$16^h\ 22^m\ 32.83^s \pm 0.02^s$	$23^o\ 52'\ 13.5'' \pm 0.5''$
Component B:	$16^h\ 22^m\ 31.97^s \pm 0.02^s$	$23^o\ 51'\ 55.1'' \pm 0.5''$
Component C:	$16^h\ 22^m\ 32.3^s \pm 0.1^s$	$23^o\ 52'\ 0.0'' \pm 1.0''$
Optical QSO:	$16^h\ 22^m\ 32.45^s \pm 0.05^s$	$23^o\ 52'\ 0.7'' \pm 0.5''$

Component C appears to coincide with the optical QSO, both of which are closer to component B than to component A.

1340+60: Hogg {19} gives the position of the radio components, and Hunstead[N-20] gives the position of the 18.1^m QSO as:

	R. A. (1950)	DEC (1950)
Component A:	$13^h\ 40^m\ 29.47^s \pm 0.10^s$	$60^o\ 36'\ 48.1'' \pm 1.0''$
Component B:	$13^h\ 40^m\ 30.34^s \pm 0.10^s$	$60^o\ 36'\ 47.7'' \pm 1.0''$
Optical QSO:	$13^h\ 40^m\ 29.94^s \pm 0.01^s$	$60^o\ 36'\ 48.4'' \pm 0.1''$

Optically, Wyndham[N-21] has observed a red galaxy ($\sim 16.5^m$) about 45" W of the optical QSO. This galaxy may be a member of the near by cluster ZW 1341.0 + 5930 ($Zc \leq 0.05$) observed by Searle and Balton[N-22].

1040+12: The positions of the radio components as given by Lyne's {25} lunar occultation observations and the position of the 17.3^m QSO given by Hunstead[N-23] are:

	R. A. (1950)	DEC (1950)
Component A:	$10^h\ 40^m\ 6.05^s \pm 0.04^s$	$12^o\ 19'\ 16.0'' \pm 1.0''$
Component B:	$10^h\ 40^m\ 5.72^s \pm 0.06^s$	$12^o\ 19'\ 18.0'' \pm 1.0''$
Component C:	$10^h\ 40^m\ 6.14^s \pm 0.07^s$	$12^o\ 19'\ 15.3'' \pm 1.0''$
Optical QSO:	$10^h\ 40^m\ 6.02^s \pm 0.02^s$	$12^o\ 19'\ 15.9'' \pm 0.3''$

It is most likely that the stronger component (A) coincides with the optical QSO, both of which are between components B and C, but closer to the weaker component (C). Optically, Bahcall, et.al.[N-24] has noted that this quasar lies about 27' from the galaxy NGC 3351, which suggests that there may be another cluster member near by.

0003-00: The lunar occultation observations at 408 MHz by Lyne [25] are somewhat hard to interpret by a simple double structure, however, the quoted component sizes are consistent with both the lower and higher frequency observations. Lyne also notes the presence of a faint luminous optical jet (~21^m) on the blue plates of the Palomar Survey. This luminosity appears to extend some 4" to 8" from the 19.4^m QSO. Lyne considers the radio data to be consistent with the assumption that the weaker radio component (B) coincides with this optical jet, however, it is just as plausible, in view of the structural uncertainties, that some of the radio emissions may be from a foreground galaxy corresponding to the optical jet. Also, the present data suggests that the brighter component (A) coincides with the optical QSO. MacDonald and Miley [27] observe this source to be only partially resolved, using a lower resolution from the NRAO three-element interferometer with a baseline ~2000 m. operating at 2695 MHz. They place an upper limit on the flux ratio of the two components of about 6, however, the entire spectrum of the source is very straight with a spectral index ~-0.5 from 100 MHz to 10,000 MHz, suggesting that the flux ratio is constant (~1.5) over this frequency range.

2230+114: Hazard and Sanitt[N-25] note that this 17.3^m QSO lies about 5.1' from the galaxy NGC 7305 ($\sim 15.1^m$), which suggests that a cluster may be near by.

1328+254: This source has at least three distinct radio components. The lower resolution observations by Donaldson, et.al. {13} and Kellermann, et.al. {23} only partially resolve the two close components (B and C), but all listed observations are consistent with a source structure consisting of larger and more intense component (A) (~0.2") and two close but equal intensity (~0.1") components (B and C), which are separated from component A by ~0.5". The data also implies that while the components B and C have about a constant flux ratio (~1.1) from 448 MHz to 2300 MHz, component A gets more intense with increasing frequencies.

0833+65: Pooley and Henbest {30} observe this extended source to have at least four components which are subcomponents of the two strongest components (A and B) observed by MacKay {28} and Hogg {19}. The position of these radio components and the position of the 18.2^m QSO are:

	R. A. (1950)	DEC (1950)
Component a:	$8^h\ 33^m\ 16.01^s \pm 0.03^s$	$65^\circ\ 24'\ 6.2" \pm 0.5"$
Component b:	$8^h\ 33^m\ 20.97^s \pm 0.03^s$	$65^\circ\ 24'\ 3.1" \pm 0.5"$
Component c:	$8^h\ 33^m\ 15.37^s \pm 0.03^s$	$65^\circ\ 24'\ 5.0" \pm 0.5"$
Component d:	$8^h\ 33^m\ 18.07^s \pm 0.03^s$	$65^\circ\ 24'\ 4.1" \pm 0.5"$
Optical QSO:	$8^h\ 33^m\ 18.15^s \pm 0.01^s$	$65^\circ\ 24'\ 3.9" \pm 0.2"$

The high resolution observation is consistent with the lower resolution observations by considering the component groups: A → a + c and B → b + d. It is also likely that the weakest component, d, (~5 times weaker than component a) is coincident with the optical QSO.

1046+05: The IPS observations by Harris {17} at 430 MHz are consistent with the short baseline interferometer observations by Wardle and Miley {32} at 2695 MHz and 8085 MHz, in that more than 30% of the total flux is contained in a region $\lesssim$1.0". The relative optical and radio positions are not very well known for this source, but it seems likely that the 18.9^m QSO is about midway between the two radio components.

0333+32: The overall spectrum of this radio source is very complex, yet the flux ratio of its components is remarkably constant (~1.6) from 400 MHz to 8000 MHz.

1206+43: Pooley and Henbest {30} observe this source to consist of at least three components. The positions of the radio components and the position of the 18.4^m QSO are:

	R. A. (1950)	DEC (1950)
Component A:	$12^h\ 6^m\ 41.83^s \pm 0.02^s$	$43^\circ\ 55'\ 58.2" \pm 0.3"$
Component B:	$12^h\ 6^m\ 42.42^s \pm 0.02^s$	$43^\circ\ 56'\ 6.0" \pm 0.5"$
Component C:	$12^h\ 6^m\ 42.10^s \pm 0.02^s$	$43^\circ\ 56'\ 2.3" \pm 0.7"$
Optical QSO:	$12^h\ 6^m\ 41.98^s \pm 0.06^s$	$43^\circ\ 55'\ 59.9" \pm 0.6"$

It seems quite likely that the brighter component (A) coincides with the optical QSO. Kristian[N-26] observes several faint galaxies (~20^m) around the QSO, one which is only 2.5" S and one ($\lesssim 20^m$) some 4" E and 5" N. Kristian also suggests that these galaxies may be members of a galaxy cluster with median redshift $Z_c \sim 0.35$.

0835+58: Pooley and Henbest {30} observe this source to have a triple structure. The radio and optical positions are:

	R. A. (1950)	DEC (1950)
Component A:	$8^h\ 35^m\ 9.80^s \pm 0.02^s$	$58^\circ\ 4'\ 42.9'' \pm 0.3''$
Component B:	$8^h\ 35^m\ 10.30^s \pm 0.02^s$	$58^\circ\ 4'\ 58.4'' \pm 0.3''$
Component C:	$8^h\ 35^m\ 10.02^s \pm 0.05^s$	$58^\circ\ 4'\ 51.5'' \pm 0.5''$
Optical QSO:	$8^h\ 35^m\ 10.02^s \pm 0.02^s$	$58^\circ\ 4'\ 51.4'' \pm 0.1''$

It is most likely that the weaker component (C) coincides with the 17.6^m QSO, both of which are about midway between components A and B. The component C is about 15 times weaker than component A, which is probably why it was not also detected by the lower resolution measurements of Hogg {19} at 2695 MHz. Optically, Kristian[N-27] observes a very diffuse red stellar object ~18.2^m, perhaps a red galaxy, some 21" from the optical QSO.

1258+40: The positions of the radio components and the optical position given by Hogg {19} are:

	R. A. (1950)	DEC (1950)
Component A:	$12^h\ 58^m\ 13.05^s \pm 0.2^s$	$40^\circ\ 25'\ 18.8'' \pm 3.0''$
Component B:	$12^h\ 58^m\ 14.57^s \pm 0.2^s$	$40^\circ\ 25'\ 11.2'' \pm 3.0''$
Optical QSO:	$12^h\ 58^m\ 14.15^s \pm 0.2^s$	$40^\circ\ 25'\ 15.3'' \pm 3.0''$

It is likely that the 19.5^m QSO is about midway between components A and B. Kristian[N-28] notes several near by faint galaxies, one in particular (~18.5^m) is about 47" E and 25" S of the optical QSO.

0017+15: The radio positions as given by Pooley and Henbest {30} and the optical position of the 18.2^m QSO given by Hunstead[N-29] are:

	R. A. (1950)	DEC (1950)
Component A:	$0^h\ 17^m\ 50.13^s \pm 0.02^s$	$15^o\ 24'\ 11.2" \pm 0.5"$
Component B:	$0^h\ 17^m\ 49.71^s \pm 0.02^s$	$15^o\ 24'\ 19.3" \pm 0.5"$
Optical QSO:	$0^h\ 17^m\ 49.92^s \pm 0.02^s$	$15^o\ 24'\ 16.2" \pm 0.4"$

and θ_2 are apparent angular halfwidths of the source and D_s is apparent "angular diameter" distance to the source. It is sufficient in this case to examine the "ratio" of the surface brightness, rather than absolute values themselves. If we denote the apparent angular diameter of two images, a and b, of one object, for example, θ_{a_1} and θ_{a_2}, and θ_{b_1} and θ_{b_2}, while denoting their radiation fluxes by S_a and S_b, respectively, then we have for the ratio of their surface brightness,

$$\Sigma_{ab} = \frac{S_a}{S_b} \cdot \left(\frac{\theta_{b_1} \cdot \theta_{b_2}}{\theta_{a_1} \cdot \theta_{a_2}} \right) ,$$

and since $S_a/S_b = R_{ab}$, the flux ratio of image a to image b, we have that,

$$\Sigma_{ab} = R_{ab} \cdot \left(\frac{\theta_{b_1} \cdot \theta_{b_2}}{\theta_{a_1} \cdot \theta_{a_2}} \right) ,$$

which should be on the order of unity for real gravitational images. Thus, by knowing the flux ratio of our radio quasars as well as their apparent dimensions, in principle, a rather severe observational restriction for verifying gravitational imaging can be placed on them. In practice, however, we are just as severely limited by many observation restrictions. The following are good examples of such limitations:

1. In order to specify an "angular dimension" of a diffusely radio emitting region, one must define an appropriate observational parameter as a standard cutoff or boundary for the radiation region. This is much the same observational difficulty that optical astronomers encounter when seeking to measure an optical magnitude of a diffuse galaxy. Most radio astronomers attempt to circumvent this problem by assuming a particular type of radiation distribution (for example, a Gaussian distribution)

and measuring to the "halfwidth" of the radio region. While such assumptions on the distribution of the radiation field may seem appealing, it is just a nice assumption.

2. Even if a realistic standard measuring technique is established in defining the angular extent of a given radio region, one still has to cope with the usual sources of errors (e.g., noise, directionality, polarization, signal distortion, et cetera). In addition, the resolution of the observing equipment depends critically upon the receiving frequencies. In general, the higher-frequency observations "see" a smaller region than a comparable resolution observation at a lower frequency. Consequently, one must execute considerable caution when comparing two sets of observations made at different frequencies.

3. In most techniques used to derive the radio-structural parameters of a source, one may regard such quantities as the flux ratio and angular separation of two radio components as first-order parameters of the model-fitting method, while estimations of the angular sizes of the components themselves are more like second-order parameters of the model. This leads to very large errors (i.e., generally on the order of 15% to 20% for good data, but more like 25% to 50% in many cases).

If one takes a very conservative estimation of the errors of the quoted angular dimensions of two radio components, for example, 20%, and assuming an error in the estimated flux ratio of about 5%, then the error in estimating the surface brightness ratio (Σ-ratio) is at least ~45%. With these limitations in mind, an attempt has been made to compute the Σ-ratios for the 40 radio quasars having similar component spectra. These values are also listed in Table III.

If the Σ-ratio can be taken seriously here, it is found that five sources have $\Sigma>1$, seven sources with $\Sigma<1$, and 28 sources with $\Sigma\sim1$. This would then imply that about 70% of the sources having similar

spectra components meet the surface brightness test. We next consider the third radio selection criterion in order to filter out the best gravitational image candidates.

Maximum Angular Separations of Images

It was seen in Chapter II that in the point-mass deflector limit, the angular separation (ϕ_d) of two gravitational images should be proportional to $\sqrt{M}$, where M is the gravitational mass of the deflector. Thus, if one believes that there exists a practical upper limit to the mass of a deflecting galaxy, then one can place an upper limit on the expected angular separations of any resulting images. However, at the same time, the distance parameters involved must be considered. In order to see this more explicitly, Equation II-6 can be written as, $\phi^2 = 4G/c^2 \cdot f(R) \cdot M \cdot {}^{\circ}D$, where the subscript (d) has now been dropped on the angular separation (ϕ),

$$f(R) = \frac{(\sqrt{R} + 1)^2}{\sqrt{R}} \quad , \text{ and } \quad {}^{\circ}D = \frac{D_{ds}}{D_d \cdot D_s} \quad .$$

This last quantity, ${}^{\circ}D$, which shall be referred to as the "separation-distance parameter," has a different functional behavior as compared to the "deflection-distance parameter,"

$$D = \frac{D_d \cdot D_{ds}}{D_s} \quad ,$$

which was introduced in Chapter II. These two parameters have the following functional characteristics:

1. As $D_d \to D_s$, ${}^{q}D \to 0$ as does D.

2. As $D_d \to 0$, ${}^{q}D \to \infty$, but $D \to 0$.

3. The parameter ${}^{q}D(Z_d,Z_s)$ has no extremum in the variables Z_d and Z_s, while the parameter $D(Z_d,Z_s)$ has a "maximum" at some deflector redshift (Z_d), denoted by $(Z_d)_{max}$, for a fixed value of the source redshift (Z_s) and specified cosmological deceleration parameter, q_o (see, for example, Appendix A).

The fact that ${}^{q}D \to \infty$ as $D_d \to 0$ (i.e., as $Z_d \to 0$) is a simple consequence that if a finite deflector mass is brought sufficiently close to the observer, one would observe a large angular separation of the images of a distant source behind the deflector. However, at the same time, the flux ratio of the images would rapidly increase (i.e., one would not likely be able to observe such a situation). Although the parameter ${}^{q}D\{(Z_d)_{max},Z_s\}$ is not a true maximum, as is $D\{(Z_d)_{max},Z_s\}$, it is indicative of an "optimum" value.

In order to facilitate such a "maximum separation test" (or in this sense an "optimum separation test") on our sample of image candidates, the sources may conveniently be divided into two groups, according to their observed angular separations. Somewhat arbitrarily, the first group shall be denoted as the "extended sources," taking this to mean those sources whose angular separations of their radio components are greater than one second of arc. The remaining sources will then be denoted as the "compact sources." The compact class, with separations $\lesssim 1"$, do not require very massive deflectors (i.e., $\lesssim 10^{11}\ m_\odot$). For the extended group, we shall adopt an upper limit for the mass of the deflector of about $10^{13}\ m_\odot$ and an upper limit to the flux ratio of

~50, since this value is well beyond the present sensitivity of the radio data. Denoting the maximum expected angular separation as ϕ_{max}, one then has $(\phi_{max})^2$ and ${}^{q_o}\mathcal{D}_{max}$, where ${}^{q_o}\mathcal{D}_{max} = {}^{q_o}\mathcal{D}_{max}\{q_o : (Z_d)_{max}, Z_s\}$ and $(Z_d)_{max} = (Z_d)_{max}(Z_s)$, for a given source redshift. It is then useful to make a simple linear plot of ϕ versus Z_s for the extended sources. Such a plot is shown in Figure 3-3. In this plot, the solid curve represents the values of ϕ_{max} as a function of Z_s, so that all the sources which lie above this curve are assumed not to satisfy our third selection criterion for imaging. The first selection criterion (the similarity of component spectra) is already included here, while the second criterion (the Σ-ratio test) is reflected here and in Figure 3-4 (which is a similar plot for the compact sources) by the following symbolism:

1. A filled triangle, (▲), indicates an estimated Σ-ratio which is significantly greater than unity.
2. A filled circle, (●), indicates that $\Sigma \sim 1$.
3. An open square, (□), indicates an Σ-ratio which is substantially less than unity.

Figure 3-3 does not contain two sources which have component separations greater than 50". These two quasars are 1049-09 (3C 246) with $\Sigma \sim 1$ and 0133+20 (3C 47) with $\Sigma > 1$. The interpretation of these results is somewhat open here, although it appears that the sources with Σ-ratios significantly greater than unity tend to be extended, and those sources with Σ-ratios less than unity tend to be compact, while the sources with Σ-ratios ~1 seem to be randomly distributed between these two classes. Whether this is a general trend or just a selection

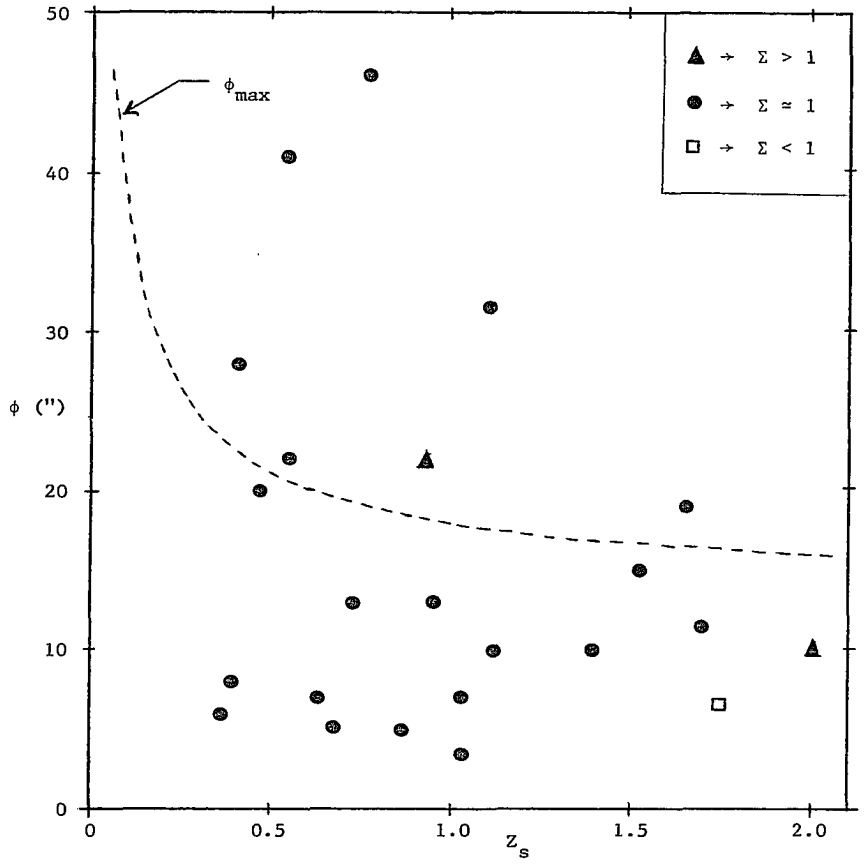

FIGURE 3-3: Plot of component angular separations, ϕ, (in arc-seconds) versus the redshifts of the sources, Z_s, for the "extended" radio quasars. The "dashed" curve represents the "ϕ_{max}" curve as discussed in the text. (The estimated values of the "Σ-ratios" are indicated by the top right legend.)

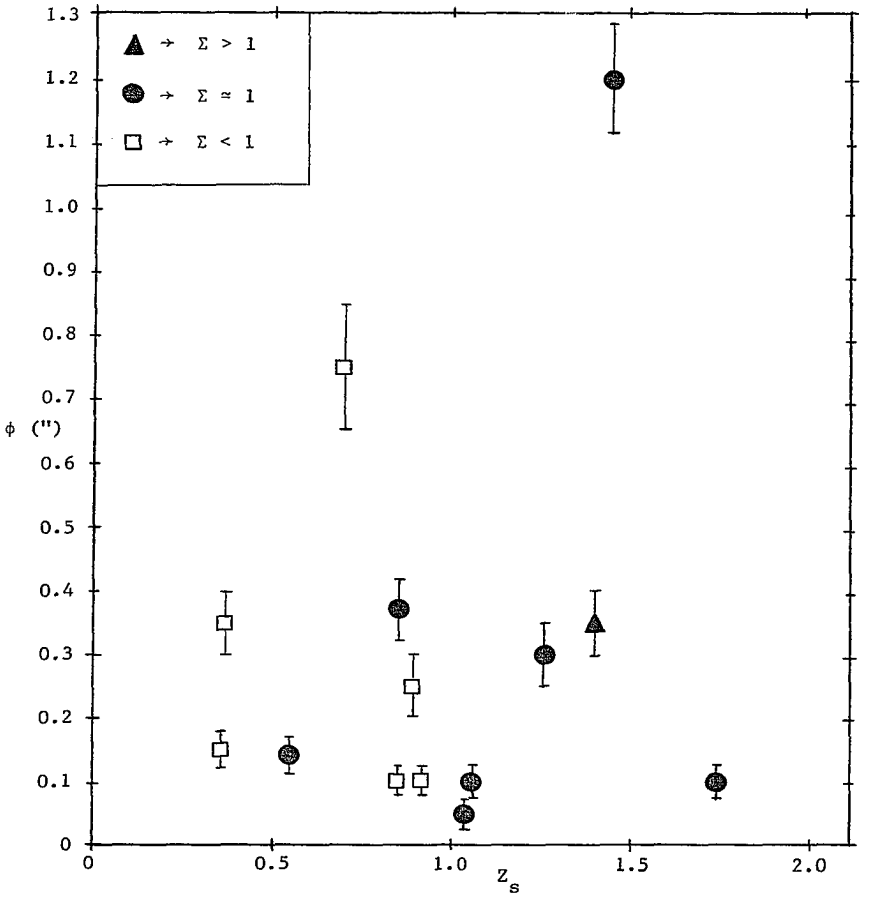

FIGURE 3-4: Plot of the component angular separations (in arc-sec. with error bars included) versus the redshifts for the "compact" radio quasars (The estimated values of the Σ-ratios are indicated by the top left legend.)

effect, one cannot at this point be sure and, thus, needs further investigations.

Applying the three main radio selection criteria, it is found that there are 21 sources which fulfill all three, which would imply a radio imaging probability of 21/130 ~ 0.16 at this point. Further restrictions can be imposed, however, by considering the optical data of the image candidates. These are discussed in the next chapter.

CHAPTER IV

FURTHER SELECTION CRITERIA AND IMAGE MODELS

In the last chapter, three main radio selection criteria were used to select the image candidates. If radio imaging is actually being observed in these sources, then there should also exist a complementary set of "optical images." In the case of the extended sources, the angular separations of these optical images should be large enough to be observed, provided that the "secondary" image is not too faint to be seen. For the compact sources, having possible image separations $\lesssim$½", any existing optical images would not likely be resolvable. In this sense, one can see that considerably more imaging restrictions can be imposed on the extended sources than on the compact sources. In the next section, these types of additional selection criteria will be discussed in order to test for gravitational imaging.

Observability of the Secondary Optical Images

First, let us consider the case where the optical quasar coincides with the brightest radio component. If such a system is suffering gravitational imaging, and if we assume that the weaker radio component is the secondary radio image, then we should expect that the "observed" optical object is the primary optical image and that the secondary optical image is coincident with the secondary radio image.

In such an imaging system, the source must consist intrinsically (i.e., in the absence of the presumed deflecting mass) of a predominantly single optical object with an associated region of radio emission. In the case of the extended quasars, which generally have component separations ~5" to 10", the question of the observability of such a secondary optical image arises. Assuming that the observed radio components are images, having a flux ratio (R), then the "optical flux ratio" of the optical images should also be of the same value. That is, in terms of an optical magnitude system, the difference between the optical magnitude of the primary (m_p) and secondary (m_s) optical images should be, $m_s - m_p \equiv \Delta m = 2.5 \cdot \log(R)$. Here, we are taking $R \geq 1$, so that $m_s \geq m_p$. Thus, for example, those sources with $R \sim 1$ might be expected to have images with approximately equal optical magnitudes. This situation is not very likely to occur, since such "double" optical quasars having the same magnitude and redshift have not as of yet been observed. However, it is an observed fact that the majority of radio quasars do not have coincident optical and radio components. This fact is evident from Table II, where all but one of the non-similar component spectra radio quasars have their associated optical object randomly distributed between or around the observed radio components. In these cases, one must exercise caution in assuming that the flux ratio of a set of optical images is the same as the corresponding radio images. We shall now consider these "non-coincident" cases, as it relates to gravitational imaging.

Let us assume that we are observing a system of real radio images having an observed angular separation (ϕ) and flux ratio (R). Then, as pointed out in Chapter II, the position of the deflector, with respect to the primary (+) and secondary (-) images, is specified by the two simple relations,

$$\phi^{+} = \left(\frac{\sqrt{R}}{\sqrt{R}+1}\right)\cdot\phi \quad \text{and} \quad \phi^{-} = \left(\frac{1}{\sqrt{R}+1}\right)\cdot\phi \ .$$

If we then denote the angular separations of the optical images by ψ, then we have a similar restriction on the relative positions of the deflector and the optical images, but in general, having a different value for the optical flux ratio, R_o,

$$(\text{e.g.,} \quad \psi^{+} = \left(\frac{\sqrt{R_o}}{\sqrt{R_o}+1}\right)\cdot\psi \quad \text{and} \quad \psi^{-} = \left(\frac{1}{\sqrt{R_o}+1}\right)\cdot\psi \ ).$$

However, the radio-image quantities ϕ and R must be related to the optical-image quantities ψ and R_o, since the same deflector mass and distance parameter must be involved. This relation can be more explicitly seen by rewriting Equation II-6 as, $M\cdot\mathfrak{D} = c^2/4G\cdot g(R)\cdot\phi^2$, where

$$g(R) = \frac{\sqrt{R}}{(\sqrt{R}+1)^2} \equiv \frac{1}{f(R)} \ .$$

Then we must have $\{M\cdot\mathfrak{D}\}(\phi,R) = \{M\cdot\mathfrak{D}\}(\psi,R_o)$, which implies that,

$$g(R_o) = g(R)\cdot\left(\frac{\phi}{\psi}\right)^2 \ .$$

From this result, one must require that $\psi \geq \phi$, in order for $R_o \geq R \geq 1$ (i.e., fainter optical images as compared to that obtained using the radio flux ratios).

From an examination of the extended sources, one finds that there are 14 sources which fulfill all three of the radio imaging criteria. Of these, there are 9 sources which have been observed to have their optical counterparts fall in between the radio components (i.e., for these sources $\psi < \phi \rightarrow R_o < R$), so these sources are probably not suitable image candidates, since the "secondary" optical image would be brighter than the observed QSO. The remaining five sources, 1704+60 (3C 351), 1229-021 (4C-02.55), 1111+40 (3C 254), 0003-00 (3C 2), and 1206+43 (3C 268.4), either have the brightest radio component coincident with the optical QSO (i.e., $\psi \simeq \phi \rightarrow R_o \simeq R$) or have an optical separation such that $\psi^+ > \phi$, so that $R_o > R$. These extended image candidates are discussed more fully in the next section.

Considering the 14 compact sources, there are 7 sources meeting the three radio imaging criteria. These compact image candidates have angular separations which are generally too small to apply the above optical test. In these cases, we must rely on the feasibility of the proposed "image models," which are discussed separately for the extended and compact candidates in the following sections.

Image Modeling Procedure

Having applied the selection criteria for imaging to the source sample, we now seek to construct plausible image models for the image candidates. We first consider the extended candidates, where we can utilize the two following modeling procedures, which are described more fully below.

1. Construction of the "deflector mass-distance curves"
2. Estimation of the deflector distance

The Deflector Mass-Distance Curves

Proceeding on the assumption that the image candidates are exhibiting radio imaging, we solve Equation II-6 for the required mass of the deflector (M), obtaining,

$$M = \frac{c^2}{4G} \cdot g(R) \cdot \phi^2 \cdot \frac{1}{\mathfrak{D}} \quad ,$$

where all quantities are as previously defined. For each source, we have the observed quantities, ϕ, R, and Z_s. Thus, by varying the redshift of the deflector (Z_d) from zero to Z_s (the source's redshift), we can find how the mass of the required deflector depends on its distance. We shall use as a distance parameter the "luminosity distance," $A_d(q_o:Z_d)$, (see Appendix A). In these models, we shall assume a simple cosmology using cosmological constants with the values, $H_o = 50$ (km/sec)/Mpc and $q_o \simeq 0$. It turns out, however, that the "separation-distance parameter," $\mathfrak{D}(q_o:Z_d,Z_s)$, is not very sensitive to an assumed value of q_o (see Appendix B). These numerical calculations involve a suitable choice of physical constants and dimensions, which are presented in Appendix C.

Estimation of the Deflector Distance

Knowledge of the deflector mass as a function of its distance allows us to estimate its mass, assuming that one can determine the

distance of the deflector. This is not a straightforward problem, since one must make quite stringent assumptions about the physical nature of the deflector itself. In this last regard, we shall assume that the required deflector is a member of a normal class of galaxies whose mass-luminosity relation is generally known. Proceeding under this type of assumption, we can then distinguish the two following cases encountered in estimating the distances of the deflecting galaxies for our image candidates.

In the first case, if we are fortunate enough to find a likely candidate for the deflecting galaxy, such as an observed optical object in the immediate neighborhood of the optical field of the quasar, then we can use its estimated optical magnitude, m_d, to estimate its mass by using the simple astronomical relation, $M = (M/L) \cdot (A_d)^2 \cdot 10^{-md/2.5} \times 10^{12}$, where $A_d(q_o:Z_d)$ is the luminosity distance of the deflecting galaxy (in Mpc) and M/L is its assumed mass-luminosity value in solar units. This equation in its present form will then give the mass of the deflecting galaxy in solar mass units ($m_\odot$), provided that we choose appropriate values for A_d, M/L, and m_d, which we shall take in most cases as the observed "photographic visual" magnitude. Since $M \propto (A_d)^2$, a plot of M versus A_d on a logarithmic scale will be a straight line with a slope of 2 and intercept which is numerically related to the assumed values of M/L and m_d. Plotted in this manner, points lying above the "luminosity lines," for given values of m_d and M/L, will reflect those deflecting galaxies which should be optically visible down to

the magnitude m_d. Also, here, both the deflecting galaxy's mass and distance will be determined by the intersection point(s) of this line and the computed "mass-distance curve" plotted on the same graph. The crucial points involved in actually carrying out this procedure are as follows:

1. The "suspect" deflector must have been observed to be reasonably positioned with respect to the optical quasar, so as to be consistent with the image formulae. That is, if we take the observed angular separation of the QSO and the suspect deflector as being the quantity, ψ^+ (i.e., assuming the QSO as the primary optical image), then we can, for example, compute the optical flux ratio between the primary and secondary optical images by the relation,

$$\sqrt{R_o} = \left(\frac{\psi^+}{\phi}\right)^2 \cdot f(R).$$

With this value of R_o, we then compute the angular separation of the deflector and secondary image (ψ^-) and thus the total angular separation of the optical images (ψ) from the simple relations,

$$\psi = \left(\frac{\sqrt{R_o} + 1}{\sqrt{R_o}}\right) \cdot \psi^+ \quad \text{and} \quad \psi^- = \left(\frac{1}{\sqrt{R_o} + 1}\right) \cdot \psi \ .$$

One can then find the relative magnitudes of such optical images from the relation, $\Delta m = 2.5 \log(R_o)$, and then determine whether or not the secondary optical image should be observed. In this latter connection, one should consider the two following cases:

   a. If $\psi^- \gtrsim 0.5"$ (i.e., above the maximum optical resolution for most optical telescopes), then the secondary image should be observable on the same plate containing the suspect deflecting galaxy, down to a particular plate limit (which is generally $\lesssim 21^m$ photographic visual).

   b. If $\psi^- \lesssim 0.5"$, then the deflecting galaxy and secondary optical image will not be resolved, thus the object actually observed will be a superposition of the two, in which case one can compute the "combined magnitude" (m_c), and by an interative

process, place a lower limit on the magnitude of the secondary optical image.

2. Caution must be applied when using the estimated magnitude of the deflecting galaxy syspect, since in many cases these are already at or near the optical plate limit. In general, one can conservatively assume an error in the quoted magnitude of around 0.5^m.

3. Assuming a value for the mass-luminosity ratio for the suspect deflecting galaxies is a somewhat uncertain aspect here. In the following image models, we shall take the following ranges of M/L values:

   a. For the irregular and spiral types of galaxies, we adopt a lower limit ~5 (Page[28]) and an upper limit ~200 (Turner and Gott[29]).

   b. For the elliptical type of galaxies, we adopt a lower limit ~20 (Noonan[30]) and a general upper limit ~200 (Avrett[31]).

   c. For those cases where the distance of the suspect deflector is estimated from an observation of a redshift system, the value of M/L is adjusted such that the deflecting galaxy just becomes visible down to the magnitude m_d at that distance.

Image Models for the Extended Sources

With the above method of attack, we shall now consider the image models of the extended class of image candidates. Each source is

---

[28]T. Page, Astrophysical Journal (Letters), Vol. 136, (1962), p. L 685.

[29]E. Turner and J. R. Gott, Astrophysical Journal, Vol. 209, (1976), p. 6.

[30]T. W. Noonan, Publications of the Astronomical Society of the Pacific, Vol. 83, (1971), p. 479.

[31]E. H. Avrett, Frontiers of Astrophysics, (Cambridge, Massachusetts: Harvard University Press, 1976), p. 510.

discussed individually below, including some short tables (Tables IV-1 through IV-3) summarizing the model parameters. The format of these tables is outlined as follows.

I. The Radio Image System

A. The observed flux ratio (R) of the radio components.

B. The relative positions of the radio images (in arc-sec.).

1. The observed angular separation (ϕ) of the radio images.

2. The computed relative positions of the deflector and the primary and secondary radio images denoted respectively by ϕ^+ and ϕ^-.

C. Distance of the radio source (assumed to be essentially the same for both the radio and optical systems). Here, (Z_S) denotes the observed redshift of the optical quasar, and (A_S) is the computed luminosity distance in Mpc (assuming $H_o = 50$ and $q_o \simeq 0$).

D. System observed?: This column always indicates a "yes," since we are assuming that the radio components are images.

II. The Optical Image System

A. The intensity parameters of the optical image system.

1. R_o: the calculated value of the optical flux ratio.

2. m_p: the photographic visual magnitude of the observed QSO, assumed to be the primary image.

3. m_s: the calculated magnitude expected for the secondary image.

B. The relative position of the optical images (in arc-sec.).

1. The calculated angular separation of the images (ψ).

2. The computed relative positions of the deflector and the primary and secondary optical images, denoted respectively by ψ^+ and ψ^-.

3. System observed?: The primary optical image is assumed to be an observed QSO. The secondary

image is generally too faint to be seen, but there may be some evidence of observability (denoted by NO?).

III. The Deflecting Galaxy

A. The observed or computed optical magnitude (m_d) of the deflecting galaxy.

B. The assumed or adjusted mass-luminosity (M/L) ratio used in the estimation of the deflector distance.

C. The computed gravitational mass of the deflecting galaxy, in solar mass ($m_\odot$).

D. The computed distance of the deflector. Here, (Z_d) denotes the computed (or observed) redshift of the deflector, and (A_d) is the resulting computed luminosity distance of the deflector. (Using $H_o = 50$ and $q_o \simeq 0$.)

E. System observed?: Those cases in which the deflector is possibly observed are denoted by (YES?). Those which are definitely observed are denoted by (YES!).

IV. The Image Time Delay

A. The "geometrical term," $(\Delta t)g$, as computed from Equation II-8, and using the assumed distance of the deflector. In some cases, an upper limit is computed; in other cases, the assumed error is taken as ~20% to 30%.

B. The "gravitational potential term," $(\Delta t)p$, as computed from Equation II-9, and using the estimated deflector mass. In the better cases, the assumed error here is taken as ~30% to 40%.

C. The "total time delay," $(\Delta t)_{tot} = (\Delta t)_g + (\Delta t)_p$. Unless stated as an upper limit, the assumed errors are taken as a weighted average of the errors of the two contributing terms.

D. Observed time delays: The notation, OV (?) and RV (?), indicates that the source has been observed to be "optically variable" and/or "radio variable," but the nature of the time variations are not clear enough to establish a "measured" time delay.

TABLE IV-1

IMAGE MODEL FOR THE EXTENDED QUASAR 1704+60 (3C 351)

SYSTEM	MEASURED/CALCULATED QUANTITIES			OBSERVED?	IMAGING STATUS
	Intensities	Positions	Distances		
RADIO	$R = 2.7 \pm 0.3$	$\phi = 5.6" \pm 0.8"$ $\phi^+ = 3.5" \pm 0.5"$ $\phi^- = 2.1" \pm 0.3"$	$Z_s = 0.371$ $A_s = 2639$ Mpc	YES	FAVORABLE
OPTICAL	$R_o \simeq 17{,}000$ $m_p = 15.3 \pm 0.1$ $m_s = 26.0 \pm 1.0$	$\psi = 36" \pm 5"$ $\psi^+ = 31" \pm 3"$ $\psi^- = 5" \pm 2"$		NO ?	
DEFLECTOR	$m_d \geq 20.5$ $M/L \simeq 150$ MASS $\lesssim 2 \times 10^{12}\ m_\odot$		$Z_d \lesssim 0.20$ $A_d \lesssim 1400$ Mpc	NO !	
TIME DELAYS	$(\Delta t)_g < 280$ Days, $(\Delta t)_p < 230$ Days $(\Delta t)_{tot} < 510$ Days			NO (not variable)	

TABLE IV-2

IMAGE MODEL FOR THE EXTENDED QUASAR 0003-00 (3C 2)

SYSTEM	MEASURED/CALCULATED QUANTITIES			OBSERVED?	IMAGING STATUS
	Intensities	Positions	Distances		
RADIO	$R = 1.5 \pm 0.3$	$\phi = 3.5" \pm 0.5"$ $\phi^+ = 1.9" \pm 0.5"$ $\phi^- = 1.6" \pm 0.4"$	$Z_s = 1.037$ $A_s = 9448$ Mpc	YES	FAVORABLE !
OPTICAL	$R_o = 1.5 \pm 0.3$ $m_p = 19.4 \pm 0.1$ $m_s = 20.0 \pm 0.3$	$\psi = 3.5" \pm 0.5"$ $\psi^+ = 1.9" \pm 0.5"$ $\psi^- = 1.6" \pm 0.4"$		YES ?	
DEFLECTOR	$m_d = 21.0 \pm 1.0$ $M/L \simeq 20$ MASS $\simeq 2.5 \times 10^{12}\ m_\odot$		$Z_d \simeq 0.633$ $A_d \simeq 5000$ Mpc	YES ?	
TIME DELAYS	$(\Delta t)_g = 180 \pm 45$ Days, $(\Delta t)_p = 115 \pm 40$ Days $(\Delta t)_{tot} = 295 \pm 60$ Days			OV (?) RV (?)	

TABLE IV-3

IMAGE MODEL FOR THE EXTENDED QUASAR 1206+43 (3C 268.4)

SYSTEM	MEASURED/CALCULATED QUANTITIES			OBSERVED?	IMAGING STATUS
	Intensities	Positions	Distances		
RADIO	$R = 4.6 \pm 0.4$	$\phi = 9.8'' \pm 1.0''$ $\phi^+ = 6.4'' \pm 0.8''$ $\phi^- = 3.4'' \pm 0.5''$	$Z_s = 1.400$ $A_s = 1.4 \times 10^4$ Mpc	YES	VERY FAVORABLE !
OPTICAL	$R_o = 4.6 \pm 0.4$ $m_p = 18.4 \pm 0.1$ $m_s = 20.1 \pm 0.4$	$\psi = 10'' \pm 1''$ $\psi^+ = 6.5'' \pm 0.7''$ $\psi^- = 3.5'' \pm 0.5''$		YES ?	
DEFLECTOR	$m_d \lesssim 20.0$ $M/L \simeq 80$ MASS $\simeq 5.0 \times 10^{12}\ m_\odot$		$Z_d \simeq 0.35$ $A_d \simeq 2400$ Mpc	YES ?	
TIME DELAYS	$(\Delta t)_g = 1463 \pm 370$ Days, $(\Delta t)_p = 868 \pm 300$ Days $(\Delta t)_{tot} = 2331 \pm 470$ Days			OV (?)	

V. Imaging Status

Each source is indicated by: "Not Favorable," "Favorable ?," "Favorable," or "Very Favorable," which is taken from the consideration of all the aspects of the imaging model.

1704+60 (3C 351)

The faint (~20^m) stellar object observed by Wyndham (see Notes to Table III) is the nearest interesting optical object to the 15.3^m QSO ($Z_s = 0.371$). From the finding chart provided by Lynds[32] this object is observed to be near the plate limit ($\leq 20.5^m$) and lies 15" N and 9" E of the QSO. Considering the optical position of the QSO and the radio position of the radio components (a and b) (see Figure 4-1), it is seen that this stellar object is some 34" away from the position of the required deflector, assuming that these radio components are images. Thus, the object is not a good suspect deflector. Without a suitably observed suspect deflector, we can maintain the assumption of gravitational imaging in the radio components here only by assuming that the deflector is below ~20.5^m (i.e., the plate limit) and placing an upper limit on its required mass and distance. This requires a M/L value ≥ 150 which places an upper limit to the deflector's mass of $\leq 2 \times 10^{12}$ $m_\odot$ placed at a distance ≤ 1400 Mpc ($Z_d \leq 0.20$) (see Figure 4-2). The QSO is also about 27" away from the nearest radio component (component a), which implies that any secondary optical image of this

[32] C. R. Lynds, et.al., Astrophysical Journal, Vol. 142, (1965), p. 1667.

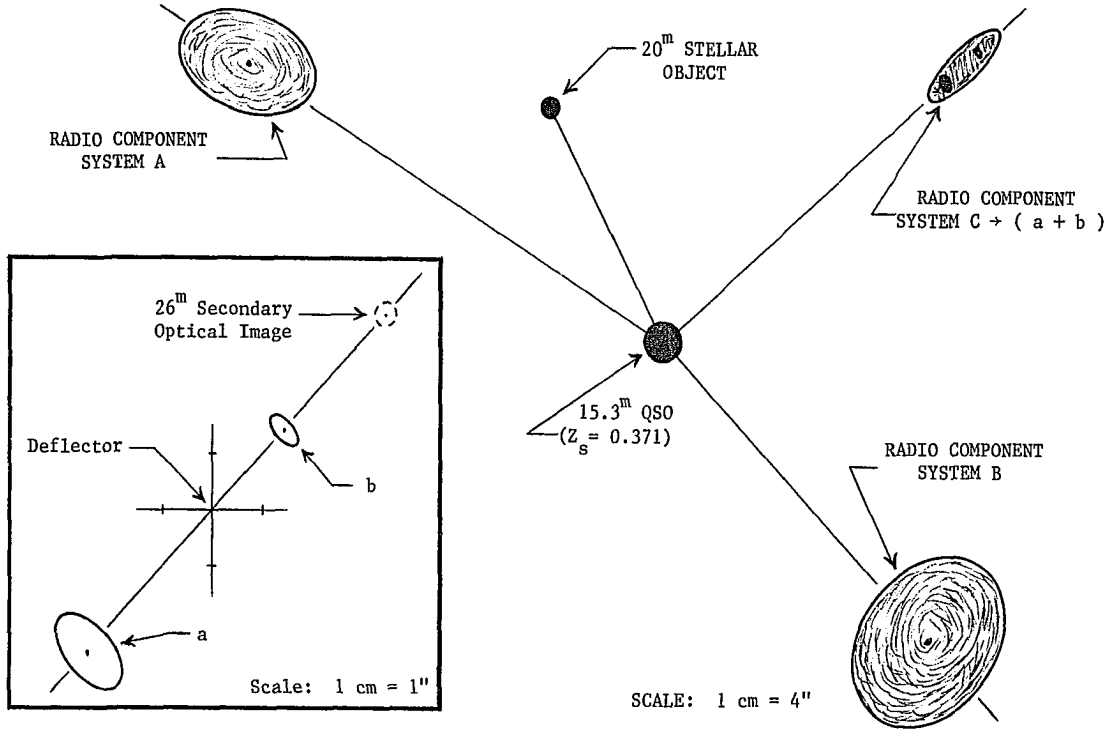

FIGURE 4-1: Positional sketch of the radio and optical systems in the quasar 1704+60 (3C 351). The insert shows an enlargement of the radio component system C, which contains the proposed radio images (a and b).

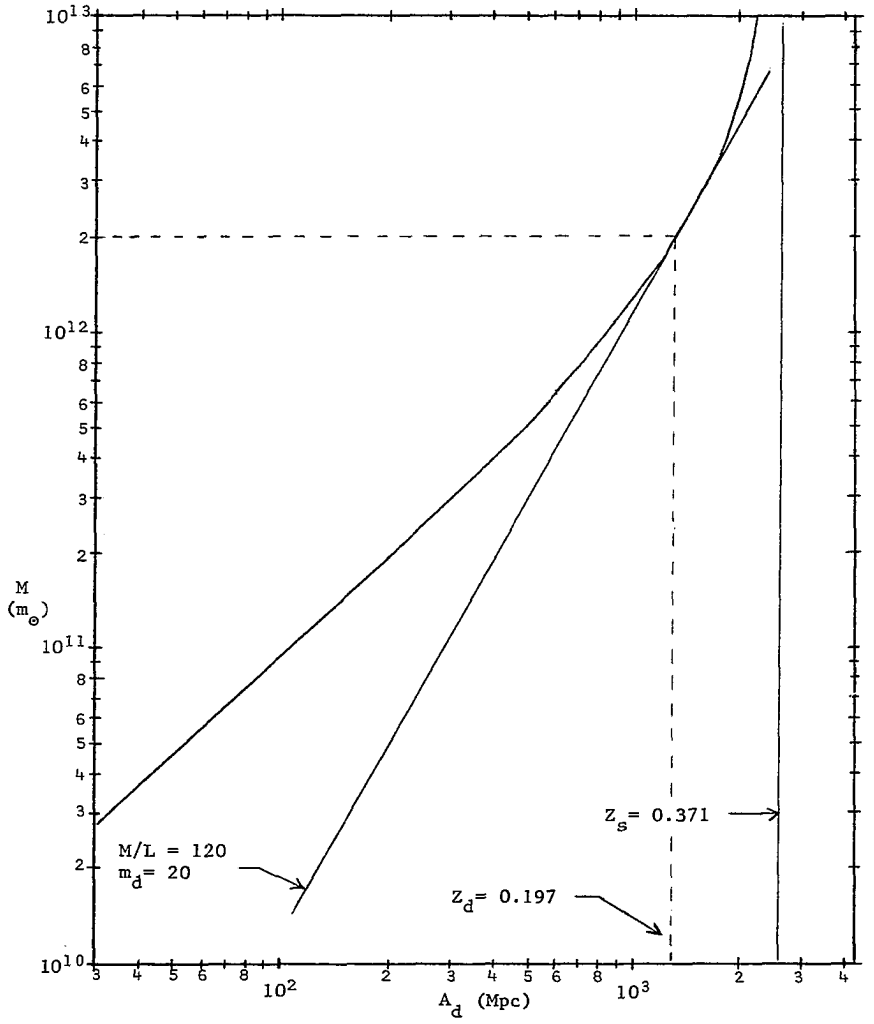

FIGURE 4-2: Logarithmic plot of the "deflector-mass" and "deflector-luminosity" curves for the image candidate 1704+60 (3C 351)

object should be $m_s = 26^m \pm 1^m$ and be about 5" ± 2" away from the required deflector. Such an optical image would not be detectable on any present optical plates. So, we conclude without further optical data that this quasar is a favorable candidate for exhibiting the gravitational lens effect.

1229-021 (4C-02.55)

The optical and radio data suggest that the brightest radio component is coincident with the 16.8^m QSO ($Z_s = 0.388$). With a flux ratio ~2.7, the magnitude of the secondary optical image (which should coincide with the weaker radio component) would be ~18^m and lie about 3" away from the required deflector. Neither the image or a suspect deflecting object is seen on the finding chart provided by Bolton and Kinman[33] (plate limit ~20^m). No image model is computed for this source since the imaging status here is very unfavorable.

1111+40 (3C 254)

This source is similar to the quasar 1229-021 in that the 18.0^m QSO ($Z_s = 0.734$) coincides with the brightest radio component. With a flux ratio ~1.2, the secondary optical image would be about 18.2^m and lie about 13" NW away from the QSO. No such object is observed on the available optical plates, although Wyndham (see Notes to Table III)

---

[33]J. G. Bolton and T. D. Kinman, Astrophysical Journal, Vol. 145, (1966), p. 951.

notes an 18^m red galaxy some 20" NE of the optical QSO. This quasar is likewise a poor candidate for gravitational imaging.

0003-00 (3C 2)

This source also has its brightest radio component coincident with the optical QSO (19.4^m, $Z_s = 1.037$). With a flux ratio ~1.5 to 1.8, the secondary image should be ~20^m and lie some 4" E of the QSO. Lyne (see Notes to Table III) observes some faint luminosity (~20^m to 21^m) extending some 4" to 8" E of the 19.4^m QSO. It would appear, in view of this information, that this luminosity may be a manifestation of both a deflecting galaxy and a secondary optical image. There is no direct indication of the distance of such a galaxy, but we can impose an upper limit by using a M/L value ~20 to obtain a distance ~5000 Mpc ($Z_d \simeq 0.63$). If this is a genuine lens system, then the upper limit to the deflector's mass is ~2.5×10^{12} $m_\odot$ (see Figure 4-3). This quasar is also noted to be both optically and radio variable, in which case one may be able to make a time delay check here, but the periodicity of these variations are not yet well established. This source is considered to be a favorable image candidate.

1206+43 (3C 268.4)

This quasar has its brightest radio component coincident with the 18.4^m QSO ($Z_s = 1.400$). Thus, taking $R_o \simeq R \simeq 4.6 \pm 0.4$, we should expect the secondary optical image to be $\gtrsim 20.1^m$ and lie some 10" NE of

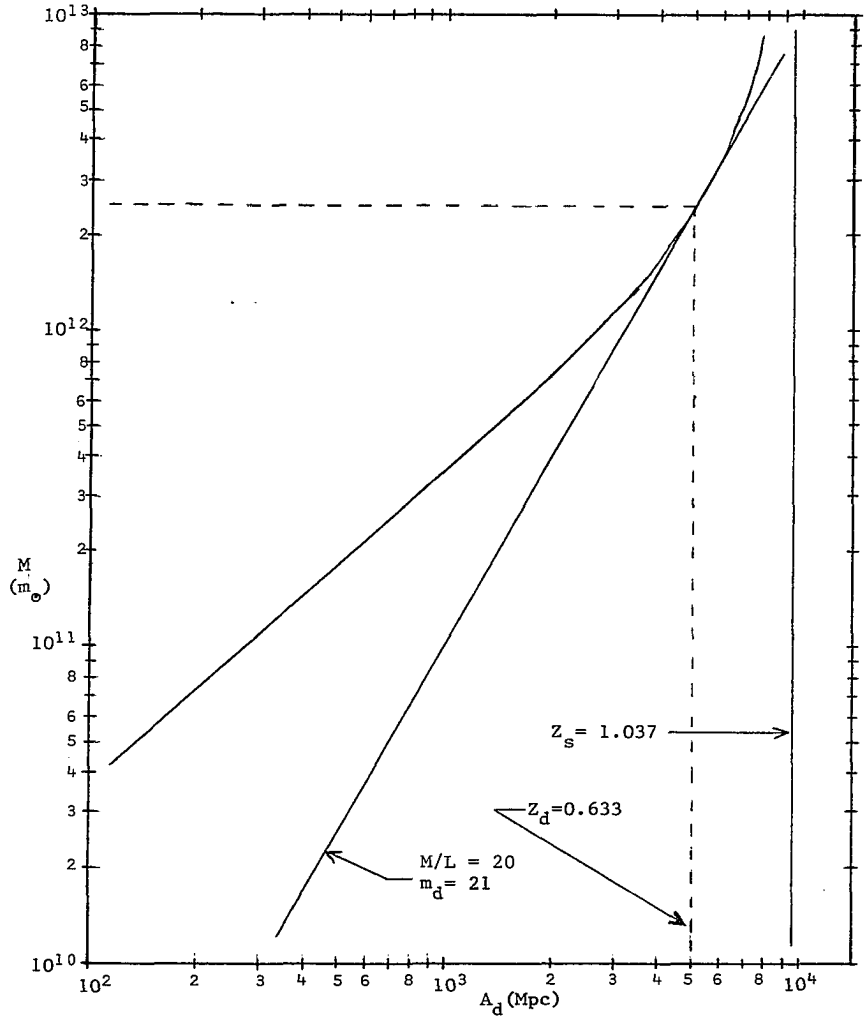

FIGURE 4-3: Logarithmic plot of the "deflector-mass" and "deflector-luminosity" curves for the image candidate 0003-00 (3C 2)

the QSO. The faint galaxy ($\lesssim 20^m$, which is near the plate limit on Wyndham's finding chart) which is about 5" N and 4" E of the QSO is positioned very favorably to be the required deflector for this system. It is also noted that the weak radio component (C) is apparently coincident with this galaxy (see Figure 4-4), thus suggesting that one may be observing radio emissions from the galaxy itself (i.e., this may be a radio galaxy). In this case, since the secondary optical image is probably $\sim 0.5^m$ below the plate limit, it is reasonable to assume that this optical image has not yet been observed. If we take the median redshift ($Z_c \sim 0.35$) of the galaxy cluster as a distance indicator for this proposed deflecting galaxy, we obtain a distance of ~2400 Mpc (see Figure 4-5). At this distance (and with $m_d \sim 20^m$), one needs a M/L value ~80 for this galaxy. From these values, we find that the mass of the deflecting galaxy must be $\sim 5 \times 10^{12}\ m_\odot$. This quasar has also been suggested as exhibiting gravitational imaging by Sanitt[34], who only considers the optical imaging case and uses the nearer galaxy ($\sim 20^m$, 2.5" S of the QSO), and thus obtains a smaller value for the mass of the deflector (i.e., $\sim 6 \times 10^{11}\ m_\odot$). This quasar is also reportedly optically variable[35], but the nature of this variability is not yet clear enough to establish a time delay measurement. This quasar is perhaps the best studied case for the feasibility of the gravitational lens effect.

---

[34]N. Sanitt, Monthly Notices of the Royal Astronomical Society, Vol. 174, (1976), p. 91.

[35]J. V. Peach, Nature, Vol. 222, (1969), p. 439.

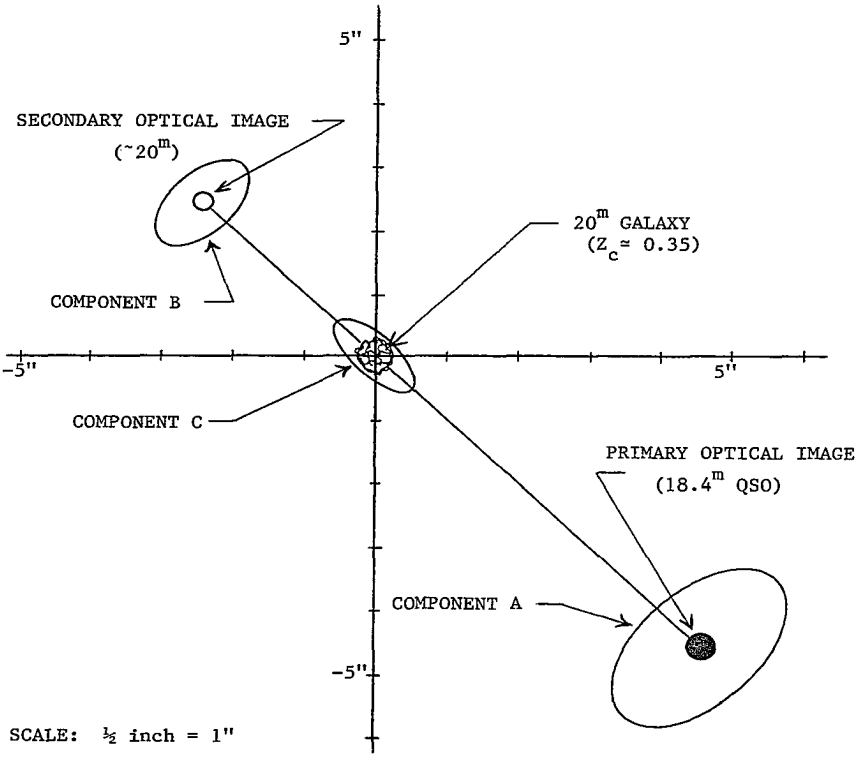

FIGURE 4-4: Positional sketch of the proposed imaging system in the quasar 1206+43 (3C 268.4)

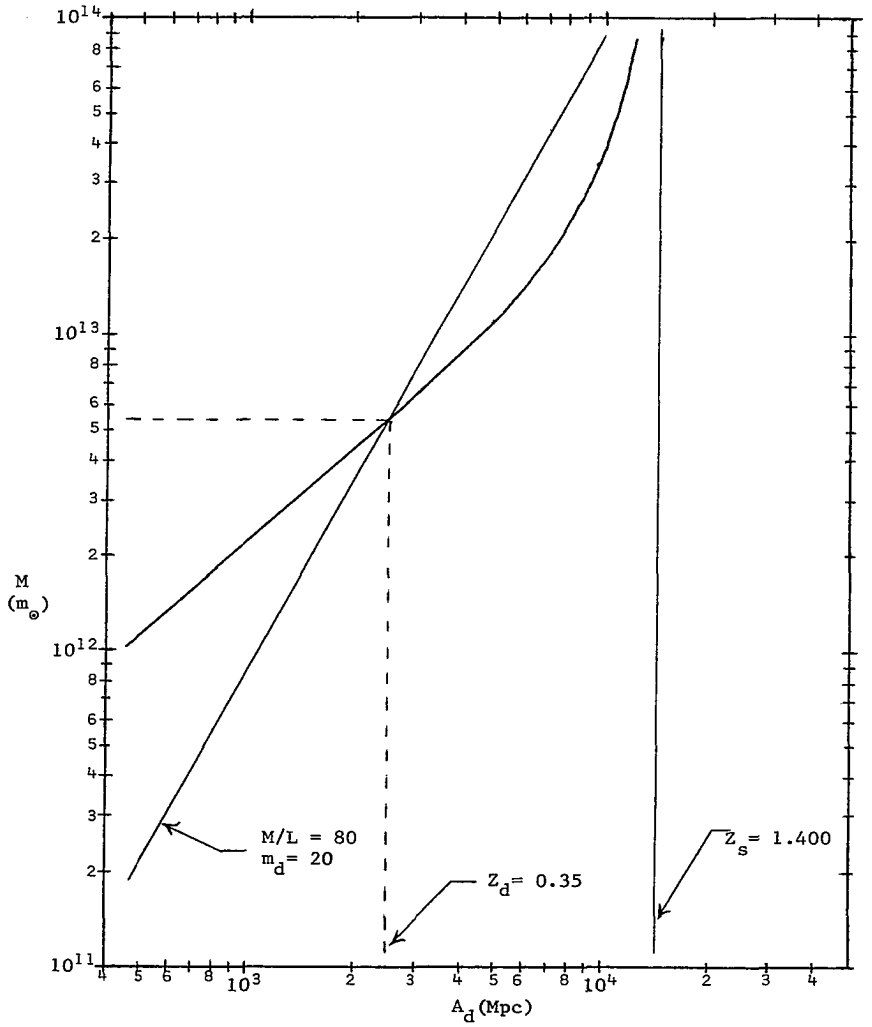

FIGURE 4-5: Logarithmic plot of the "deflector-mass" and "deflector-luminosity" curves for the image candidate 1206+43 (3C 268.4)

Image Models for the Compact Sources

We shall now consider the image models for the compact image candidates. Each of these sources is discussed individually below with a similar summary table (Tables V-1 through V-7) as used above for the extended sources. The format of these tables is similar to that presented for the extended candidates, with the following exceptions:

1. Since all of these sources have an overall angular size $\lesssim 1''$, we cannot impose the same type of optical constraints as previously used. So, without further information regarding the relative positions of the optical and radio components, we take the predicted optical flux ratio (R_o) to be roughly the same as the observed radio flux ratio (R). Also, all of the optical objects (i.e., both images and the deflecting object) will be similarly confined to such small angular regions. Thus, the observed optical magnitude of the QSO will be labeled, m_c, denoting the combined magnitudes of all these objects.

2. With the small angular separations of the images involved, the required deflector masses will be correspondingly smaller (i.e., $\sim 10^9 - 10^{11}\ m_\odot$), so that for a wide range of assumed mass-luminosity ratios of the deflector, the deflecting object would not be optically visible below most plate limits ($\sim 21^m$). So, we adopt here a M/L value of around 15 to 25 (characteristic of giant elliptical galaxies) and then estimate the expected apparent optical magnitudes.

3. Except for two candidates, which have indirect evidence of a deflecting mass located at some distance, one cannot place a reasonable guess on the distance of the required deflector. In these cases, we used the optimum redshift parameter, $(Z_d)_{max}$, for the deflector's distance.

TABLE V-1

IMAGE MODEL FOR THE COMPACT QUASAR 0538+49 (3C 147)

SYSTEM	MEASURED/CALCULATED QUANTITIES			OBSERVED?	IMAGING STATUS
	Intensities	Positions	Distances		
RADIO	$R = 1.2 \pm 0.1$	$\phi = 0.14'' \pm 0.03''$ $\phi^+ = 0.07'' \pm 0.02''$ $\phi^- = 0.07'' \pm 0.02''$	$Z_s = 0.545$ $A_s = 4160$ Mpc	YES	FAIR
OPTICAL	$R_o = 1.2 \pm 0.1$ $m_c = 17.8 \pm 0.1$	$\psi = 0.14'' \pm 0.03''$ $\psi^+ = 0.07'' \pm 0.02''$ $\psi^- = 0.07'' \pm 0.02''$		YES ?	
DEFLECTOR	$m_d \lesssim 25$ $M/L \simeq 15$ MASS $\sim 2 \times 10^9\ m_\odot$		$(Z_d)_{max} = 0.25$ $A_d \simeq 1690$ Mpc	NO	
TIME DELAYS	$(\Delta t)_g \simeq 1.02$ Hours, $(\Delta t)_p \simeq 1.00$ Hours $(\Delta t)_{tot} \simeq 2.02$ Hours			OV (?) RV (?)	

TABLE V-2

IMAGE MODEL FOR THE COMPACT QUASAR 1328+307 (3C 286)

SYSTEM	MEASURED/CALCULATED QUANTITIES			OBSERVED?	IMAGING STATUS
	Intensities	Positions	Distances		
RADIO	$R = 2.1 \pm 0.3$	$\phi = 0.37'' \pm 0.05''$ $\phi^+ = 0.22'' \pm 0.05''$ $\phi^- = 0.15'' \pm 0.03''$	$Z_s = 0.849$ $A_s = 7256$ Mpc	YES	VERY GOOD !
OPTICAL	$R_o = 2.1 \pm 0.3$ $m_c = 17.3 \pm 0.1$	$\psi = 0.37'' \pm 0.05''$ $\psi^+ = 0.22'' \pm 0.05''$ $\psi^- = 0.15'' \pm 0.03''$		YES ?	
DEFLECTOR	$m_d \lesssim 25$ $M/L \simeq 20$ MASS $\simeq$ (5 to 8) x 10^{10} $m_\odot$		$Z_d = 0.692$ $A_d = 5589$ Mpc	YES !	
TIME DELAYS	$(\Delta t)_g = 216 \pm 70$ Hours, $(\Delta t)_p = 136 \pm 40$ Hours $(\Delta t)_{tot} = 352 \pm 80$ Hours			RV (?)	

TABLE V-3

IMAGE MODEL OF THE COMPACT QUASAR 0420-01 (OF-035)

SYSTEM	MEASURED/CALCULATED QUANTITIES			OBSERVED?	IMAGING STATUS
	Intensities	Positions	Distances		
RADIO	$R = 1.3 \pm 0.2$	$\phi = 0.10'' \pm 0.02''$ $\phi^+ = 0.06'' \pm 0.02''$ $\phi^- = 0.04'' \pm 0.01''$	$Z_s = 1.740$	YES	GOOD
OPTICAL	$R_o = 1.3 \pm 0.2$ $m_c = 18.0 \pm 0.1$	$\psi = 0.10'' \pm 0.02''$ $\psi^+ = 0.06'' \pm 0.02''$ $\psi^- = 0.04'' \pm 0.01''$	$A_s = 1.95 \times 10^4$ Mpc	YES ?	
DEFLECTOR	$m_d \leq 28$ $M/L \simeq 20$ MASS $\simeq 3 \times 10^9 m_\odot$		$Z_d = 0.915$ $A_d = 8000$ Mpc	YES ?	
TIME DELAYS	$(\Delta t)_g = 4.3 \pm 1.0$ Hours, $(\Delta t)_p = 2.2 \pm 0.8$ Hours $(\Delta t)_{tot} = 6.5 \pm 1.3$ Hours			RV (?)	

TABLE V-4

IMAGE MODEL OF THE COMPACT QUASAR 2230+114 (CTA 102)

SYSTEM	MEASURED/CALCULATED QUANTITIES			OBSERVED?	IMAGING STATUS
	Intensities	Positions	Distances		
RADIO	$R = 5.1 \pm 0.5$	$\phi = 0.05" \pm 0.01"$ $\phi^+ = 0.04" \pm 0.02"$ $\phi^- = 0.01" \pm 0.01"$	$Z_s = 1.038$ $A_s = 9460$ Mpc	YES	FAIR
OPTICAL	$R_o = 5.1 \pm 0.5$ $m_c = 17.3 \pm 0.1$	$\psi = 0.05" \pm 0.01"$ $\psi^+ = 0.04" \pm 0.02"$ $\psi^- = 0.01" \pm 0.01"$		YES ?	
DEFLECTOR	$m_d \leq 30$ $M/L \simeq 20$ MASS $\geq 1 \times 10^9 m_\odot$		$(Z_d)_{max} = 0.826$ $A_d \simeq 7000$ Mpc	NO	
TIME DELAYS	$(\Delta t)_g \geq 8.7$ Hours, $(\Delta t)_p \geq 4.5$ Hours $(\Delta t)_{tot} \geq 13.2$ Hours			RV (?) OV (?)	

TABLE V-5

IMAGE MODEL OF THE COMPACT QUASAR 1328+254 (3C 287)

SYSTEM	MEASURED/CALCULATED QUANTITIES			OBSERVED?	IMAGING STATUS
	Intensities	Positions	Distances		
RADIO	$R = 1.1 \pm 0.1$	$\phi = 0.10'' \pm 0.02''$ $\phi^+ = 0.05'' \pm 0.02''$ $\phi^- = 0.05'' \pm 0.02''$	$Z_s = 1.055$ $A_s = 9670$ Mpc	YES	FAIR
OPTICAL	$R_o = 1.1 \pm 0.1$ $m_c = 17.7 \pm 0.1$	$\psi = 0.10'' \pm 0.02''$ $\psi^+ = 0.05'' \pm 0.02''$ $\psi^- = 0.05'' \pm 0.02''$		YES ?	
DEFLECTOR	$m_d \leq 28$ M/L = 20 MASS $\simeq 1 \times 10^9 m_\odot$		$(Z_d)_{max} \simeq 0.35$ $A_d \simeq 2470$ Mpc	NO ?	
TIME DELAYS	$(\Delta t)_g \simeq 0.8$ Hours, $(\Delta t)_p \simeq 0.5$ Hours $(\Delta t)_{tot} \simeq 1.3$ Hours			NO (not variable)	

TABLE V-6

IMAGE MODEL OF THE COMPACT QUASAR 0333+32 (4C 32.14)

SYSTEM	MEASURED/CALCULATED QUANTITIES			OBSERVED?	IMAGING STATUS
	Intensities	Positions	Distances		
RADIO	$R = 1.6 \pm 0.2$	$\phi = 0.30'' \pm 0.05''$ $\phi^+ = 0.17'' \pm 0.04''$ $\phi^- = 0.13'' \pm 0.03''$	$Z_s = 1.258$	YES	FAIR
OPTICAL	$R_o = 1.6 \pm 0.2$ $m_c = 18.3 \pm 0.1$	$\psi = 0.30'' \pm 0.05''$ $\psi^+ = 0.17'' \pm 0.04''$ $\psi^- = 0.13'' \pm 0.03''$	$A_s = 1.23 \times 10^4$ Mpc	YES ?	
DEFLECTOR	$m_d \leq 26$ $M/L = 20$ MASS $\simeq 7 \times 10^9 m_\odot$		$(Z_d)_{max} \simeq 0.40$ $A_d \simeq 2880$ Mpc	NO	
TIME DELAYS	$(\Delta t)_g \simeq 13.5$ Hours, $(\Delta t)_p \simeq 9.0$ Hours $(\Delta t)_{tot} \simeq 22.5$ Hours			RV (?)	

TABLE V-7

IMAGE MODEL OF THE COMPACT QUASAR 1416+067 (3C 298)

SYSTEM	MEASURED/CALCULATED QUANTITIES			OBSERVED?	IMAGING STATUS
	Intensities	Positions	Distances		
RADIO	$R = 1.8 \pm 0.2$	$\phi = 1.2" \pm 0.2"$ $\phi^+ = 0.7" \pm 0.2"$ $\phi^- = 0.5" \pm 0.1"$	$Z_s = 1.439$ $A_s = 1.49 \times 10^4$ Mpc	YES	FAIR
OPTICAL	$R_o = 1.8 \pm 0.2$ $m_c = 16.8 \pm 0.1$	$\psi = 1.2" \pm 0.2"$ $\psi^+ = 0.7" \pm 0.2"$ $\psi^- = 0.5" \pm 0.1"$		YES ?	
DEFLECTOR	$m_d \leq 22$ M/L = 20 MASS $\simeq 1.3 \times 10^{11}\ m_\odot$		$(Z_d)_{max} \simeq 0.45$ $A_d \simeq 3300$ Mpc	NO	
TIME DELAYS	$(\Delta t)_g \simeq 300$ Hours, $(\Delta t)_p \simeq 510$ Hours $(\Delta t)_{tot} \simeq 810$ Hours			RV (?)	

4. Since all of the compact sources are already favorable image candidates in the sense that they fulfill all of the available imaging criteria and only need reasonable deflector masses, then the imaging status is given the terminology: "Fair," "Good," or "Very Good," depending upon whether or not suitable evidence is available for the required deflecting mass.

0538+49 (3C 147)

The radio structure of this source is a simple triple component system with the weaker two components (B and C) having a constant flux ratio ~1.2, while the larger component (A) does not appear to have a frequency-independent radio spectrum. Since the separation of this component (A) is ~0.6" from the two image candidates (B and C), which have a separation ~0.1", the radio image of component A would be ~40 times weaker, and this could be why such a "fourth" component is not observed. Thus, the components (B and C) appear to be reasonable radio image candidates. However, no evidence is at present available to confirm or deny the presence of a suitable deflector. We, thus, adopt $(Z_d)_{max} \simeq 0.25$ ($A_d \simeq 1690$ Mpc), which gives a mass ~2 x 10^9 $m_\odot$. By using a M/L value ~15, we see (Figure 4-6) that such a deflecting galaxy would not be visible above a magnitude of ~25^m. The optical QSO has been observed to be somewhat variable at both optical and radio wavelengths, so that a time delay measurement may be obtainable, but the time variations are not yet clear enough to measure any existing such time delay. Thus, we consider this source to be a fair image candidate.

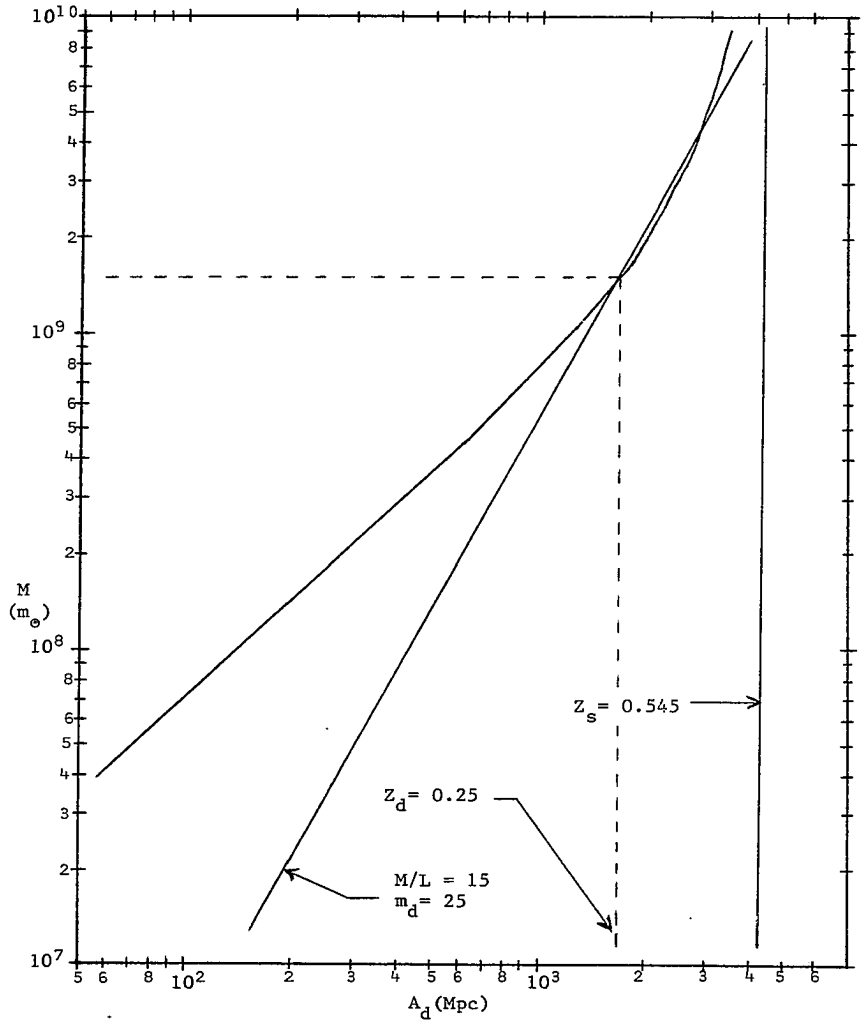

FIGURE 4-6: Logarithmic plot of the "deflector-mass" and "deflector-luminosity" curves for the image candidate 0538+49 (3C 147)

1328+307 (3C 286)

Brown and Roberts (see Notes to Table III) have observed a 21-cm. absorption redshift of ~0.692, which they attribute to the presence of an intervening galaxy. The weak third radio component observed by Clarke[36] could be the radio emission from such a galaxy. Using the redshift as an indication of the galaxy's distance (i.e., $A_d \sim 5589$ Mpc), we obtain a mass of about (5 to 8) x 10^{10} $m_\odot$, which is very reasonable. Also, if we adopt a M/L value ~20 for this galaxy (which is very indicative of gaseous spiral galaxies), we see that the galaxy would be fainter than about 25^m at this distance, and hence is probably why it has not been detected optically. Figure 4-7 shows the maximum and minimum deflector-mass curve, obtained from the assumed errors in the observed quantities, ϕ and R. The quasar is not reported as being optically variable, but there is good evidence that it is radio variable.[37] This quasar, then, is a very good candidate for exhibiting the gravitational lens effect.

0420-01 (OF-035)

This quasar has a controversial redshift of 0.915 or 1.740. If we take the lower reported redshift as a possible absorption redshift

---

[36]R. W. Clarke, et.al., Monthly Notices of the Royal Astronomical Society, Vol. 146, (1969), p. 381.

[37]B. H. Grahl and M. Grewing, Astrophysical Letters, Vol. 4, (1969), p. 107.

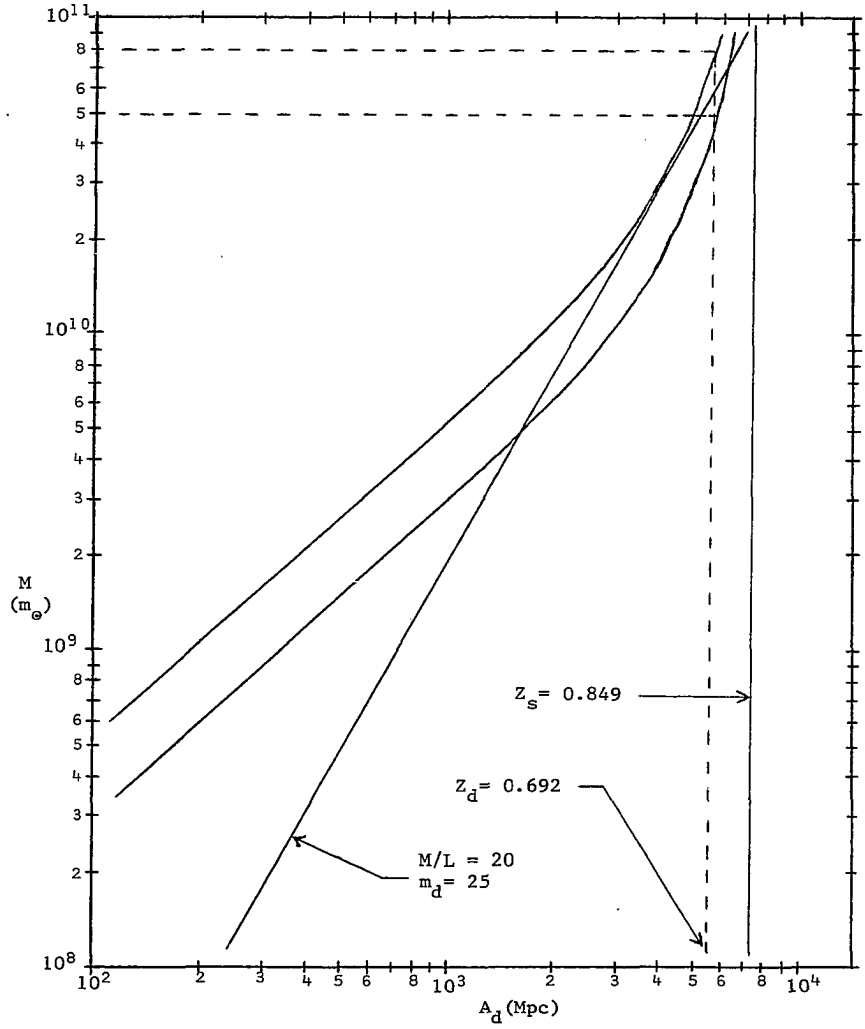

FIGURE 4-7: Logarithmic plot of the "deflector-mass" and "deflector-luminosity" curves for the image candidate 1328+307 (3C 286)

system, due to some intervening galaxy, then we arrive at a deflector mass value ~3 x 10^9 $m_\odot$ at a distance of ~8000 Mpc ($Z_d \simeq 0.915$). Adopting a M/L value ~20 (i.e., a reasonable lower value), we see that such an object would not be visible above ~28^m (see Figure 4-8). The radio quasar is reportedly pronouncedly variable (see Notes to Table III) at radio wavelengths, and with an estimated time delay ~6 hours, this should be an interesting object for investigation. This source is considered as a good prospect for imaging.

2230+114 (CTA 102)

This quasar has no reported evidence of a suitable deflector, although the observed flux ratio ~5 seems favorable for a possible image system. Taking an optimum redshift of ~0.83, we find that a mass of only ~1 x 10^9 $m_\odot$ is required for a deflector here. Even if the M/L value of such a small galaxy is ~20, it would not be visible above ~30^m. This source is considered a fair image candidate.

1328+254 (3C 287)

The radio structure of this quasar is very similar to the source 0538+49 (3C 147) having the brighter radio component (A) ~0.5" from the image candidates (components B and C). Likewise, this is a favorable image system, but no prospective deflector system has been observed. Using an optimum deflector redshift ~0.35 (A_d ~ 2470 Mpc) gives a mass ~1 x 10^9 $m_\odot$. Such a deflecting galaxy would not be visible

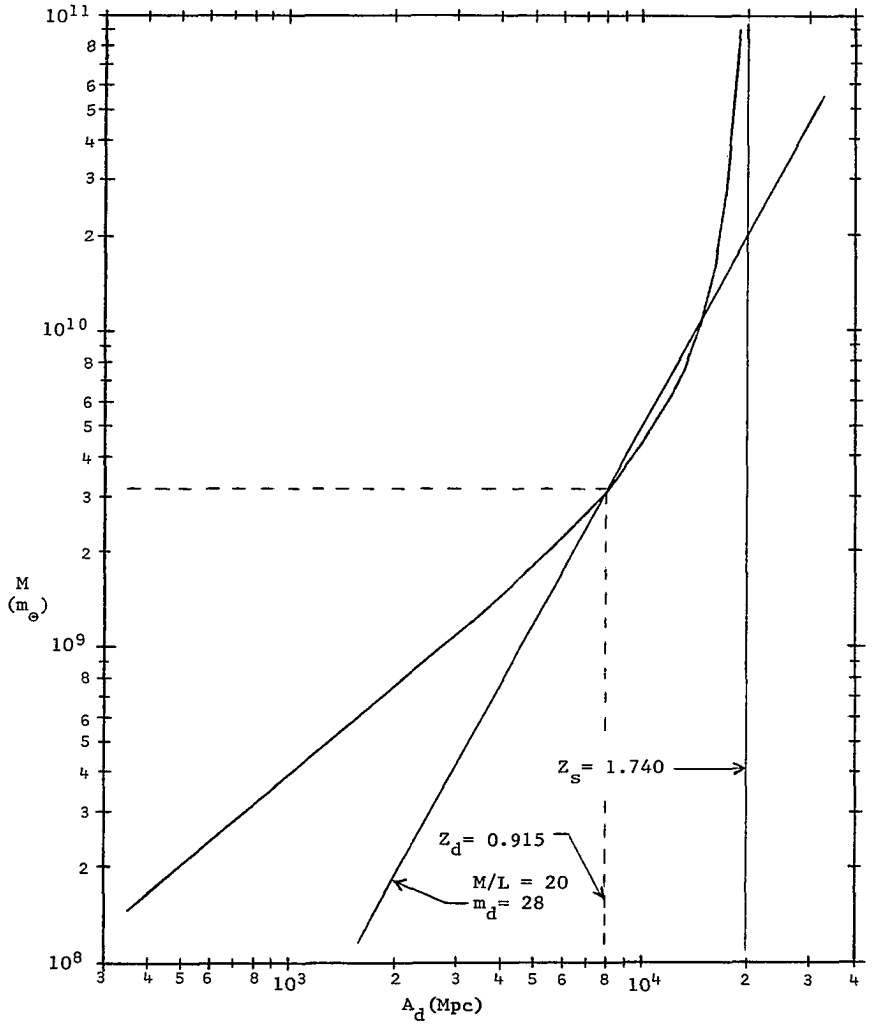

FIGURE 4-8: Logarithmic plot of the "deflector-mass" and "deflector-luminosity" curves for the image candidate 0420-01 (OF-035)

above ~28^m, assuming a M/L value as low as ~20. No significant variability has been observed in this quasar system. This source is also considered to be only a fair image candidate.

0333+32 (4C 32.14)

This radio quasar has been observed to have a simple double radio structure with ϕ ~ 0.3" and R ~ 1.6, but again no prospective deflector object has been detected. Using $(Z_d)_{max}$ ~ 0.40 gives a mass ~7×10^9 $m_\odot$ at a distance, A_d ~ 2880 Mpc. Assuming a M/L value ~20, one probably could not be expected to observe such an optical object down to ~26^m. The quasar is, however, reportedly radio variable.[38] Without further evidence, this source is also considered as only a fair image candidate.

1416+067 (3C 298)

This source is also listed as having no observed suitable deflector. With $(Z_d)_{max}$ ~ 0.45, one obtains a mass ~1.3×10^{11} $m_\odot$, which is quite a reasonable value. With this mass range and an assumed M/L value ~20, such a potential deflecting galaxy should be visible below ~22^m, which might be bright enough to be detected with good optical plates. This source should then be considered as a prospective, but only fair, candidate for exhibiting gravitational imaging.

---

[38] I. I. K. Pauliny-Toth and K. I. Kellermann, Astrophysical Journal, Vol. 146, (1966), p. 634.

CHAPTER V

CONCLUSION

Summary of the Results

From the theory of gravitational imaging due to point-mass deflectors and its application to the present observational data of radio emitting quasars, we have seen that the radio imaging criteria employed here are necessary, but not sufficient, to select only those sources which may be exhibiting the gravitational lens effect. However, when combined with the optical restrictions in the case of the extended sources or the consideration of indirect evidence for a suitable deflector in the case of the compact sources, we obtain a small filtered sample of sources which just might contain gravitationally lensed objects.

Starting with a total sample of 130 radio emitting quasars having determined radio structures, it was found that the imposition of the radio imaging criteria reduced the sample to 21. Of these, only 10 were found to satisfy the optical imaging criteria for the observability of secondary optical images or the required mass deflectors. If we consider only the best two imaging candidates here, 1206+43 (3C 268.4, $Z_s = 1.400$) and 1328+307 (3C 286, $Z_s = 0.849$), then we would obtain an estimated probability of ~2% for observing gravitational imaging.

This compares quite well with the theoretical predictions by Bourassa and Kantowski[39] which give an imaging probability of $\lesssim 5\%$ (considering only double images with flux ratios < 10, with sources out to a redshift of 1.5). However, there are a few points which should be mentioned here, which may affect the validity of this conclusion.

1. The question of the assumption that the radio sources are not significantly extended might arise. However, for the listed image candidates, the angular sizes of the radio components are all less than 1.8" (with an average value ~1.0") in the case of the extended sources, while the compact candidates all have component sizes $\lesssim 0.5$" (with an average value $\lesssim 0.04$"). These source sizes are not considered to be significantly extended, especially in the case of the compact image candidates.

2. There is no doubt that some inherent selection effects are embedded in the procedure adopted in this investigation which might tend to include some non-imaged sources. Such sources may "accidentally" survive the selection criteria imposed here. For example, one might argue that the similarity of the radio spectra in the components of these sources is automatically correlated with their angular separations or their surface brightnesses, due to the physical nature of the systems themselves. Such correlations have not yet been established, and to this end, much further knowledge must be obtained concerning the physical processes occuring in these systems, if one is to resolve this question.

Suggestions for Further Investigations

In an attempt to seek further evidence, either for or against, gravitational imaging, one needs more observational data, both at optical and radio wavelengths. Particularly in the latter case, much further

---

[39]R. R. Bourassa and R. Kantowski, Astrophysical Journal, Vol. 205, (1976), p. 674.

insight could be gained by higher resolutional radio data, but more importantly, from good observations at many different wavelengths. With improved radio structural data of the radio emitting quasars, one may be able to deduce the "projected axial ratios" of their radio components with sufficient accuracy to apply another radio selection criterion, which would help resolve the selection problems stated in the second point above. Such a test would again require a much more detailed knowledge of the distribution of the radiation fields of the source than presently exists, as well as requiring the use of more realistic mass distributions of the required deflecting system. However, the radio sources discussed in this paper may serve as good choices for such further and more intensive investigations.

Another valuable observational consideration for such further work would be the measurement of any "time delays" in the variable quasars, particularly at radio wavelengths. Such observations could possibly resolve the more fundamental question of the "local" or "non-local" hypotheses of the quasars themselves.[40] At the same time, time delay observations could place very useful limits on the estimation of both the mass and distance of gravitational lenses, particularly in view of the concepts of this paper. The determination of the distances of gravitational lenses would then enable one to place good limits on the Hubble constant and the deceleration parameter. In fact, the Hubble constant, H_o, measured in this manner, could be determined to

---

[40] J. H. Cooke and R. Kantowski, op. cit.

essentially the same degree of accuracy as the relevant measurable quantities (i.e., perhaps $\lesssim$10%). The deceleration constant, q_o, on the other hand, would be much more difficult to measure accurately, since the parameter, $\mathcal{D}$, is not very sensitive to q_o. However, if the probability of observing gravitational images is as high as proposed in this paper (i.e., 2% to 5%), then a sufficient statistical sample of gravitational lens systems might be available from which q_o could be derived to an accuracy that is at least comparable to any of the present existing methods. It would then be most fitting if the apparently weak nature of the gravitational lens effect turns out to be an important factor for the determination of the state of the cosmos, which is ruled by gravity itself.

APPENDIX A

COSMOLOGICAL DISTANCE PARAMETERS

This appendix presents the pertinent distance parameters used in the calculations of the gravitational image models discussed in this paper. The following formulae pertain to the various assumed cosmological constants, H_o and q_o, assuming a simple Friedmann cosmology with calculations to be performed in a Robertson-Walker spacetime. These distance formulae are written in their dimensionaless forms for convenience. Absolute values are calculated by scaling with the numerical factor, c/H_o, (refer to Appendix C).

Luminosity Distances

$$A(q_o:Z) = \frac{Z}{q_o} + \frac{(q_o-1)}{{q_o}^2} \cdot \left[\sqrt{1 + 2q_oZ} - 1\right] \qquad \text{(A-1a)}$$

Inverting to solve for Z:

$$Z + 1 = q_o \cdot (1 + A) + (1 - q_o) \cdot \sqrt{1 + 2A} \qquad \text{(A-1b)}$$

The distance parameter, $A(q_o:Z)$, is plotted in Figure A-1 for a few selected values of q_o and can be expressed more simply for the three following special cases:

1. $A(Z) = Z \cdot (1 + Z/2), \quad (q_o = 0)$
2. $A(Z) = 2Z - 2 \cdot (\sqrt{1 + Z} - 1), \quad (q_o = \frac{1}{2})$
3. $A(Z) = Z, \quad (q_o = 1)$

Apparent Angular Diameter Distances

The apparent angular diameter distances are expressed in terms of the luminosity distance for a given deflector redshift, Z_d.

$$D_d(q_o:Z_d) = \frac{A(q_o:Z_d)}{(1 + Z_d)^2} = \frac{A_d}{(1 + Z_d)^2} \qquad \text{(A-2)}$$

In the above and below expressions, the notations, $A_d = A(q_o:Z_d)$ and $A_s = A(q_o:Z_s)$, are used. The distance parameter, $D_d(q_o:Z_d)$, is plotted for various values of q_o as a function of Z_d in Figure A-2.

Imaging Distance Parameters

The Deflector-Source Distance:

$$D_{ds}(q_o:Z_d,Z_s) = \frac{A_s - A_d}{(1 + Z_d)\cdot(1 + Z_s)^2} \qquad \text{(A-3)}$$

The Position-Distance Parameter:

$$D(q_o:Z_d,Z_s) = \frac{D_d\cdot D_{ds}}{D_s} = \frac{A_d}{A_s} \cdot \left[\frac{A_s - A_d}{(1 + Z_d)^3}\right] \qquad \text{(A-4)}$$

The Separation-Distance Parameter:

$$\mathcal{D}(q_o:Z_d,Z_s) = \frac{D_{ds}}{D_d\cdot D_s} = (1 + Z_d)\cdot \left[\frac{A_s - A_d}{A_s\cdot A_d}\right] \qquad \text{(A-5)}$$

These parameters are plotted in Figures A-3 through A-6 for various values of q_o and as a function of Z_d.

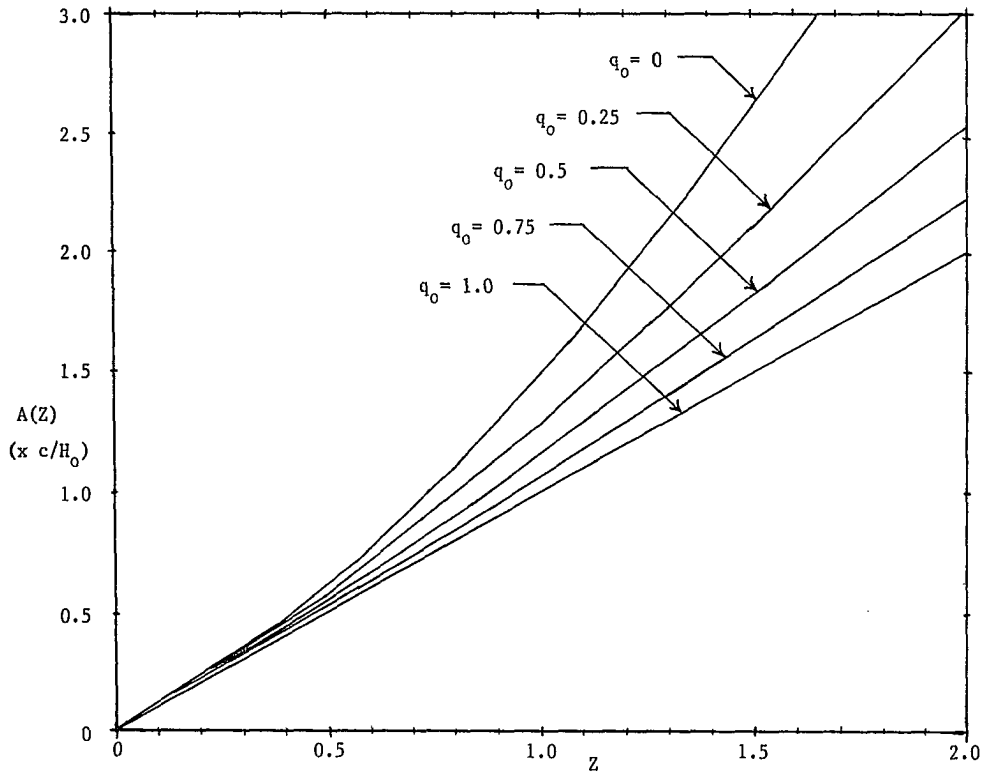

FIGURE A-1: Plot of A(Z) versus Z for various values of q_0

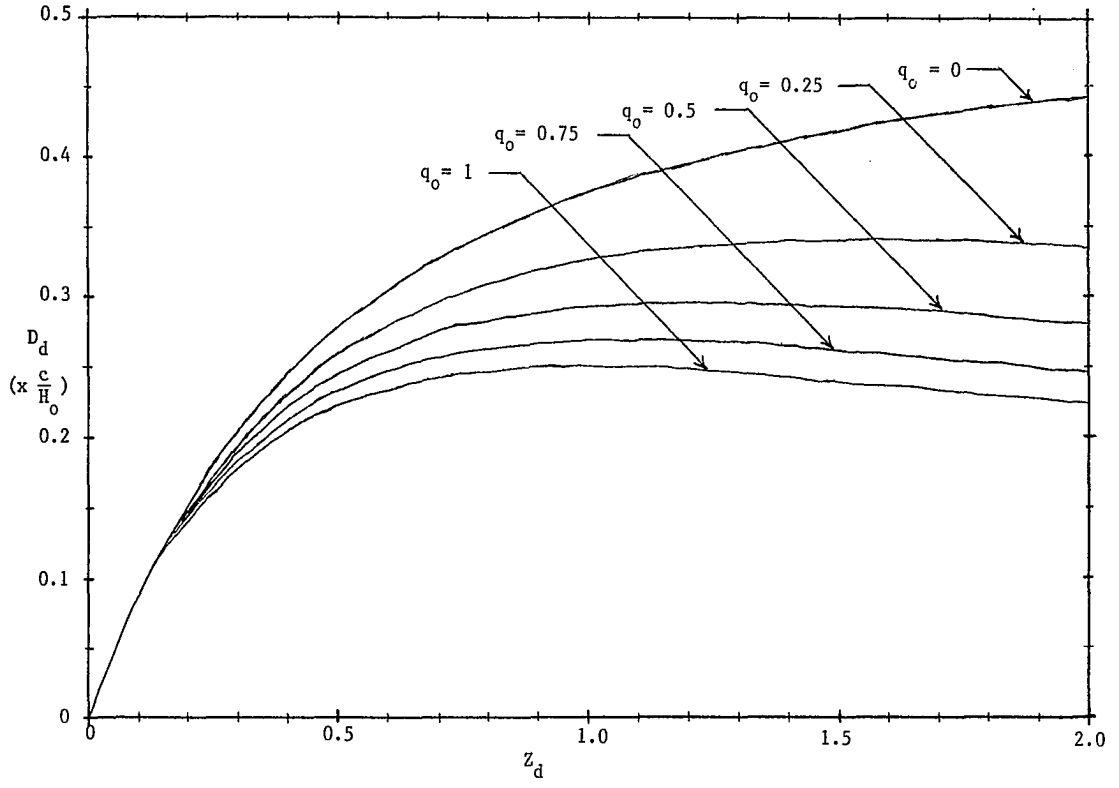

FIGURE A-2 : Plot of D_d versus Z_d for various values of q_o

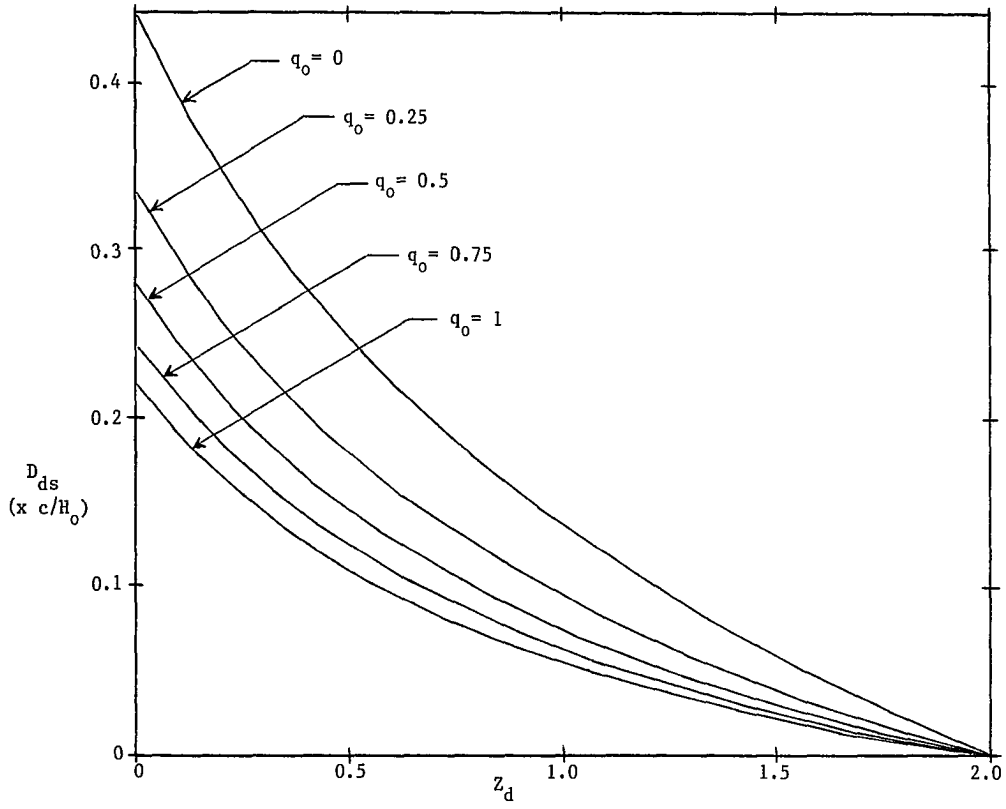

FIGURE A-3: Plot of D_{ds} versus Z_d (with Z_s= 2) for various values of q_o

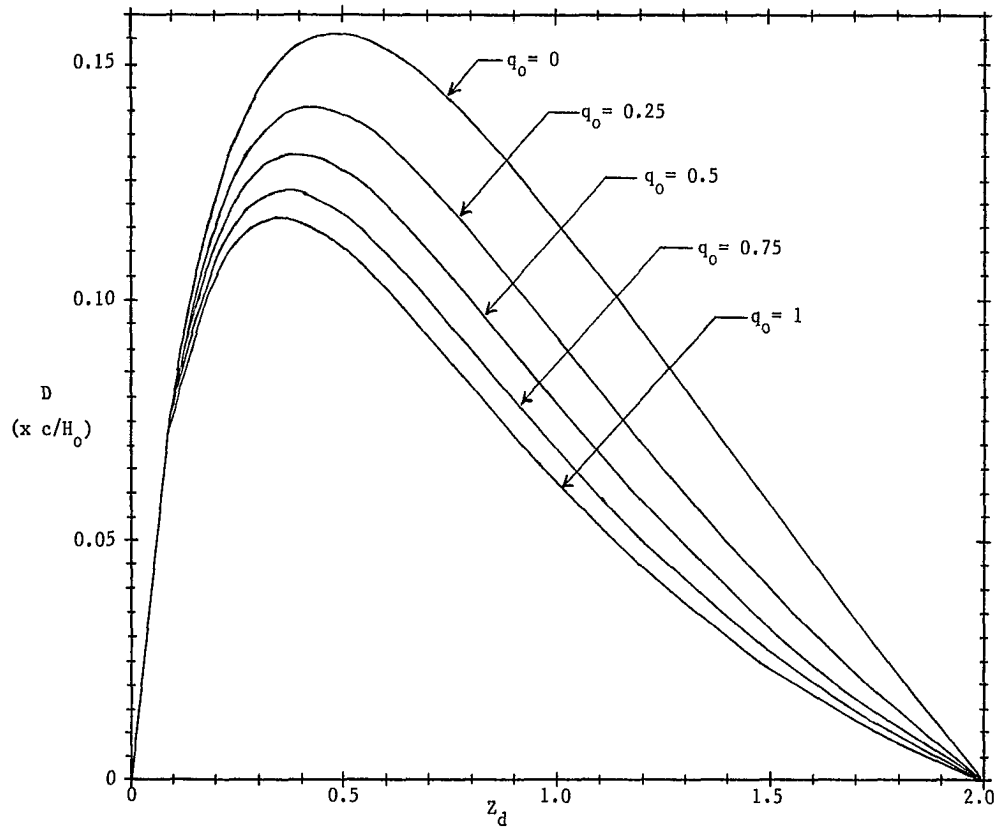

FIGURE A-4: Plot of D versus Z_d (with $Z_s = 2$) for various values of q_o

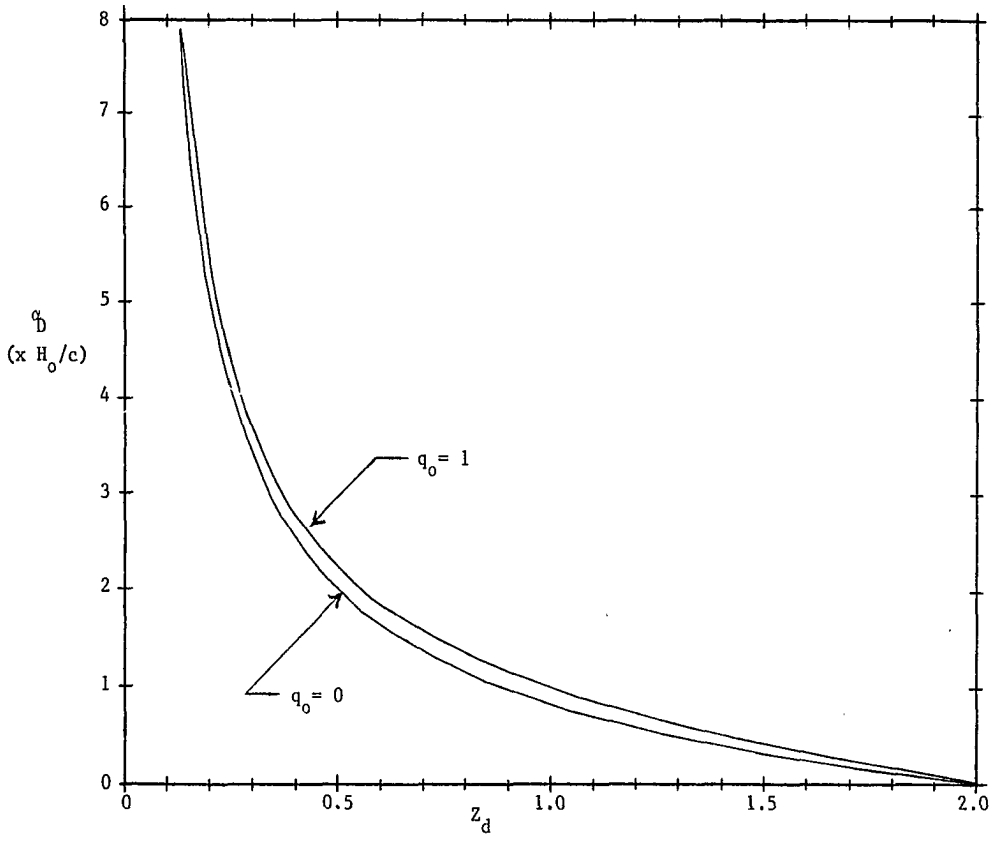

FIGURE A-5: Plot of α_D versus Z_d (with $Z_s = 2$) for $q_o = 0$ and $q_o = 1$

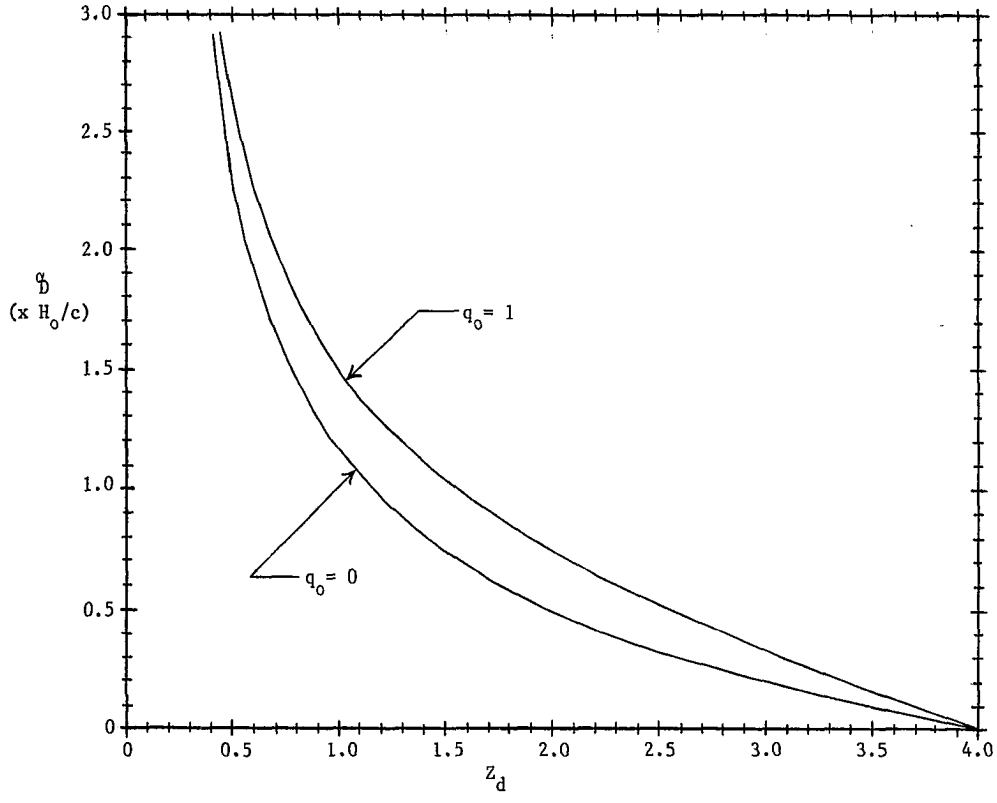

FIGURE A-6: Plot of α_D versus Z_d (with Z_s= 4) for q_o= 0 and q_o= 1

APPENDIX B

MAXIMIZATION OF $D(q_o:Z_d,Z_s)$

From Figure A-4, it is seen that the position-distance parameter, $D(q_o:Z_d,Z_s)$, has a maximum, D_{max}, at a particular deflector redshift, $(Z_d)_{max}$, for a given value of the source redshift, Z_s, and of the deceleration constant, q_o. This appendix presents the analytic solutions for these extremum values.

We seek,

$$\frac{d\left[D(q_o:Z_d,Z_s)\right]}{d\ (Z_d)} = 0 \rightarrow (Z_d)_{max} \rightarrow D_{max} .$$

From Equation A-4, and by using Equations A-1a and A-1b, we can write this condition as,

$$\frac{d\left[D(q_o:Z_d,Z_s)\right]}{d\ (Z_d)} = \frac{\partial\left[D(q_o:A_d,A_s)\right]}{\partial\ (A_d)} \cdot \frac{\partial\left[A_d(q_o:Z_d,Z_s)\right]}{\partial\ (Z_d)} = 0.$$

Since the function, $A_d(q_o:Z_d,Z_s)$, has no maximum with respect to the variable, $Z_d(Z_d \neq 0)$, this condition reduces to

$$\frac{\partial\left[D(q_o:A_d,A_s)\right]}{\partial\ (A_d)} = 0.$$

The solution to this equation, for arbitrary values of q_o and for fixed values of Z_s, is given by,

$$(1 - q_o) \cdot \left[A_s - A_d \cdot (A_s + A_d + 2)\right] + q_o \cdot \sqrt{1 + 2A_d} \cdot \left[A_s + A_d \cdot (A_d - 2A_s - 2)\right] = 0.$$

This equation simplifies for the following two particular values of q_o:

$$\underline{q_o = 0}$$

$$(Z_d)_{max} = \sqrt{1 + 2 \cdot (A_d)_{max}} - 1, \text{ where here,}$$

$$(A_d)_{max} = \tfrac{1}{2} \cdot \left[-(A_s + 2) + \sqrt{(A_s + 2)^2 + 4A_s} \right], \text{ and} \qquad \text{(B-1a)}$$

$$A_s = Z_s \cdot (1 + Z_s/2).$$

$$\underline{q_o = 1}$$

$$(Z_d)_{max} = (A_d)_{max}, \text{ where here,}$$

$$(A_d)_{max} = A_s + 1 - \sqrt{A_s \cdot (A_s + 1) + 1}, \text{ and} \qquad \text{(B-1b)}$$

$$A_s = Z_s$$

The function, $(Z_d)_{max}\{q_o : Z_s\}$ is plotted as a function of Z_s, for $q_o = 0$ and $q_o = 1$, in Figure B-1.

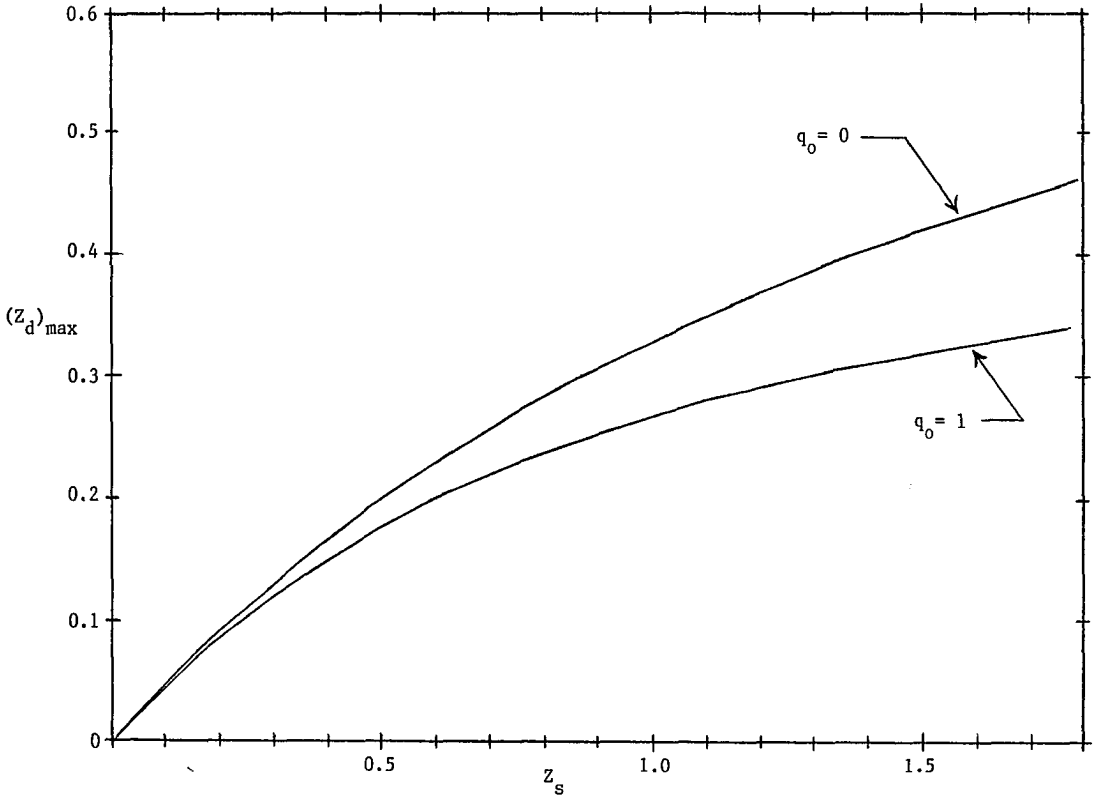

FIGURE B-1: Plot of the quantity, $(Z_d)_{max}$, versus the source redshift, Z_s, for $q_o = 0$ and $q_o = 1$

APPENDIX C

VALUES AND DIMENSIONS OF CONSTANTS

This appendix provides the pertinent constants which are used for the computational methods of this paper.

Fundamental Physical Constants

Speed of light: $c = 2.998 \times 10^5$ Km./Sec.

Gravitational constant: $G = 6.670 \times 10^{-11}$ Nt-m^2/Kg^2

$= 6.670 \times 10^{-20}$ $Km^3/Kg\text{-}Sec.^2$

Solar mass unit: $m_\odot = 1.989 \times 10^{30}$ Kg.

Mass of the galaxy: $m_g \simeq 1.5 \times 10^{11}\ m_\odot$.

Megaparsec: Mpc $= 3.086 \times 10^{19}$ Km.

Derived Constants

Light deflection constant: $c^2/4G = 5.227 \times 10^{18}\ m_\odot/Mpc$.

Time delay constant: $4G/c^3 = 1.969 \times 10^{-5}$ Sec./$m_\odot$

$= 2.279 \times 10^{-10}$ Day/$m_\odot$

$= 6.239 \times 10^{-13}$ Yr./$m_\odot$.

Hubble constant: $H_o = h \cdot 100$ (Km./Sec.)/Mpc ($h = \frac{1}{2} \rightarrow H_o = 50$).

Distance scale factor: $c/H_o = 2998\ h^{-1}$ Mpc ($h = \frac{1}{2} \rightarrow c/H_o \simeq 6000$ Mpc)

LITERATURE CITED

References to Tables II and III

{1} Anderson, B. and Donaldson, W., Monthly Notices of the Royal Astronomical Society, Vol. 137, (1967), p. 81.

{2} Bhandari, S. M., et.al., Australian Journal of Physics, Vol. 27, (1974), p. 121.

{3} Branson, N., et.al., Monthly Notices of the Royal Astronomical Society, Vol. 156, (1972), p. 377.

{4} Burnell, S. J. B., Astronomy and Astrophysics, Vol. 16, (1972), p. 379.

{5} Clark, B. C. and Hogg, D. E., Astrophysical Journal, Vol. 145, (1966), p. 21.

{6} Clark, B. C., et.al., Astrophysical Journal, Vol. 153, (1968), p. 705.

{7} Clarke, R. W., et.al., Monthly Notices of the Royal Astronomical Society, Vol. 146, (1969), p. 381.

{8} Cohen, M. H., et.al., Astrophysical Journal, Vol. 170, (1971), p. 207.

{9} Critchley, F., et.al., Monthly Notices of the Royal Astronomical Society, Vol. 160, (1972), p. 271.

{10} Ibid., p. 283.

{11} Ibid., p. 305.

{12} Donaldson, W., et.al., Monthly Notices of the Royal Astronomical Society, Vol. 146, (1969), p. 213.

{13} Donaldson, W., et.al., Monthly Notices of the Royal Astronomical Society, Vol. 152, (1971), p. 145.

{14} Donaldson, W. and Smith, H., Monthly Notices of the Royal Astronomical Society, Vol. 151, (1971), p. 253.

{15} Fanaroff, B. L. and Blake, G. M., Monthly Notices of the Royal Astronomical Society, Vol. 157, (1972), p. 41.

{16} Fomalont, E. B., Astronomical Journal, Vol. 76, No. 6, (1971), p. 513.

{17} Harris, D. E., Astronomical Journal, Vol. 78, No. 5, (1973), p. 369.

{18} Högbom, J. A. and Carlsson, I., Astronomy and Astrophysics, Vol. 34, (1974), p. 341.

{19} Hogg, D. E., Astrophysical Journal, Vol. 155, (1968), p. 1099.

{20} Jauncey, D. L., et.al., Astrophysical Journal, Vol. 160, (1970), p. 337.

{21} Kapahi, V. K., et.al., Astronomical Journal, Vol. 78, No. 8, (1973), p. 673.

{22} Kellermann, K. I., et.al., Astrophysical Journal (Letters), Vol. 153, (1968), p. L 209.

{23} Kellermann, K. I., et.al., Astrophysical Journal, Vol. 161, (1970), p. 803.

{24} Kellermann, K. I., et.al., Astrophysical Journal, Vol. 169, (1971), p. 2.

{25} Lyne, A. G., Monthly Notices of the Royal Astronomical Society, Vol. 158, (1972), p. 431.

{26} MacDonald, G. H., et.al., Monthly Notices of the Royal Astronomical Society, Vol. 138, (1968), p. 259.

{27} MacDonald, G. H. and Miley, G. K., Astrophysical Journal, Vol. 164, (1971), p. 237.

{28} MacKay, C. D., Monthly Notices of the Royal Astronomical Society, Vol. 145, (1969), p. 31.

{29} Miley, G. K., Monthly Notices of the Royal Astronomical Society, Vol. 152, (1970), p. 477.

{30} Pooley, G. G. and Henbest, S. N., Monthly Notices of the Royal Astronomical Society, Vol. 169, (1974), p. 527.

{31} Rao, A. P., et.al., American Journal of Physics, Vol. 27, (1974), p. 105.

{32} Wardle, J. F. C. and Miley, G. K., Astronomy and Astrophysics, Vol. 30, (1974), p. 305.

References to Notes to Table III

N - 1 Hunstead, R. W., Monthly Notices of the Royal Astronomical Society, Vol. 152, (1971), p. 277.

N - 2 Kristian, J., Astrophysical Journal (Letters), Vol. 179, (1973), p. L 61.

N - 3 Wyndham, J. D., Astrophysical Journal, Vol. 144, (1966), p. 459.

N - 4 Bahcall, J. N., et.al., Astrophysical Letters, Vol. 10, (1972), p. 147.

N - 5 Hunstead, R. W., op. cit.

N - 6 Bahcall, J. N., Astrophysical Journal (Letters), Vol. 157, (1964), p. L 151.

N - 7 Hunstead, R. W., op. cit.

N - 8 Carr, T. D., et.al., Astrophysical Journal (Letters), Vol. 153, (1968), p. L 139.

N - 9 Hunstead, R. W., op. cit.

N-10 Bahcall, J. N., op. cit., (1964).

N-11 Wyndham, J. D., op. cit.

N-12 Bahcall, J. W., op. cit., (1964).

N-13 Hunstead, R. W., op. cit.

N-14 Wyndham, J. D. op. cit.

N-15 Brown, R. L. and Roberts, M. S., Astrophysical Journal (Letters), Vol. 184, (1973), p. L 7.

N-16 Kristian, J., op. cit.

N-17 Peterson, B. A., Astronomical Journal, Vol. 75, No. 6, (1970), p. 695.

N-18 Wyndham, J. D., op. cit.

N-19 Burbidge, G. R., et.al., Astrophysical Journal, Vol. 175, (1972), p. 601.

N-20 Hunstead, R. W., op. cit.

N-21 Wyndham, J. D., op. cit.

N-22 Searle, L. and Bolton, J. G., Astrophysical Journal (Letters), Vol. 154, (1968), p. L 101.

N-23 Hunstead, R. W., op. cit.

N-24 Bahcall, J. W., op. cit., (1972).

N-25 Hazard, C. and Sanitt, N., Astronomical Journal (Letters), Vol. 11, (1972), p. 77.

N-26 Kristian, J., op. cit.

N-27 Kristian, J., op. cit.

N-28 Kristian, J., op. cit.

N-29 Hunstead, R. W., op. cit.

Bibliography

Books

Avrett, E. H., Frontiers of Astrophysics. Cambridge, Massachusetts: Harvard University Press, 1976, p. 510.

Bergmann, P. G., Introduction to the Theory of Relativity. New York, New York: Prentice-Hall, Inc., 1950, p. 184.

Periodicals

Barbieri, C.; Capaccioli, M.; and Zanban, M., Memorie Della Società Astronomica Italiana, Vol. 46, No. 4, (1975), p. 461.

Barnothy, J. M. and Barnothy, M. F., Astronomical Journal, Vol. 70, (1965), p. 666.

Barnothy, J. M. and Barnothy, M. F., Science, Vol. 162, (1968), p. 348.

_____. and _____., Soviet Astronomy (Astrophysics), Vol. 11, No. 5, (1968), p. 895.

Bolton, J. G. and Kinman, T. D., Astrophysical Journal, Vol. 145, (1966), p. 951.

Bourassa, R. R. and Kantowski, R., Astrophysical Journal, Vol. 195, (1975), p. 13.

_____. and _____., Astrophysical Journal, Vol. 205, (1976), p. 674.

_____.; _____.; and Norton, T. D., Astrophysical Journal, Vol. 185, (1973), p. 747.

Burnell, S. J., Astronomy and Astrophysics, Vol. 16, (1972), p. 379.

Clark, E. E., Monthly Notices of the Royal Astronomical Society, Vol. 158, (1972), p. 233.

Clarke, R. W., et.al., Monthly Notices of the Royal Astronomical Society, Vol. 146, (1969), p. 381.

Cooke, J. H. and Kantowski, R., Astrophysical Journal (Letters), Vol. 195, (1975), p. L 11.

Einstein, A., Science, Vol. 84, (1936), p. 506.

Etherington, I. M. H., Philosophical Magazine, Vol. 15, (1933), p. 761.

Gott, J. R. and Gunn, J. E., Astrophysical Journal (Letters), Vol. 190, (1974), p. L 105.

Grahl, B. H. and Grewing, M., Astrophysical Letters, Vol. 4, (1969), p. 107.

Harris, D. E., Astronomical Journal, Vol. 78, No. 5, (1973), p. 369.

Hewish, A. and Burnell, S. J., Monthly Notices of the Royal Astronomical Society, Vol. 150, (1970), p. 141.

Kapahi, V. K., et.al., Astronomical Journal, Vol. 78, No. 8, (1973), p. 673.

Kellermann, K. I., et.al., Astrophysical Journal, Vol. 169, (1971), p. 1.

Liebes, S., Physical Review, Vol. 133, (1964), p. 835.

Lynds, C. R., et.al., Astrophysical Journal, Vol. 142, (1965), p. 1667.

Lyne, A. G., Monthly Notices of the Royal Astronomical Society, Vol. 158, (1972), p. 431.

Noonan, T. W., Publications of the Astronomical Society of the Pacific, Vol. 83, (1971), p. 479.

Pacholczyk, A. G. and Weymann, R., Astronomical Journal, Vol. 73, (1968), p. 836.

Page, T., Astrophysical Journal (Letters), Vol. 136, (1962), p. L 685.

Pauliny-Toth, I. I. K. and Kellermann, K. I., Astrophysical Journal, Vol. 146, (1966), p. 634.

Peach, J. V., Nature, Vol. 222, (1969), p. 439.

Pooley, G. G. and Henbest, S. N., Monthly Notices of the Royal Astronomical Society, Vol. 169, (1974), p. 477.

Press, W. H. and Gunn, J. E., Astrophysical Journal, Vol. 185, (1973), p. 397.

Refsdal, S., Monthly Notices of the Royal Astronomical Society, Vol. 128, (1964), p. 295.

Sanitt, N., Monthly Notices of the Royal Astronomical Society, Vol. 174, (1976), p. 91.

_____., Nature, Vol. 234, (1971), p. 199.

Turner, E. and Gott, J. R., Astrophysical Journal, Vol. 209, (1976), p. 6.

Zwicky, F., Physical Review, Vol. 51, (1937), p. 679.

Unpublished Material

Rousey, C. E., "Possible Evidence of the Gravitational Lens Effect from Observations of the Radio Properties of Quasistellar Objects." Unpublished M. S. thesis, University of Oklahoma, 1974.